Operator-Based Modeling and Inversion

An Operator Approach to the Forward and Inverse Scattering Problems

Hammad, H.I.A.

DOI
10.4233/uuid:9367ebbb-6a82-4d68-9c30-6785566cbe54

Publication date
2021

Document Version
Final published version

Citation (APA)
Hammad, H. I. A. (2021). *Operator-Based Modeling and Inversion: An Operator Approach to the Forward and Inverse Scattering Problems*. [Dissertation (TU Delft), Delft University of Technology]. https://doi.org/10.4233/uuid:9367ebbb-6a82-4d68-9c30-6785566cbe54

Important note
To cite this publication, please use the final published version (if applicable).
Please check the document version above.

H.I.A. Hammad

Operator-Based Modeling and Inversion

Operator-Based Modeling and Inversion

An Operator Approach to the Forward and Inverse Scattering Problems

H.I.A. Hammad

OPERATOR-BASED MODELING AND INVERSION

AN OPERATOR APPROACH TO THE FORWARD AND INVERSE SCATTERING PROBLEMS

OPERATOR-BASED MODELING AND INVERSION

AN OPERATOR APPROACH TO THE FORWARD AND INVERSE SCATTERING PROBLEMS

Proefschrift

ter verkrijging van de graad van doctor
aan de Technische Universiteit Delft,
op gezag van de Rector Magnificus prof. dr. ir. T.H.J.J. van der Hagen,
voorzitter van het College voor Promoties,
in het openbaar te verdedigen op donderdag 23 december 2021 om 10:00 uur

door

Hussain Ibrahim A. HAMMAD

Master of Science in Geology and Geophysics
University of Calgary, Canada
geboren te Tarout, Saoedi-Arabië.

Dit proefschrift is goedgekeurd door de

Promotors: Dr. ir. D.J. Verschuur
Prof. dr. S. Stallinga

Samenstelling promotiecommissie:

Rector Magnificus,	voorzitter
Dr. ir. D.J. Verschuur,	Technische Universiteit Delft
Prof. dr. S. Stallinga,	Technische Universiteit Delft

Onafhankelijke leden:

Prof. dr. ir. C.P.A. Wapenaar,	Technische Universiteit Delft
Prof. dr. W.A. Mulder,	Technische Universiteit Delft
Dr. ir. M.D. Verweij,	Technische Universiteit Delft
Prof. J. Virieux,	Université Joseph Fourier
Dr. ir T. van Leeuwen,	Centrum Wiskunde & Informatica

Keywords: Seismic Modeling, Operator-based modeling, inverse scattering

Printed in The Netherlands by Ridderprint

ISBN 978-94-6458-002-0

"Our Lord, Thou embracest everything in mercy and knowledge."

Ghafir:7

To my parents, grandparents, especially Saleh Al-Sunni.

To my wife, kids, siblings and niblings.

To the First and Second Teachers.

CONTENTS

SUMMARY

The seismic method has many applications. It is important in the critical sector of energy. Besides being used in imaging oil and gas reservoirs, it is also utilized in other sectors of energy such as geothermal energy exploration and development. It also plays a role in extracting other resources such as minerals or in the process of monitoring CO2 sequestration to reduce the carbon footprint of humankind. While seismic waves can occur naturally, their study gives insight in analysing the occurrence of and mitigating risks related to earthquakes. As far as active-source seismic is concerned: seismic images make it possible to see what is in the subsurface with minimal expensive and invasive operations such as drilling unnecessary holes in the subsurface — similar to what medical professionals use ultrasound or X-ray images for.

Several methods have been proposed to analyze seismic data. A popular method nowadays is full waveform inversion (FWI), for instance, which attempts to fit all the recorded waveform with a model. This process solves, in fact, a very complicated highly non-linear inverse problem. Another process that uses such inversion process, but which tries to separate classes of parameters to reduce non-linearity, is joint migration inversion (JMI), in which scattering properties of the subsurface are separated from the propagation properties of seismic waves. Currently those two methods, FWI and JMI, are generally model-dependent — that is they have been formulated to fit specific physics model such as isotropic acoustic media, transversally isotropic media with or without absorption. Hence, they would tend to have biases towards those particular models.

Another paradigm is the so-called data-driven paradigm, or data-adaptive paradigm, and since it is formulated in terms of operators, one could also refer to it as operator-based. Since it contains less biases towards a particular physics model or require no detailed knowledge of model parameters, beforehand, some also refer to it as model-independent, as it does not need to force the data to fit a specific model, rather the process adapts to the model contained within the data. A process such as surface-related multiple elimination follows this paradigm. Another process, which is also shown in this dissertation, separates the surface multiples scattering-order-by-scattering-order without the need to assume a specific physics model. The process is referred to as scattering order decomposition. So, this dissertation looks into the problem of extending the inversion process to the model-independent or the operator-based paradigm.

This dissertation looks first into the theoretical underpinning of this problem, where integral representations are used to study it. These representations are divided into four categories: first model-based representations are derived and presented as directional and non-directional. So, it places in context those theories. Next, the operator-based representations are also divided into directional and non-directional. Finally, four representations are derived, in this dissertation, which have the potential for applications in modeling, inversion and various seismic data analysis processes.

Modeling is needed before any inversion since the inverse problem is ill-posed or ill-conditioned and hence no unique solutions exist but rather preconditioned or regularized solutions to these problems are normally used. Moreover, the inverse problem uses modeling iteratively and also back-projects the data residuals with the forward modeling mechanism. Therefore, the next chapters study operator generation and the subsequent modeling of wavefields with these derived operators.

The forward modeling method is implemented into two primary steps: operator generation and subsequent wavefield modeling. The involved operators are the generalized-wavenumber, reflection and transmission operators. The operators are implemented using a staggered-grid central finite difference discretization scheme in order to accommodate the situation of laterally heterogeneous media. For certain inhomogeneous models, the wavenumber operators are analyzed by converting them to the slowness domain and deriving slowness curves from them. While the slowness curves are generally known for homogeneous anisotropic media, the modeled curves in this dissertation show how slowness curves vary in laterally heterogeneous media. Those curves are numerically computed and shown to vary by frequency and, hence, are dispersive for such media unlike under the laterally homogeneous assumption that is usually adopted. As a consequence, such changes also impact the reflection and transmission operators.

Once the operators are created, one can then use them to generate the full directional wavefields. The wavefields are modeled numerically and iteratively using the so-called Neumann's method. Then, the entire modeling engine, with both of its components, is run on a few modeling examples. The first example shows a benchmarking result with an analytical solution and the two solutions are found to be consistent and in agreement. Next, diving waves are modeled using the x-direction as a direction of preference, and, as it turns out, a single iteration is sufficient using such configuration in order to model the diving wave for a model that changes linearly with depth. Finally, a more complex model is used to recursively model several scattering orders. The evolution of the wavefield in terms of the scattering order in both frequency- and time-domains are shown. Such an example shows that this method is useful for such cases where one is interested in understating the wavefields in terms of their scattering order in media as general as those of vertical and laterally heterogeneity.

While Neumann's method seems to be straight forward to implement the modeling scheme with, it is perhaps not the optimal one. Thus, three different methods that represent a generalization of the Neumann's solution are used: one is a preconditioned over-relaxation, and the other two are a preconditioned conjugate gradient and a truncated Krylov method, the so-called GMRes. The convergence of all those methods is compared, as well as, stationary and successive over-relaxation methods without preconditioning. As it turns out, such truncated Krylov method, i.e., GMRes, is overall faster to converge and requires no preconditioning to ensure convergence. Two examples are shown: one using a velocity model linearly increasing with depth and one using a complex salt model adapted from the SEG SEAM model. In the first model, full wavefield modeling provides the upgoing and the downgoing diving waves including the horizontally propagating constituents, while in the second model, it provides the evolution of the scattering process with different iterations, providing insight into the actual scattering process.

Next, the modeling scheme is extended to the anisotropic situation. By considering a quasi-elastodynamic formulation where the elastodynamic generalized vertical wavenumber operator for P-waves is embedded in the acoustic formulation, anisotropy is introduced in the full wavefield modeling method. The method has been implemented and two examples are shown. One example shows the typical behavior of anisotropy in the homogeneous situation, whereas the other one shows both the incident and the scattered wavefields in an anisotropic heterogeneous medium. The anisotropy examples show clear kinematic and curvature differences compared to the isotropic situation. This development paves the road to not only understanding different phenomena, such as multiples, in anisotropic media but also (and more importantly) to understanding model-independent joint migration inversion (which is treated last in this dissertation) whose goal is to obtain wavefield operators rather than model parameters from the measured data.

Then, the full wavefield modeling method is extended to the elastodynamic situation. While the acoustic situation encompasses directional decomposition — where upgoing and downgoing wavefields are modeled for heterogeneous media through modal decomposition — the elastodynamic situation encompasses three types of decomposition: directional, polarizational and modal. The polarizational decomposition separates the wavefields into its constituent polarizations: quasi-P, quasi-SV, and quasi-SH waves. Two formulations are presented: one is simpler to implement as it contains no polarizational decomposition, while the other one handles all three types of decomposition. Although we begin with the most general equations for anisotropic inhomogeneous media, we reduce those equations to the isotropic situation, and we consider only P-SV waves for simplicity. We implement only the square-root wavenumber operator, whose implementation closely resembles that of the acoustic situation.

Finally, the proposed operator-based inversion process, which is referred to as model-independent joint migration inversion (MI-JMI), is investigated. The operators ultimately sought by the proposed MI-JMI method are reflection and augmented transmission operators (the sum of slowness and transmission operators), yet the reference/background operators are only the simpler Green's primary-only operators. The proposed method is an operator-based model-independent approach to the inverse problem, in contrast to the model-dependent conventional approach of full waveform inversion, which not only uses the physical model parameters, velocity and density in the acoustic situation, but also forces the data to obey a certain model, e.g. isotropic or anisotropic. Two frameworks are proposed in this dissertation: one where those operators are inverted directly and another where those operators are inverted via what is referred to as phantom sources — a combination of operator contrasts and wavefields. A first implementation of the direct framework shows that the method is capable of distinguishing between the relatively easily-obtained vertical heterogeneity, embedded in the reflection operator, and the more difficulty-obtained lateral heterogeneity, embedded in the augmented transmission operator. This feature, among others, is expected to have a major influence on the inversion process, including its convergence properties.

To summarize, this dissertation has investigated theoretical and practical aspects. It investigated the wavefield operators, and developed the forward full directional wavefield modeling method for acoustic, quasi-elastic anisotropic and elastic media and it

laid the ground for the inverse problem using such operator-based description.

SAMENVATTING

De seismische methode kent vele toepassingen. Het is belangrijk in de kritieke energiesector. Behalve dat het wordt gebruikt voor het in beeld brengen van olie- en gasreservoirs, wordt het ook gebruikt in andere energiesectoren, zoals de exploratie en ontwikkeling van geothermische energie. Het speelt ook een rol bij de winning van andere natuurlijke bronnen zoals mineralen of bij het monitoren van de ondergrondse CO2-opslag om de ecologische voetafdruk van de mensheid te verkleinen. Hoewel seismische golven van nature kunnen voorkomen, geeft hun onderzoek inzicht in het beschrijven van aardbevingen en het verminderen van de daarbij behorende risico's. Wat betreft actieve seismiek: de daarmee verkregen seismische beelden maken het mogelijk om te zien wat zich in de ondergrond bevindt met minimale kosten en invasieve operaties zoals het boren van onnodige gaten in de ondergrond — vergelijkbaar met wat medische professionals gebruiken voor ultrasone echografie of röntgen-gebaseerde afbeeldingen.

Er zijn verschillende methoden voorgesteld om seismische gegevens te analyseren. Een populaire methode tegenwoordig is bijvoorbeeld volledige golfveldinversie (FWI), die probeert alle geregistreerde golfvormen met een model van de ondergrond te verklaren. Dit proces lost in feite een zeer gecompliceerd, zeer niet-lineair invers probleem op. Een ander proces dat een dergelijk inversieproces gebruikt, maar dat probeert klassen van parameters te scheiden om niet-lineariteit te verminderen, is gezamenlijke migratieinversie (JMI), waarbij verstrooiingseigenschappen van de ondergrond worden gescheiden van de voortplantingseigenschappen van seismische golven. Momenteel zijn deze twee methoden, FWI en JMI, over het algemeen modelafhankelijk — dat wil zeggen dat ze zijn geformuleerd om te passen in een specifiek natuurkundig model zoals isotrope akoestische media, transversaal isotrope media met of zonder absorptie. Daarom hebben ze de neiging om een bias te hebben richting die specifieke modellen.

Een ander paradigma is het zogenaamde datagedreven paradigma, of data-adaptieve paradigma, en aangezien het is geformuleerd in termen van operatoren, zou men het ook operator-gebaseerd kunnen noemen. Omdat het minder aannames bevat ten opzichte van een bepaald natuurkundig model of vooraf geen gedetailleerde kennis van modelparameters vereist, noemen sommigen het ook modelonafhankelijk, omdat het de gegevens niet hoeft te forceren om in een specifiek model te passen, maar het proces zelf past zich aan aan het model verborgen in de gegevens. Een proces zoals verwijdering van oppervlakte-gerelateerde meervoudige reflecties volgt dit paradigma. Een ander proces, dat ook in dit proefschrift wordt gedemonstreerd, scheidt de meervoudige oppervlak reflecties verstrooiing-orde-voor-verstrooiing-orde zonder de noodzaak om een specifiek natuurkundig model aan te nemen. Het proces wordt verstrooiingsordeontleding genoemd. Dit proefschrift onderzoekt dus het probleem van het uitbreiden van het inversieproces naar het modelonafhankelijke of het op de operator gebaseerde paradigma.

Dit proefschrift gaat eerst in op de theoretische onderbouwing van dit probleem,

waarbij integraalrepresentaties worden gebruikt om het te bestuderen. Deze representaties zijn onderverdeeld in vier categorieën: Eerst worden modelgebaseerde representaties afgeleid en gepresenteerd als directioneel en niet-directioneel. Het plaatst die theorieën dus in een context. Vervolgens worden de operatorgebaseerde representaties ook onderverdeeld in directioneel en niet-directioneel. Tenslotte worden in dit proefschrift vier representaties afgeleid die potentie hebben voor toepassingen in modellering, inversie en verschillende seismische data-analyseprocessen.

Modellering is nodig vóór elke inversie, omdat het inverse probleem slecht gesteld of slecht geconditioneerd is en er daarom geen unieke oplossingen bestaan. Het zijn juist geconditioneerde of geregulariseerde oplossingen voor deze problemen die normaal gesproken worden gebruikt. Bovendien gebruikt het inverse probleem iteratief modelleren en worden de gegevensresiduen ook teruggeprojecteerd met het voorwaartse modelleringsmechanisme. Daarom bestuderen de volgende hoofdstukken het genereren van operatoren en de daaropvolgende modellering van golfvelden met deze operatoren.

De voorwaartse modelleringsmethode wordt geïmplementeerd in twee primaire stappen: operatorgeneratie en daaropvolgende golfveldmodellering. De betrokken operators zijn de gegeneraliseerde golfgetal-, reflectie- en transmissie-operatoren. De operatoren worden geïmplementeerd met behulp van een centraal discretisatieschema met gespreide rasters, om rekening te houden met de situatie van lateraal heterogene media. Voor bepaalde inhomogene modellen worden de golfgetaloperatoren geanalyseerd door ze te converteren naar het traagheidsdomein en er traagheidscurven uit af te leiden. Hoewel de traagheidscurven algemeen bekend zijn voor homogene anisotrope media, laten de gemodelleerde curven in dit proefschrift zien hoe traagheidscurven variëren in lateraal heterogene media. Die curven worden numeriek berekend en laten zien dat ze variëren in frequentie en zijn daarom dispersief voor dergelijke media, in tegenstelling tot de lateraal homogene aanname die gewoonlijk wordt aangenomen. Bijgevolg hebben dergelijke veranderingen ook gevolgen voor de reflectie- en transmissie-operatoren.

Zodra de operators zijn gemaakt, kan men ze gebruiken om de volledige directionele golfvelden te genereren. De golfvelden worden numeriek en iteratief gemodelleerd met behulp van de zogenaamde Neumann-methode. Vervolgens wordt het hele modelleringsproces, met zijn beide componenten, uitgevoerd op een paar modelleringsvoorbeelden. Het eerste voorbeeld toont een benchmarkresultaat met een analytische oplossing en de twee oplossingen blijken consistent en in overeenstemming te zijn. Vervolgens worden duikgolven gemodelleerd met de x-richting als voorkeursrichting, en het blijkt dat een enkele iteratie voldoende is om een dergelijke configuratie te gebruiken om de duikgolf te modelleren voor een snelheidsmodel dat lineair verandert met de diepte. Hierna wordt een complexer model gebruikt om recursief meerdere verstrooiingsorden te modelleren. De evolutie van het golfveld in termen van de verstrooiingsorde in zowel frequentie- als tijddomeinen wordt getoond. Een dergelijk voorbeeld laat zien dat deze methode nuttig is voor gevallen waarin men geïnteresseerd is in het schatten van de golfvelden in termen van hun verstrooiingsorde in media die algemeen zijn in termen van verticale en laterale heterogeniteit.

Hoewel de methode van Neumann geschikt lijkt om het modelleringsschema mee te implementeren, is het misschien niet het meest optimale. Daarom worden er drie verschillende methoden gebruikt die een generalisatie van de Neumann-oplossing verte-

genwoordigen: de ene is een voorgeconditioneerde over-relaxatie en de andere twee zijn een voorgeconditioneerde geconjugeerde gradiënt en een afgeknotte Krylov-methode, de zogenaamde GMRes. De convergentie van al die methoden wordt vergeleken, evenals stationaire en opeenvolgende over-relaxatie methoden zonder preconditionering. Het blijkt dat een dergelijke verkorte Krylov-methode, (d.w.z. GMRes), over het algemeen sneller convergeert en geen preconditionering vereist om convergentie te garanderen. Er worden twee voorbeelden getoond: een met een snelheidsmodel dat lineair toeneemt met de diepte en een met een complex zoutmodel dat is aangepast van het SEG SEAM-model. In het eerste model geeft volledige golfveldmodellering de opgaande en neergaande duikgolven inclusief de zich horizontaal voortplantende delen, terwijl in het tweede model de evolutie van het verstrooiingsproces met verschillende iteraties wordt gegeven, waardoor inzicht wordt verkregen in het werkelijke verstrooiingsproces.

Vervolgens wordt het modelleringsschema uitgebreid tot de anisotrope situatie. Door een quasi-elastodynamische formulering aan te nemen, waarbij de elastodynamische gegeneraliseerde verticale golfgetaloperator voor P-golven is ingebed in de akoestische formulering, wordt anisotropie geïntroduceerd in de volledige golfveldmodelleringsmethode. De methode is geïmplementeerd en twee voorbeelden worden getoond. Het ene voorbeeld toont het typische gedrag van anisotropie in de homogene situatie, terwijl het andere zowel de invallende als de verstrooide golfvelden in een anisotroop heterogeen medium toont. De anisotropievoorbeelden laten duidelijke kinematische en krommingsverschillen zien in vergelijking met de isotrope situatie. Deze ontwikkeling maakt de weg vrij om niet alleen verschillende fenomenen, zoals meervoudige reflecties, in anisotrope media te begrijpen, maar ook (en belangrijker) om modelonafhankelijke gezamenlijke migratie-inversie te begrijpen (welke als laatste in dit proefschrift wordt behandeld), waarvan het doel is om uit de gemeten gegevens golfveldoperators te verkrijgen in plaats van modelparameters.

Vervolgens wordt de volledige golfveldmodelleringsmethode uitgebreid naar de elastodynamische situatie. Terwijl de akoestische situatie directionele decompositie omvat — waarbij opgaande en neergaande golfvelden worden gemodelleerd voor heterogene media door middel van modale decompositie — omvat de elastodynamische situatie drie soorten decompositie: directioneel, polarisatie en modaal. De polarisatiedecompositie scheidt de golfvelden in de samenstellende polarisaties: quasi-P, quasi-SV en quasi-SH golven. Er worden twee formuleringen gepresenteerd: de ene is eenvoudiger te implementeren omdat deze geen polarisatie-ontleding bevat, terwijl de andere alle drie de soorten ontleding behandelt. Hoewel we beginnen met de meest algemene vergelijkingen voor anisotrope inhomogene media, reduceren we die vergelijkingen tot de isotrope situatie en beschouwen we voor de eenvoud alleen P-SV-golven. We implementeren alleen de kwadratische golfgetaloperator, waarvan de uitvoering sterk lijkt op die van de akoestische situatie.

Tenslotte wordt het voorgestelde op de operator gebaseerde inversieproces, welke modelonafhankelijke gezamenlijke migratie-inversie (MI-JMI) wordt genoemd, onderzocht. De operatoren die uiteindelijk worden gezocht door de voorgestelde MI-JMI-methode zijn reflectie- en geaugmenteeerde-transmissie-operators (de som van traagheids- en transmissie-operators), terwijl de referentie-/achtergrondoperators alleen de eenvoudigere (alleen-enkelvoudige) Greense operatoren zijn. De voorgestelde

methode is een operator-gebaseerde modelonafhankelijke benadering van het inverse probleem, in tegenstelling tot de modelafhankelijke conventionele benadering van volledige golfvorminversie, die niet alleen de fysieke modelparameters, snelheid en dichtheid in de akoestische situatie, gebruikt, maar ook de data dwingt om een bepaald model te gehoorzamen, bijvoorbeeld isotroop of anisotroop. In dit proefschrift worden twee raamwerken voorgesteld: een waarbij die operatoren direct worden geïnverteerd en een andere waarbij die operatoren worden geïnverteerd via zogenaamde fantoombronnen — een combinatie van operatorcontrasten en golfvelden. Een eerste implementatie van het directe raamwerk toont aan dat de methode in staat is om onderscheid te maken tussen de relatief gemakkelijk te verkrijgen verticale heterogeniteit, ingebed in de reflectie-operatoren, en de moeilijker te verkrijgen laterale heterogeniteit, ingebed in de uitgebreide transmissie-operatoren. Onder andere deze eigenschap zal naar verwachting een grote invloed hebben op het inversieproces, inclusief de convergentie-eigenschappen.

Samenvattend heeft dit proefschrift theoretische en praktische aspecten onderzocht. Het onderzocht de golfveldoperatoren en ontwikkelde de voorwaartse volledig-directionele golfveldmodelleringsmethode voor akoestische, quasi-elastische anisotrope en elastische media en legde de basis voor het inverse probleem met behulp van een dergelijke operatorgebaseerde beschrijving.

1

INTRODUCTION

"Technology is a gift of God. After the gift of life, it is perhaps the greatest of God's gifts. It is the mother of civilizations, of arts and of sciences."

Freeman Dyson, [1, p. 270]

We introduce the motivation of the thesis in this chapter and we give an overview of its chapters. This dissertation presents a solution to the seismic modeling problem with the aim of model-independent inversion in mind. Although a process such as surface-related multiple elimination (SRME) is less biased towards a model, and hence can be referred to as model-independent, imaging and inversion are still not so; they are model-dependent. Since the model-independent formulation involves operators, one could also refer them as operator-based methods. We propose a representation that could realize such model-independent or operator-based inversion. However, we first need to investigate the forward problem, especially in heterogeneous media. Although, one might need to reparametrize the actual model parameters in order to gain more robustness in the inversion, model-independent or operator-based inversion seems to be more of a radical departure of reparameterization. It indeed belongs to a different paradigm than the established conventional paradigm of seismic data analysis and that of full waveform inversion.

1

1.1. MOTIVATION: MODEL-INDEPENDENT INVERSION

Classical seismic inversion methods focus on retrieving model parameters, such as velocity and/or density. Travel time inversion such as the so-called tomography, or amplitude inversion such as AVO (amplitude variation with offset) inversion or wavefield inversion such as the so-called full waveform inversion (FWI) focus on this goal. While those methods are well developed to some extent, what I would like to investigate is another less developed paradigm; the one that focuses on data and operators.

In other words, I am looking for a data-driven (data-adaptive) approach rather than a model-driven one.

An example of a data-driven method is surface related multiple elimination (SRME) [e.g 2–4]. Instead of requiring a velocity model that would be used to model the multiples and then remove them from the data, what SRME does is use the data themselves to predict those multiples for later subtraction; hence it is a data-driven approach as it builds operators from the data to predict those multiples. See Figure 1.1 for an example of not only SRME but also scattering order decomposition (SOD), which does not only separate all the multiples from the data but it also separates each individual order of surface multiples [5].

While SRME works for surface-multiples, Weglein *et al.* [6] introduced an extension to internal multiples in a data-driven manner. With this method, based on the inverse scattering theory, he could describe the removal of internal multiples without using any information of the subsurface. They use a homogeneous background model to facilitate the prediction of the internal multiples but the output is data without internal multiples located at the surface.

If one is interested to move into the medium instead, then the Marchenko methodology provides a way to do so, with compensation of all scattering in the overburden, using only knowledge of direct arrivals from the surface to the chosen subsurface locations. More importantly, the Marcheko method does not require any knowledge of the scatterers in the overburden [e.g. 7].

However, the majority of imaging and inversion methodologies follow the classic model-driven paradigm. Full wavefield migration (FWM) and joint migration inversion (JMI) methodologies, as proposed by Berkhout [8, 9] are in-between solutions. They are operator-based inversion methods, where as much as possible, exact knowledge of the subsurface is hidden in the operators. Along this line of thinking, I would like to investigate methodologies that are more data-driven and thereby do not need prior knowledge/assumptions on anisotropy or attenuation, for instance.

While model-independent thinking seems to be more of a radical departure of the model-dependent paradigm, we point out that even when using model-dependent methods, it is often justifiable to seek a different set of parameters than the original ones. For instance, using different set of anisotropy parameters, one could get different data sensitivities and hence one set of parameters is probably more useful than another [10]. Another common example is instead of using P-and S-wave velocity and density, one could use Lamé parameters, λ and μ [11].

Therefore, we could see that even if we opt for a model-dependent approach, we might need to reparametrize a set of parameters into a different one. Or we could take a more radical approach and abandon those parameters altogether and seek more of a

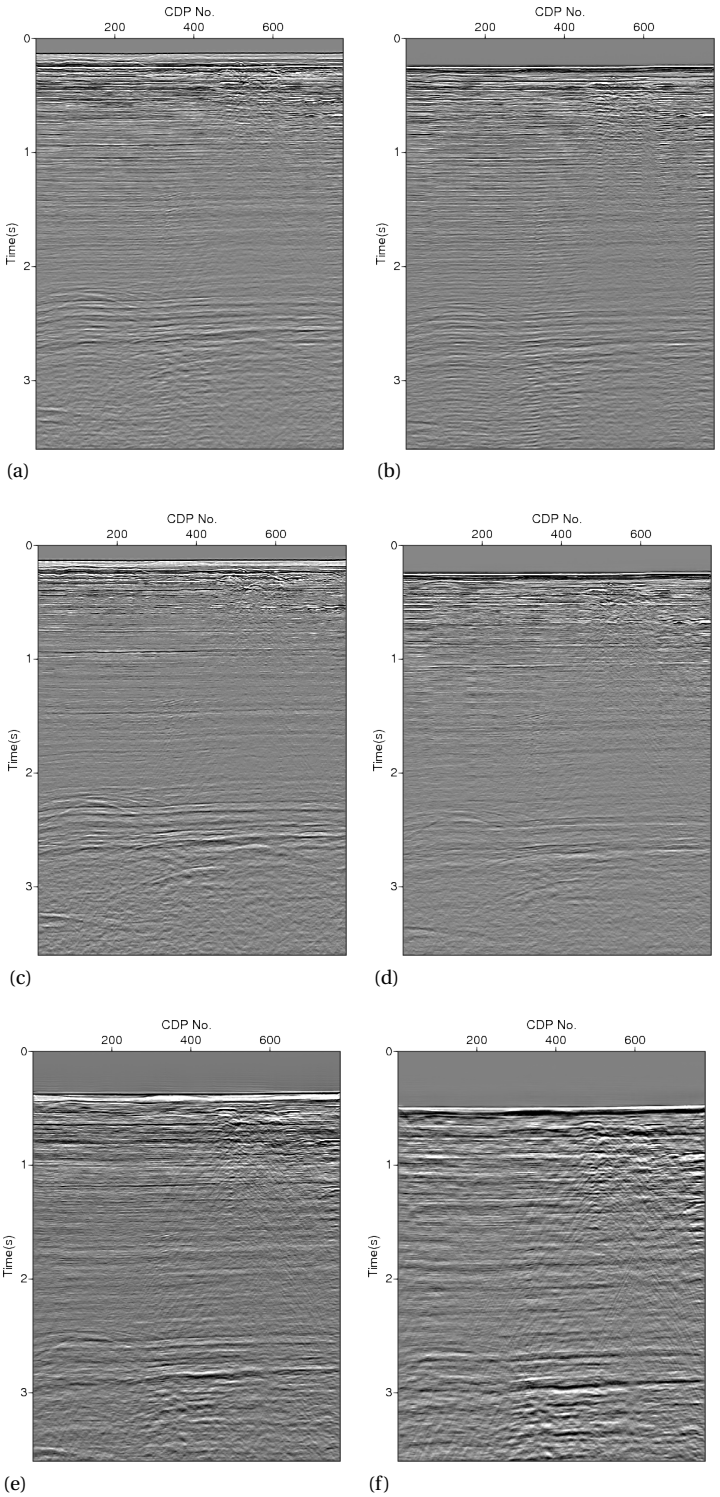

Figure 1.1 *Scattering order decomposition (SOD) of the Nelson field data in the North Sea. (a) Input common offset section, (b) all multiples, (c) primaries and (d)-(f) separated multiples of first to third orders respectively, obtained using SOD, a model-independent process.*

model-independent formulation, similar to SRME.

Whether model-dependent or model-independent (data-driven), one could argue that those two different paradigms are based on fundamentally different types of reasoning. One starts from observations and derives a hypothesis, a model, while the other starts from a hypothesis, a model and validates it with observations [e.g. 12].

This thesis investigates different approaches of posing the model-independent problem and we pick a certain representation, which generalizes the one arrived at by Berkhout [8]. But we realize that one of the reasons the model-independent approach has not been fully developed yet for imaging and inversion, is that some obstacles are present. One of them is understanding the forward problem, especially in the context of heterogeneous media.

So, this thesis dives into the forward problem as a means of understanding and addressing the impact of heterogeneity and as an enabler for implementing a model-independent inversion approach.

But let us take a step back and see what exactly we are proposing in comparison to different existing paradigms.

1.2. DIFFERENT TECHNOLOGY PARADIGMS

Let us first take a look at the established paradigm of analyzing seismic data after a pre-processing step is applied to them. Figure 1.2 shows this conventional workflow. The workflow consists of imaging and model building that are done iteratively and result in a macro model, as well, as an image or reflectivity. The reflectivity, in turn, is analyzed for amplitudes, often using Zoeppritz equations, or a linearized form, and a micro reservoir model is produced. But the amplitude analysis step assumes that the model is not too complex, otherwise it may not work. The books of Yilmaz [13] and the newer version [14], are about this established technology and the book of Simm and Bacon [15], among others, details the steps of AVO analysis and their mapping to rock physics models.

Figure 1.3 shows the workflow that involves a state-of-the-art technology, namely full waveform inversion, whose ultimate objective is to output model parameters directly from the seismic data [e.g. 16, 17]. However, since those parameters are not as well resolved as reflectivity, a broad-band reflectivity image is still produced by imaging the data. In addition, AVO inversion is applied to those reflectivity amplitudes in order to produce a micro model if AVO analysis works; that is to say if the medium is not too complex.

Figure 1.4 shows what we propose in this thesis. We propose that seismic data are mapped into operators that are model-independent. If those operators need to be interpreted as belonging to a specific model, then they can be inverted in a model-dependent step.

However, modeling is needed before any inversion is applied since the inversion process is not unique; that is multiple estimated operators could fit the data equally well [e.g. 18–20]. The other reason is that those operators are only well understood for essentially homogeneous media, or media that are at least piece-wise homogeneous (e.g. consisting of laterally homogeneous layers). Since we are dealing with the Earth, which is known to be heterogeneous, one would need to know those operators for general heterogeneous media so that we could verify any inversion process. In other words, it is easier to design

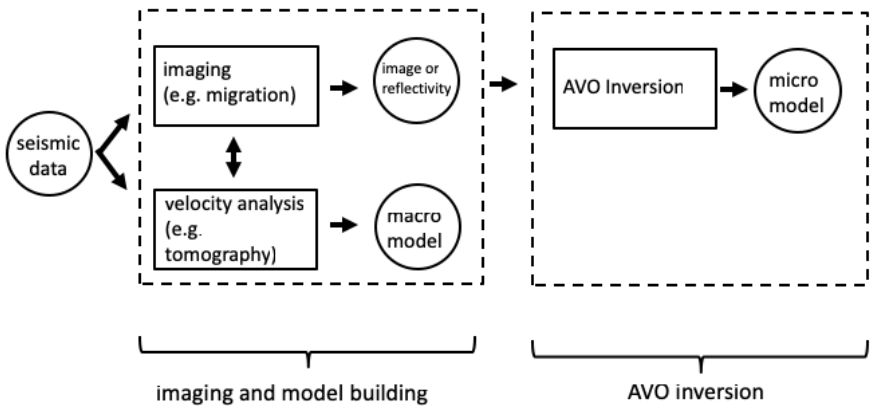

Figure 1.2 *Workflow of established or conventional technology.*

methods that steer the solution to the true one once the family of true solutions is generally known by modeling. In contrast, if one does not know the true solution, it is difficult to steer the solutions, produced by inversion, in the right direction.

Although we present the modeling as a means of seeking model-independent inversion, it is important to point out that, regardless of the success of such a pursuit, the modeling method is indeed useful on its own for different situations of modeling and inversion. It is especially useful in situations where Zoeppritz' equations are used to model reflection coefficients, as this method can replace Zoeppritz' equations for heterogeneous media [21, 22] including situations related to acoustic or SH-waves. Compared to different methods such as that of Kennett [23], two-way wave equation [e.g. 24, 25], or Lippmann-Schwinger equation [e.g. 26], it computes wavefield operators explicitly for heterogeneous media. In contrast, such methods either compute those operators only for homogeneous media or include them implicitly and hence those operators cannot be obtained.

While different modeling methods such as that of Kennett [23], two-way wave equation [e.g. 24, 25], or Lippmann-Schwinger equation [e.g. 26], either use operators for laterally homogeneous media or use them implicitly and hence cannot be obtained.

But let's now take an overview of the different chapters of this thesis.

1

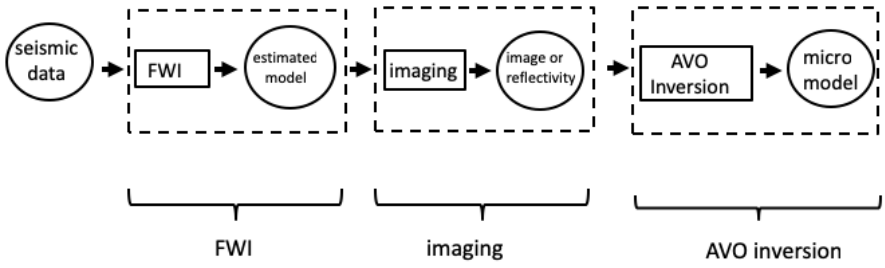

Figure 1.3 *Workflow of FWI, a state-of-the-art technology.*

1.3. THESIS OBJECTIVE AND OVERVIEW

While the model-dependent methods such as FWI are fairly developed, the objective of this thesis is to investigate the other paradigm, the model-independent one. But before any inversion work, one would need first to tackle the forward problem; that is using operators to model the full wavefield. Therefore, we investigate thoroughly the forward problem, especially for heterogeneous media since the Earth is in general a highly heterogeneous medium.

While we state our objectives and motivation in Chapter 1, we investigate, in Chapter 2, model-independent representations that can be used for both modeling and inversion and we compare them to model-dependent ones. What we will find is that model-independent formulations can be done using both directional and non-directional wavefields; both of which could involve different types of operators and we compare those representations to their model-based counterparts.

After we pick a certain form of representation, we model in Chapter 3 the wavefield operators only, which involve reflection, transmission and wavenumber operators. We model them using current knowledge of boundary conditions using the so-called stretch-coordinate PML (perfectly matched layer) and we also look for curves that show the variation of slowness and reflection coefficients in heterogeneous media. We also compare the conventional locally homogeneous formulation to its counterpart for gen-

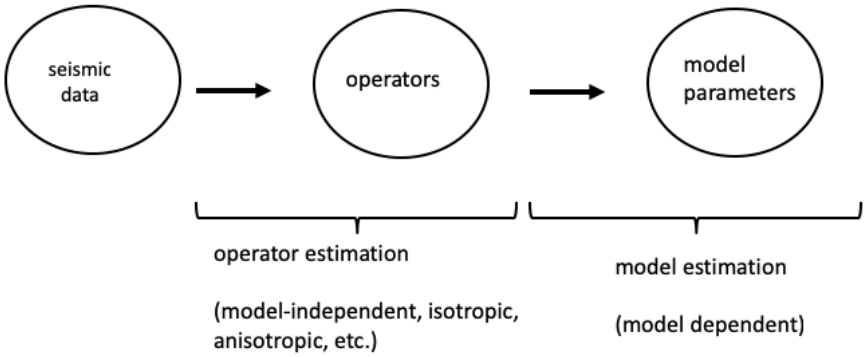

Figure 1.4 *Methodologies as proposed in this thesis.*

eral heterogeneous media.

In Chapter 4, using the operators from Chapter 3, we model the wavefields iteratively using the so-called Neumann's iterative method. We verify the modeling methods by modeling Green's functions in homogeneous media. We model diving waves and show that horizontally propagating waves are not missing in this modeling scheme. We model the wavefields fully for an inhomogeneous medium where both frequency-domain and time-domain domain data are obtained and we show different scattering orders that can be modeled using this method.

While we used Neumann's method, in Chapter 4, which is known to diverge, we examine in Chapter 5 different iterative methods for solving the forward problem. As a result, we find that unlike the application of Neumann's method to problems such as the Lippmann-Schwinger equation, Neumann's method is generally acceptable as applied to our modeling problem and provides stable results for a complex salt model.

In order to demonstrate any model-independent behavior for the inverse problem we need to model the operators beyond only the isotropic situations. So, we extend in Chapter 6 the modeling method to transversely isotropic media and we will show that we can use non-zero vertical shear-wave velocity, unlike what is typically assumed in conventional methods.

We extend in Chapter 7, the modeling method to the elastodynamic situation al-

though using flux-normalized wavefields. While the acoustic method is relatively simple, the complexity increases for the elastodyanmic situations. That's why we limit our discussion only to two-dimensional situations, where P-SV and SH waves are decoupled and treated separately. We derive those operators for this situation and we model the wavefields for P- and S-waves separately.

Given that we have modeled the operators and wavefields, can we retrieve those operators from measured data? We examine this question in Chapter 8, where we propose a method to retrieve those operators and we examine it closely for the laterally homogeneous situation. We show that this method is, in principle, capable of solving the problem through different data-fitting frameworks.

Finally, we dedicate Chapter 9 to different conclusions and further discussion.

REFERENCES

[1] F. J. Dyson, *Infinite in all directions: Gifford lectures given at Aberdeen, Scotland, April-November 1985* (Penguin, 1989).

[2] D. J. Verschuur, A. J. Berkhout, and C. P. A. Wapenaar, *Adaptive surface-related multiple elimination,* GEOPHYSICS **57**, 1166 (1992).

[3] A. J. Berkhout and D. J. Verschuur, *Estimation of multiple scattering by iterative inversion, part I: Theoretical considerations,* GEOPHYSICS **62**, 1586 (1997).

[4] R. G. van Borselen, J. T. Fokkema, and P. M. Van den Berg, *Removal of surface-related wave phenomena—the marine case,* GEOPHYSICS **61**, 202 (1996).

[5] H. I. Hammad and D. J. Verschuur, *Scattering order decomposition-separating multiples by order of scattering, 79th EAGE Conference and Exhibition 2017*, (2017).

[6] A. B. Weglein, F. A. Gasparotto, P. M. Carvalho, and R. H. Stolt, *An inverse-scattering series method for attenuating multiples in seismic reflection data,* GEOPHYSICS **62**, 1975 (1997).

[7] K. Wapenaar, J. Thorbecke, J. Van Der Neut, F. Broggini, E. Slob, and R. Snieder, *Marchenko imaging,* GEOPHYSICS **79**, WA39 (2014).

[8] A. Berkhout, *Review paper: An outlook on the future of seismic imaging, part II: Full-wavefield migration,* Geophysical Prospecting **62**, 931 (2014).

[9] A. J. Berkhout, *Review paper: An outlook on the future of seismic imaging, part III: Joint migration inversion,* Geophysical Prospecting **62**, 950 (2014).

[10] T. Alkhalifah and R.-É. Plessix, *A recipe for practical full-waveform inversion in anisotropic media: An analytical parameter resolution study,* GEOPHYSICS **79**, R91 (2014).

[11] B. Goodway, *The magic of Lamé,* The Leading Edge **29**, 1432 (2010).

[12] W. Sinnott-Armstrong and R. J. Fogelin, *Cengage Advantage Books: Understanding Arguments: An Introduction to Informal Logic* (Cengage Learning, 2014).

[13] Ö. Yilmaz, *Seismic data processing* (Society of Exploration Geophysicists, 1987).

[14] Ö. Yilmaz, *Seismic data analysis: Processing, inversion, and interpretation of seismic data* (Society of exploration geophysicists, 2001).

[15] R. Simm and M. Bacon, *Seismic Amplitude: An interpreter's handbook* (Cambridge University Press, 2014).

[16] A. Tarantola, *Inversion of seismic reflection data in the acoustic approximation,* GEOPHYSICS **49**, 1259 (1984).

[17] L. Sirgue and R. G. Pratt, *Efficient waveform inversion and imaging: A strategy for selecting temporal frequencies,* GEOPHYSICS **69**, 231 (2004).

[18] R. C. Aster, B. Borchers, and C. H. Thurber, *Parameter estimation and inverse problems* (Elsevier, 2018).

[19] W. Menke, *Geophysical data analysis: Discrete inverse theory* (Academic press, 2018).

[20] A. Tarantola, *Inverse problem theory and methods for model parameter estimation*, Vol. 89 (siam, 2005).

[21] M. V. de Hoop, *Generalization of the Bremmer coupling series,* Journal of Mathematical Physics **37**, 3246 (1996).

[22] C. P. A. Wapenaar and J. L. T. Grimbergen, *Reciprocity theorems for one-way wavefields,* Geophysical Journal International **127**, 169 (1996).

[23] B. L. N. Kennett, *Seismic Wave Propagation in Stratified Media* (Cambridge University Press, Cambridge, U.K., 1983).

[24] K. Kelly, R. Ward, S. Treitel, and R. Alford, *Synthetic seismograms: A finite-difference approach,* GEOPHYSICS **41**, 2 (1976).

[25] J. Virieux, *P-SV wave propagation in heterogeneous media: Velocity-stress finite-difference method,* GEOPHYSICS **51**, 889 (1986).

[26] R. E. Kleinman and P. M. van den Berg, *Iterative methods for solving integral equations,* Radio Science **26**, 175 (1991).

2

THEORETICAL ASPECTS: INTEGRAL REPRESENTATION THEOREMS

"All that is said by any of us can only be imitation and representation."

Plato [1, p. 528]

We present integral representations for acoustic wavefields, which can be used for different applications such as modeling, imaging, and inversion of seismic wavefields. We first organise and classify the various forms of representation into two broad categories related to directional and non-directional wavefields. Those, in turn, are classified into two further categories: those involving model parameters and those involving mainly wavefield operators. We derive five forms related to an operator-based directional representation and one form related to a directional model-based representation. We also derive another form involving operators and based on non-directional wave-fields. Although the derived representations are essentially related to the acoustic situation, all representations are extend-able to the elastodynamic and electromagnetic situations.

2.1. INTRODUCTION

The classical Lippmann-Schwinger equation and its linearised form, the so-called Born Equation, form the basis for scattering and inverse scattering theory [e.g 2]. Methods such as full waveform inversion [3] and inverse scattering theory methods [e.g 2, 4], in general, are based on this equation; albeit the forward problem can be solved using those equations [e.g. 4] or a differential equation such as the wave equation [3]. Seeking alternative representations would pave the road to different methods of modeling and inversion. This chapter investigates such alternatives, where only domain (volume integral) representations are considered rather than boundary (surface) representations or a combination of both.

For acoustic media with constant density (ρ_0), the Lippmann-Schwinger equation is given by

$$p(\mathbf{x}_d) = \int_{\mathbb{R}^3} d^3\mathbf{x}\, G_H(\mathbf{x}_d,\mathbf{x})\, s(\mathbf{x}) + \int_{\mathbb{R}^3} d^3\mathbf{x}\, \omega^2 G_H(\mathbf{x}_d,\mathbf{x})\delta m(\mathbf{x})\, p(\mathbf{x}), \tag{2.1}$$

where the model contrast $\delta m(\mathbf{x}) = \frac{1}{\rho_0}(\frac{1}{c^2(\mathbf{x})} - \frac{1}{c_0^2(\mathbf{x})})$, c being the velocity of the actual medium and c_0 that of the background medium, G_H is the Green function in the background medium, p is the pressure wave-field, $\mathbf{x}_d$ is the detector location, s is the source signature and ω is the angular frequency for which the wavefields are considered. Note also that $\mathbf{x}$ is a vector representing all spatial coordinates such that $\mathbf{x} = (x_1, x_2, x_3)$ and similarly for the detector vector $\mathbf{x}_d = (x_{d,1}, x_{d,2}, x_{d,3})$.

For media with variable density and velocity, the Lippmann-Schwinger equation can be written as [see e.g. 5, p. 172]

$$\begin{aligned} p(\mathbf{x}_d) = &\int_{\mathbb{R}^3} d^3\mathbf{x}\, G_H(\mathbf{x}_d,\mathbf{x})\, s(\mathbf{x}) \\ &+ \int_{\mathbb{R}^3} d^3\mathbf{x} \left[\omega^2 G_H(\mathbf{x}_d,\mathbf{x})\delta\kappa(\mathbf{x})\, p(\mathbf{x}) - \partial_k G_H(\mathbf{x}_d,\mathbf{x})\delta l(\mathbf{x})\partial_k p(\mathbf{x})\right], \end{aligned} \tag{2.2}$$

where the incompressibility perturbation $\delta\kappa = \kappa - \kappa_0$, the lightness (inverse of density, ρ) perturbation is $\delta l = l - l_0$, the velocity is such that $c^{-2} = \rho\kappa$ and the summation convention is assumed over repeated indices, where k can take on the values 1, 2 and 3, representing the spatial coordinates.

The objective of this chapter is to find alternatives to this classical representation for applications in modeling and inversion. All types of representations presented in this chapter are categorized in Figure 2.1, where those that involve operators are referred to as operator-based representations and those that involve solely model parameters are referred to as model-based representations. Each is further categorized as either directional or non-directional based on the wavefields they model. We start with a directional version of the Lippmann-Schwinger equation where directional, e.g. up-going and down-going wavefields, are represented instead of full, non-directional ones. We then present various forms of operator-based methods, where operators are used to encompass the perturbation instead of model parameters.

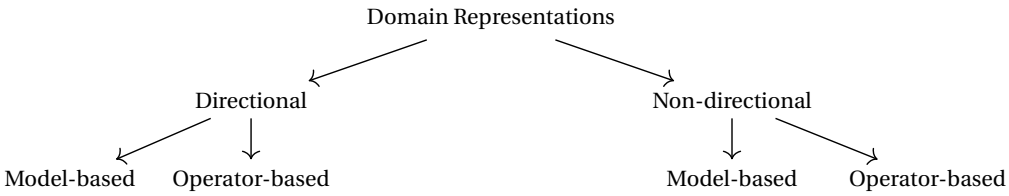

Figure 2.1 *A flow chart illustrating the order of which domain representations are presented, categorized and derived in this chapter.*

As shown in Figure 3.1, we first state the different differential forms of the governing equations, which are the ones related to the acoustic situation. From those various forms, different integral representation theorems can be derived. We then derive the domain-boundary representations, which invoke the Green functions, and we finally state the domain-representations that are more of interest to us. The domain representations are finally classified into either directional or non-directional and model-based or operator-based. The derived equations are summarized in Table 2.1.

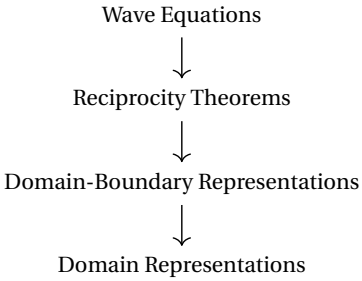

Figure 2.2 *The steps that lead to the domain representations that are used for further investigation into operator-based and model-based methods.*

2.2. WAVE EQUATIONS

We present in this section the actual differential equations that are used next for deriving the corresponding reciprocity theorems. All equations are expressed in the space-frequency domain.

2.2.1. COUPLED WAVE EQUATIONS

The governing wave equations that couple all components of particle velocity and pressure [e.g 5, 6] are given by

Table 2.1 *A table categorizing the representation theorems presented and derived in this chapter.*

	Model-based	Operator-based
Directional	Derived in this chapter: Equation 2.39.	Seven equations presented. Five are proposed in this chapter. The Equations are 2.46, 2.48, 2.50, 2.52 2.55,2.57 and 2.58.
Non-directional	Follows from Rayleigh Reciprocity theorem: Equations 2.38 2.37 and 2.36 .	Derived in this chapter: Equation 2.2

$$\begin{cases} j\omega\rho v_i + \partial_i p = f_i \\ j\omega\kappa p + \partial_i v_i = q, \end{cases} \tag{2.3}$$

where p is the pressure wavefield. In addition, v_i is the particle velocity, f_i is the force source in the x_i direction q is the volume injection source. The summation convention over repeated indexes is assumed. Equation 2.3 can also be written in another operator form shown in Appendix A.6.

2.2.2. HELMHOLTZ SCALAR WAVE EQUATION

The so-called Helmholtz equation, which only contains pressure, can be obtained from the general Equation 2.3 by eliminating particle velocity. It states that [e.g 5]

$$\partial_i(l\,\partial_i p) + \omega^2\kappa p = s, \tag{2.4}$$

where again $l = 1/\rho$ is the lightness and $s = \partial_i(l\,f_i) + \omega^2 q$. It can also be written as

$$\left[\frac{\omega^2}{c^2} + \rho\partial_i(\frac{1}{\rho}\partial_i\,\cdot)\right] p = \rho\partial_i(\frac{1}{\rho}f_i) + \omega^2\rho q. \tag{2.5}$$

where the Helmholtz operator is

$$H_{2,f} = \frac{\omega^2}{c^2} + \rho\partial_i(\frac{1}{\rho}\partial_i\,\cdot), \tag{2.6}$$

which contains the velocity, c and spatial partial derivatives in all spatial dimensions. We will later distinguish between this full Helmholtz operator, $H_{2,f}$, and the one that

contains only lateral derivatives. Substituting the Helmholtz operator in Equation 2.5 yields a more compact equation such that

$$H_{2,f}\, p = \rho \partial_i (\frac{1}{\rho} f_i) + \omega^2 \rho q. \tag{2.7}$$

In media with homogeneous density, the Helmholtz equation then turns into the the more familiar form

$$\partial_i \partial_i p + \frac{\omega^2}{c^2} p = \rho \partial_i f_i + \omega^2 \rho q. \tag{2.8}$$

2.2.3. EQUATIONS ENCOMPASSING VERTICAL PARTICLE VELOCITY AND PRESSURE

We can also express the wave equation in only vertical particle velocity and pressure [e.g 5] leading to the coupled equations

$$\begin{cases} \partial_3 p + j\omega\rho v_3 = f_3 \\ \partial_3 v_3 - \frac{1}{j\omega\rho} H_2 p = q - \frac{1}{j\omega} \partial_\alpha (\frac{1}{\rho} f_\alpha), \end{cases} \tag{2.9}$$

where

$$H_2 = \frac{\omega^2}{c^2} + \rho \partial_\alpha (\frac{1}{\rho} \partial_\alpha \cdot), \tag{2.10}$$

where α takes on the values 1 and 2, i.e. the lateral spatial coordinates. Note here the distinction between the full Helmholtz operator, $H_{2,f}$ that embeds all spatial coordinates and the lateral Helmholtz operator, H_2, that embeds only the lateral ones.

Expressed in another form, equation 2.9 can also be written as [5]

$$\partial_3 \mathbf{q} = \mathbf{A}\mathbf{q} + \mathbf{d}, \tag{2.11}$$

where

$$\mathbf{q} = \begin{pmatrix} p \\ v_3 \end{pmatrix}, \tag{2.12}$$

which encompasses the vertical particle velocity, v_3, and pressure p. Then,

$$\mathbf{A} = \begin{pmatrix} 0 & -j\omega\rho \\ \frac{1}{j\omega\rho} H_2 & 0 \end{pmatrix}, \tag{2.13}$$

and the source term is expressed as

$$\mathbf{d} = \begin{pmatrix} f_3 \\ q - \frac{1}{j\omega} \partial_\alpha (\frac{1}{\rho} f_\alpha) \end{pmatrix}. \tag{2.14}$$

2.2.4. COUPLED DIRECTIONAL WAVE EQUATIONS

One can decompose the operator, $\mathbf{A}$, mentioned above as $\mathbf{A} = -j\omega\mathbf{L}\boldsymbol{\Lambda}\mathbf{L}$, which results in the following coupled system of equations [e.g. 7, 8]

$$\begin{cases} \partial_3 p^+ + (+j\omega\Lambda^+ + T^+)\, p^+ + R^- p^- = s^+ \\ \partial_3 p^- + (-j\omega\Lambda^- + T^-)\, p^+ + R^+ p^+ = s^-, \end{cases} \tag{2.15}$$

where, p^+ and p^- are downgoing and upgoing energy flux-normalized wavefields [7, 8], respectively, Λ is the vertical slowness operator, R is the reflection operator and T is the transmission operator. Equation 2.15 can also be written as [5]

$$\partial_3 \mathbf{p} = \mathbf{B}\mathbf{p} + \mathbf{s}, \tag{2.16}$$

where the operator

$$\mathbf{B} = -j\omega\mathbf{\Lambda} + \mathbf{\Theta}, \tag{2.17}$$

such that the scattering operator

$$\mathbf{\Theta} = -\mathbf{L}^{-1}\partial_3\mathbf{L}, \tag{2.18}$$

which is expressed as

$$\mathbf{\Theta} = \begin{pmatrix} T^+ & R^- \\ R^+ & T^- \end{pmatrix}, \tag{2.19}$$

while the vertical slowness operator, $\mathbf{\Lambda}$, is expressed as

$$\mathbf{\Lambda} = \begin{pmatrix} \Lambda^+ & 0 \\ 0 & \Lambda^- \end{pmatrix}, \tag{2.20}$$

with both of its upgoing, Λ^+, and downgoing, Λ^-, constituents. The wavefields are then

$$\mathbf{p} = \begin{pmatrix} p^+ \\ p^- \end{pmatrix}, \tag{2.21}$$

and the sources

$$\mathbf{s} = \begin{pmatrix} s^+ \\ s^- \end{pmatrix}. \tag{2.22}$$

2.3. RECIPROCITY THEOREMS

Gauss' divergence theorem can be applied to each differential equation so that an integral form can be obtained. In this section we state the reciprocity theorem while paying attention to the classification we propose.

2.3.1. MODEL-BASED RECIPROCITY THEOREMS

The reciprocity theorem invokes two different states, state "a" and state "b", which are indicated as a subscript to each variable. The reciprocity for the full coupled wave equation, Equation 2.3, [e.g. 6, p. 97] state that

$$\begin{aligned} \oint_{\partial\mathbb{D}} d^2\mathbf{x}\,(p_a v_{i,b} + p_b v_{i,a})n_i = &\int_{\mathbb{D}} d^3\mathbf{x}\,(v_{i,b}f_{i,a} + p_a q_b + v_{i,a}f_{i,b} + p_b q_a) \\ &+ \int_{\mathbb{D}} d^3\mathbf{x}\, j\omega[p_a\delta\kappa\, p_b + v_{i,a}\delta\rho\, v_{i,b}], \end{aligned} \tag{2.23}$$

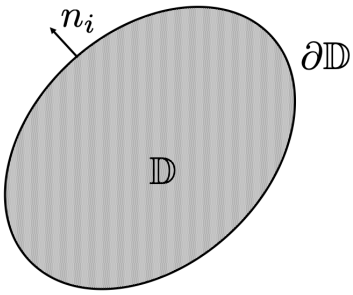

Figure 2.3 *Configuration of reciprocity theorem for non-directional wavefields, the famous "de Hoop's egg". After de Hoop [9, p.151], see also Fokkema and van den Berg [6, p. 16].*

where $\delta\rho = \rho_b - \rho_a$, $\delta\kappa = \kappa_b - \kappa_a$ and n_i is the normal to the surface $\partial\mathbb{D}$ that encloses the domain $\mathbb{D}$, shown in Figure 2.3, known as the "de Hoop egg".

The reciprocity theorem based on the Helmholtz equation [e.g. 5] is given as

$$\begin{aligned}\oint_{\partial\mathbb{D}} d^2\mathbf{x}\,[p_a\{l_b\partial_i p_b\} - p_b\{l_a\partial_i p_a\}]\,n_i = &\int_{\mathbb{D}} d^3\mathbf{x}\,[p_a s_b + p_b s_a] \\ &+ \int_{\mathbb{D}} d^3\mathbf{x}\,[\omega^2 p_a\delta\kappa\, p_b - \partial_i p_a\delta l\partial_i p_b]\,.\end{aligned} \tag{2.24}$$

We note that both reciprocity theorems, Equation 2.24 and Equation 2.23, invoke model perturbations to incompressibility and to density. In the next section the representation invoke mostly operator perturbations.

2.3.2. OPERATOR-BASED RECIPROCITY THEOREMS

We can also derive a reciprocity theorem based on the operator-based non-directional equations given by Equation 2.9. The details of the derivation are given in the Appendix A and briefly discussed by Dillen *et al.* [11]. The equation states that

$$\int_{\partial\mathbb{D}'} d^2\mathbf{x}_h\,\{\mathbf{q}_a^T\mathbf{N}\mathbf{q}_b\}n_3 = \int_{\mathbb{D}'} d^3\mathbf{x}\,\mathbf{q}_a^T\mathbf{N}\delta\mathbf{A}\mathbf{q}_b + \int_{\mathbb{D}'} d^3\mathbf{x}\,\left[\mathbf{q}_a^T\mathbf{N}\mathbf{q}_b + \mathbf{d}_a^T\mathbf{N}\mathbf{q}_b\right], \tag{2.25}$$

where $\mathbf{N} = \begin{pmatrix} 0 & 1 \\ -1 & 0 \end{pmatrix}$ and $\delta\mathbf{A} = \mathbf{A}_b - \mathbf{A}_a$. A more explicit form of Equation 2.25 is

$$\begin{aligned}\int_{\partial\mathbb{D}'} d^2\mathbf{x}_h\,[p_a v_{3,b} - v_{3,a}p_b] = &\int_{\mathbb{D}'} d^3\mathbf{x}\,[v_b f_{3,a} + p_a s_b + v_{3,a} f_{3,b} + p_b s_a] \\ &+ \int_{\mathbb{D}'} d^3\mathbf{x}\,[j\omega v_{3,b}\delta\rho\, v_{3,a} + \frac{1}{j\omega} p_a\delta\tilde{H}_2\, p_b],\end{aligned} \tag{2.26}$$

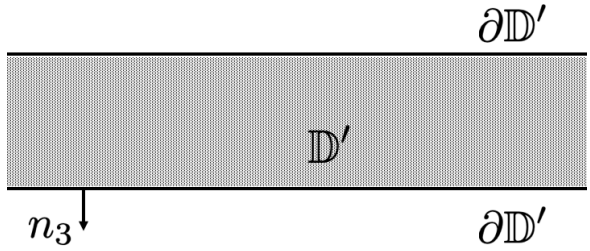

Figure 2.4 *Configuration of the reciprocity theorems involving directional wavefields or vertical particle velocity and pressure. After Wapenaar [10]. Note that while the reciprocity theorem of non-directional wave fields requires a bounded integral, this theorem allows the medium to be laterally unbounded while only vertically bounded.*

where $\delta\tilde{H}_2 = \frac{1}{\rho_b}H_{2,b} - \frac{1}{\rho_a}H_{2,a}$. The domain of integration is shown in Figure 2.4, which does not require the domain to be bounded laterally, unlike the representation for non-directional wavefield, Equation 2.23, which requires the domain to be fully bounded and thus a closed-surface integral is used.

Similarly, one could also apply Gauss' theorem to Equation 2.25, in order to obtain an operator-based directional reciprocity theorem — previously derived by Wapenaar and Grimbergen [7] — which states that

$$\int_{\partial\mathbb{D}'} d^2\mathbf{x}_h \, \{\mathbf{p}_a^T\mathbf{N}\mathbf{p}_b\} n_3 = \int_{\mathbb{D}'} d^3\mathbf{x} \, \mathbf{p}_a^T\mathbf{N}\delta\mathbf{B}\mathbf{p}_b + \int_{\mathbb{D}'} d^3\mathbf{x} \, \left[\mathbf{p}_a^T\mathbf{N}\mathbf{s}_b + \mathbf{s}_a^T\mathbf{N}\mathbf{p}_b\right], \tag{2.27}$$

where $\delta\mathbf{B} = \mathbf{B}_b - \mathbf{B}_a$. Based on these reciprocity theorems full domain-boundary representations can be obtained in the next section.

2.4. DOMAIN-BOUNDARY REPRESENTATIONS

2.4.1. MODEL-BASED REPRESENTATIONS

We can obtain a domain boundary representation involving pressure such that [e.g 6]

$$\begin{aligned}\chi(\mathbf{x}_d)\, p(\mathbf{x}_d) = &\int_{\mathbb{D}} d^3\mathbf{x}\, [G^q(\mathbf{x}_d,\mathbf{x})\, q(\mathbf{x}) - Q_i^q(\mathbf{x}_d,\mathbf{x})\, f_i(\mathbf{x})] \\ &- j\omega \int_{\mathbb{D}} d^3\mathbf{x}\, [G^q(\mathbf{x}_d,\mathbf{x})\delta\kappa(\mathbf{x})\, p(\mathbf{x}) - Q_i^q(\mathbf{x}_d,\mathbf{x})\delta\rho(\mathbf{x})\, v_i(\mathbf{x})], \\ &- \oint_{\partial\mathbb{D}} d^2\mathbf{x}\, [G^q(\mathbf{x}_d,\mathbf{x})\, v_i(\mathbf{x}) - Q_i^q(\mathbf{x}_d,\mathbf{x})\, p(\mathbf{x})]\, n_i\end{aligned} \tag{2.28}$$

where the characteristic function $\chi(\mathbf{x}_d)$ [see 5, 6] is defined as

$$\chi(\mathbf{x}_d) \begin{cases} 1 & \text{for } \mathbf{x}_d \in \mathbb{D} \\ 1/2 & \text{for } \mathbf{x}_d \in \partial\mathbb{D} \\ 0 & \text{for } \mathbf{x}_d \notin \mathbb{D} \cup \partial\mathbb{D} \end{cases}, \tag{2.29}$$

In addition, the reciprocity theorem involving particle velocity states that

$$\begin{aligned}\chi(\mathbf{x}_d)\, v_j(\mathbf{x}_d) = &-\int_{\mathbb{D}} d^3\mathbf{x}\, [G_j^f(\mathbf{x}_d,\mathbf{x})\, q(\mathbf{x}) - Q_{i,j}^f(\mathbf{x}_d,\mathbf{x})\, f_i(\mathbf{x})] \\ &+ j\omega \int_{\mathbb{D}} d^3\mathbf{x}\, [G_j^f(\mathbf{x}_d,\mathbf{x})\delta\kappa(\mathbf{x})\, p(\mathbf{x}) - Q_{i,j}^f(\mathbf{x}_d,\mathbf{x})\delta\rho(\mathbf{x})\, v_i(\mathbf{x})] \\ &- \oint_{\partial\mathbb{D}} d^2\mathbf{x}\, [G_j^f(\mathbf{x}_d,\mathbf{x})\, v_i(\mathbf{x}) - Q_{i,j}^f(\mathbf{x}_d,\mathbf{x})\, p(\mathbf{x})]\, n_i,\end{aligned} \tag{2.30}$$

and the Green functions G^q and $Q_i^q$is due to a point volume injection source and G_j^f and $Q_{i,j}^f$ are due to a point force source in x_j direction — see [6, p. 92] and [9] for details. Appendix A defines those Green's functions.

The reciprocity theorem involving the Helmholtz equation [5] is then

$$\begin{aligned}\chi(\mathbf{x}_d)\, p(\mathbf{x}_d) = &\int_{\mathbb{D}} d^3\mathbf{x}\, G_H(\mathbf{x}_d,\mathbf{x})\, s(\mathbf{x}) \\ &+ \int_{\mathbb{D}} d^3\mathbf{x}\, \left[\omega^2 G_H(\mathbf{x}_d,\mathbf{x})\delta\kappa(\mathbf{x})\, p(\mathbf{x}) - \partial_k G_H(\mathbf{x}_d,\mathbf{x})\delta l(\mathbf{x})\partial_k p(\mathbf{x})\right] \\ &+ \oint_{\partial\mathbb{D}} d^2\mathbf{x}\, \left[G_H(\mathbf{x}_d,\mathbf{x})\left\{l(\mathbf{x})\partial_k p(\mathbf{x})\right\} - p(\mathbf{x})\left\{l(\mathbf{x})\partial_k G_H(\mathbf{x}_d,\mathbf{x})\right\}\right] n_i.\end{aligned} \tag{2.31}$$

Note that Equations 2.31. and 2.28 are essentially equivalent, but the only difference is how the Green functions are defined. While one equation uses the Helmholtz Green function, G_H, the other uses explicit Green functions that correspond to a point volume injection source or a point force source in a single direction see [9, p. 158], [6, p. 124] and Appendix A for details).

2.4.2. OPERATOR-BASED REPRESENTATIONS: NON-DIRECTIONAL

The reciprocity theorem involving non-directional wavefields and is based on operators (derived in the Appendix A) states that

$$\begin{aligned}\chi(\mathbf{x}_d)\mathbf{q}(\mathbf{x}_d) = &\int_{\mathbb{D}'} d^3\mathbf{x}\, \mathbf{G}_A(\mathbf{x}_d,\mathbf{x})\mathbf{d}(\mathbf{x}) + \int_{\mathbb{D}'} d^3\mathbf{x}\, \mathbf{G}_A(\mathbf{x}_d,\mathbf{x})\delta\mathbf{A}(\mathbf{x})\mathbf{q}(\mathbf{x}) \\ &- \int_{\partial\mathbb{D}'} d^2\mathbf{x}_h\, \mathbf{G}_A(\mathbf{x}_d,\mathbf{x})\mathbf{q}(\mathbf{x})\, n_3(\mathbf{x}),\end{aligned} \tag{2.32}$$

where $\mathbf{G}_A$ is a Green function defined in Appendix A.

We can also write Equation 2.31, the one that leads to the Lippmann-Schwinger equation, in an operator form such that

$$\begin{aligned}\chi(\mathbf{x}_d)\, p(\mathbf{x}_d) = &\int_{\mathbb{D}} d^3\mathbf{x}\, G_H(\mathbf{x}_d,\mathbf{x})\, s(\mathbf{x}) \\ &+ \int_{\mathbb{D}} d^3\mathbf{x}\, G_H(\mathbf{x}_d,\mathbf{x}) \underbrace{\left[\omega^2\delta\kappa(\mathbf{x}) + \partial_k\left(\delta l \partial_k \cdot\right)\right]}_{\delta\mathcal{L}} p(\mathbf{x}) \\ &+ \oint_{\partial\mathbb{D}} d^2\mathbf{x}\left[G_H(\mathbf{x}_d,\mathbf{x})\left\{l_0(\mathbf{x})\partial_k p(\mathbf{x})\right\} - p(\mathbf{x})\left\{l(\mathbf{x})\partial_k G_H(\mathbf{x}_d,\mathbf{x})\right\}\right] n_i.\end{aligned} \tag{2.33}$$

Note that Equation 2.33 involves a contrast in Helmholtz operator, $\delta\mathcal{L}$, which in turn involves contrasts to model parameters. Going from an equation that involves model perturbation, Equation 2.1 or 2.2, to an operator-based one, Equation 2.33, is not trivial, especially in the context of the reciprocity theorem. So, we derive one from the other in Appendix A, using — surprisingly enough — Gauss' divergence theorem, and show how they are linked.

2.4.3. OPERATOR-BASED REPRESENTATIONS: DIRECTIONAL

Similarly, we can also obtain an operator-based directional representation such that [7]

$$\begin{aligned}\chi(\mathbf{x}_d)\mathbf{p}(\mathbf{x}_d) = &\int_{\mathbb{D}'} d^3\mathbf{x}\, \mathbf{G}_B(\mathbf{x}_d,\mathbf{x})\mathbf{s}(\mathbf{x}) + \int_{\mathbb{D}'} d^3\mathbf{x}\, \mathbf{G}_B(\mathbf{x}_d,\mathbf{x})\delta\mathbf{B}(\mathbf{x})\mathbf{p}(\mathbf{x}) \\ &- \int_{\partial\mathbb{D}'} d^2\mathbf{x}_h\, \mathbf{G}_B(\mathbf{x}_d,\mathbf{x})\mathbf{p}(\mathbf{x})\, n_3(\mathbf{x}),\end{aligned} \tag{2.34}$$

where $\mathbf{G}_B$ is a Green function defined in Appendix A.

However, Equation 2.34 is not the only form with which we can cast an operator-based directional representation. We can also cast Equation 2.33 — the one that leads to the operator-based Lippmann-Schwinger equation — in a directional form, resulting in

$$\begin{aligned}\chi(\mathbf{x}_d)\, p^{\pm}(\mathbf{x}_d) = &\int_{\mathbb{D}} d^3\mathbf{x}\, G_H^{\pm}(\mathbf{x}_d,\mathbf{x})\, s^{\pm}(\mathbf{x}) \\ &+ \int_{\mathbb{D}} d^3\mathbf{x}\, G_H^{\pm}(\mathbf{x}_d,\mathbf{x}) \underbrace{\left[\omega^2\delta\kappa(\mathbf{x}) + \partial_k\left(\delta l \partial_k \cdot\right)\right]}_{\delta\mathcal{L}} p(\mathbf{x}) \\ &+ \oint_{\partial\mathbb{D}} d^2\mathbf{x}\left[G_H^{\pm}(\mathbf{x}_d,\mathbf{x})\left\{l_0(\mathbf{x})\partial_k p(\mathbf{x})\right\} - p(\mathbf{x})\left\{l(\mathbf{x})\partial_k G_H^{\pm}(\mathbf{x}_d,\mathbf{x})\right\}\right] n_i,\end{aligned} \tag{2.35}$$

where $p = p^+ + p^-$ and $G_H = G_H^+ + G_H^-$; so they are pressure normalized. Note that the directional decomposition is at the detector location, $\mathbf{x}_d$.

2.5. DOMAIN REPRESENTATIONS

The following section contains domain representations, which disregard the boundary integral by assuming that the domain is unbounded, but only consider an integral involving a contrast or a perturbation over some domain $\mathbb{D}_p$, and one involving integration over sources over some domain $\mathbb{D}_s$ — see Figure 2.5 for the full configuration. Those representations are useful for modeling, imaging and inversion, but we start first with the model-based ones before we cover the ones based on operators.

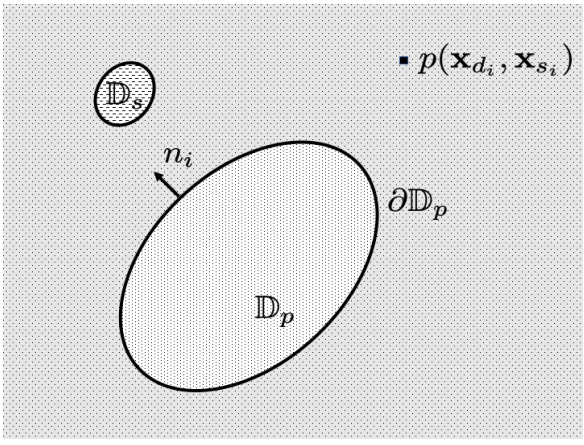

Figure 2.5 *Configuration of the scattering problem, which involves a perturbation domain, $\mathbb{D}_p$, and a source domain, $\mathbb{D}_s$. The pressure wavefield, $p(\mathbf{x}_{d_i},\mathbf{x}_{s_i})$, is indicated at an arbitrary point. Modified from de Hoop [9, p.194]*

2.5.1. MODEL-BASED REPRESENTATIONS: NON-DIRECTIONAL

One can represent the pressure wave-field using the Green functions defined using the Helmholtz equations as

$$p(\mathbf{x}_d) = \int\limits_{\mathbb{D}_s} d^3\mathbf{x}\, G_H(\mathbf{x}_d,\mathbf{x})\, s(\mathbf{x}) + \int\limits_{\mathbb{D}_p} d^3\mathbf{x}\left[\omega^2 G_H(\mathbf{x}_d,\mathbf{x})\delta\kappa(\mathbf{x})\, p(\mathbf{x}) - \partial_k G_H(\mathbf{x}_d,\mathbf{x})\delta l(\mathbf{x})\partial_k p(\mathbf{x})\right]. \tag{2.36}$$

We can also represent the pressure wavefield as

$$p(\mathbf{x}_d) = \int\limits_{\mathbb{D}_s} d^3\mathbf{x}\, [G^q(\mathbf{x}_d,\mathbf{x})\, q(\mathbf{x}) - Q_i^q(\mathbf{x}_d,\mathbf{x})\, f_i(\mathbf{x})] - j\omega \int\limits_{\mathbb{D}_p} d^3\mathbf{x}\, [G^q(\mathbf{x}_d,\mathbf{x})\delta\kappa(\mathbf{x})\, p(\mathbf{x}) - Q_i^q(\mathbf{x}_d,\mathbf{x})\delta\rho(\mathbf{x})\, v_i(\mathbf{x})]. \tag{2.37}$$

Note that while those two equations represent pressure — 2.37 and 2.36 — they are different because one invokes only pressure, Equation 2.37, and the other invokes additionally particle velocity and hence the Green functions are different.

We can also represent particle velocity as

$$v_j(\mathbf{x}_d) = -\int\limits_{\mathbb{D}_s} d^3\mathbf{x}\, [G_j^f(\mathbf{x}_d,\mathbf{x})\, q(\mathbf{x}) - Q_{i,j}^f(\mathbf{x}_d,\mathbf{x})\, f_i(\mathbf{x})] + j\omega \int\limits_{\mathbb{D}_p} d^3\mathbf{x}\, [G_j^f(\mathbf{x}_d,\mathbf{x})\delta\kappa(\mathbf{x})\, p(\mathbf{x}) - Q_{i,j}^f(\mathbf{x}_d,\mathbf{x})\delta\rho(\mathbf{x})\, v_i(\mathbf{x})]. \tag{2.38}$$

2.5.2. MODEL-BASED REPRESENTATIONS: DIRECTIONAL

Splitting the wavefield into $p = p^+ + p^-$ and the Green function into $G_H = G_H^+ + G_H^-$ and substituting those results in Equation 2.36 yields

$$p^\pm(\mathbf{x}_d) = \int\limits_{\mathbb{D}_s} d^3\mathbf{x}\, G_H^\pm(\mathbf{x}_d,\mathbf{x})\, s^\pm(\mathbf{x}) + \int\limits_{\mathbb{D}_p} d^3\mathbf{x}\, \omega^2 G_H^\pm(\mathbf{x}_d,\mathbf{x})\delta\kappa(\mathbf{x})\{p^+(\mathbf{x}) + p^-(\mathbf{x})\} + \int\limits_{\mathbb{D}_p} d^3\mathbf{x}\, \partial_k G_H^\pm(\mathbf{x}_d,\mathbf{x})\delta l(\mathbf{x})\partial_k\{p^+(\mathbf{x}) + p^-(\mathbf{x})\}. \tag{2.39}$$

We can also derive the correlation-type form leading to

$$p^\pm(\mathbf{x}_d) = \int\limits_{\mathbb{D}_s} d^3\mathbf{x}\, \{G_H^\pm\}^*(\mathbf{x}_d,\mathbf{x})\, s^\pm(\mathbf{x}) + \int\limits_{\mathbb{D}_p} d^3\mathbf{x}\, \omega^2 \{G_H^\pm\}^*(\mathbf{x}_d,\mathbf{x})\delta\kappa(\mathbf{x})\{p^+(\mathbf{x}) + p^-(\mathbf{x})\} + \int\limits_{\mathbb{D}_p} d^3\mathbf{x}\, \partial_k \{G_H^\pm\}^*(\mathbf{x}_d,\mathbf{x})\delta l(\mathbf{x})\partial_k\{p^+(\mathbf{x}) + p^-(\mathbf{x})\}. \tag{2.40}$$

In media with constant density, Equation 2.39 becomes

$$p^{\pm}(\mathbf{x}_d) = \int_{\mathbb{D}_s} d^3\mathbf{x}\, G_H^{\pm}(\mathbf{x}_d,\mathbf{x}) s^{\pm}(\mathbf{x}) + \int_{\mathbb{D}_p} d^3\mathbf{x}\, \omega^2 G_H^{\pm}(\mathbf{x}_d,\mathbf{x}) \delta m(\mathbf{x}) \{p^+(\mathbf{x}) + p^-(\mathbf{x})\}. \tag{2.41}$$

Equation 2.39 is the directional form of the non-directional model-based representation.

2.5.3. OPERATOR-BASED REPRESENTATIONS: NON-DIRECTIONAL

In this section, we list operator-based representations, which are derived from the boundary-domain representations by assuming an unbounded volume. As discussed previously, those representations are of two forms: one is for non-directional wave-fields and other for directional wave-fields. By assuming an unbounded domain, Equation 2.32 then becomes

$$\mathbf{q}(\mathbf{x}_d) = \int_{\mathbb{D}_s} d^3\mathbf{x}\, \mathbf{G}_A(\mathbf{x}_d,\mathbf{x}) \mathbf{d}(\mathbf{x}) + \int_{\mathbb{D}_p} d^3\mathbf{x}\, \mathbf{G}_A(\mathbf{x}_d,\mathbf{x}) \delta\mathbf{A}(\mathbf{x}) \mathbf{q}(\mathbf{x}). \tag{2.42}$$

Even though Equation 2.2 contains a density perturbation, the main perturbation is that of the Helmholtz operator; which contains all the isotropic or for that matter the anisotropic behavior, as well. Therefore, we refer to it as operator-based, since it contains mainly an operator perturbation.

Similarly, we can obtain an operator-based Lippmann-Schwinger equation from Equation 2.35, resulting in

$$p(\mathbf{x}_d) = \int_{\mathbb{D}_s} d^3\mathbf{x}\, G_H(\mathbf{x}_d,\mathbf{x}) s(\mathbf{x}) + \int_{\mathbb{D}_p} d^3\mathbf{x}\, G_H(\mathbf{x}_d,\mathbf{x}) \underbrace{\left[\omega^2 \delta\kappa(\mathbf{x}) + \partial_k\left(\delta l \partial_k \cdot\right)\right]}_{\delta\mathcal{L}} p(\mathbf{x}). \tag{2.43}$$

2.5.4. OPERATOR-BASED REPRESENTATIONS: DIRECTIONAL

An operator-based domain representation that invokes directional wavefields can also be obtained from Equation 2.34, resulting in

$$\mathbf{p}(\mathbf{x}_d) = \int_{\mathbb{D}_s} d^3\mathbf{x}\, \mathbf{G}_f^0(\mathbf{x}_d,\mathbf{x}) \mathbf{s}(\mathbf{x}) + \int_{\mathbb{D}_p} d^3\mathbf{x}\, \mathbf{G}_f^0(\mathbf{x}_d,\mathbf{x}) \delta\mathbf{B}(\mathbf{x}) \mathbf{p}(\mathbf{x}), \tag{2.44}$$

where the superscript, 0, in the Green function, $\mathbf{G}_f^0$, refers to the fact that the Greens function is modeled in the background/reference model.

Another form of this kind of representation can be obtained from Equation 2.35 resulting in

$$p^{\pm}(\mathbf{x}_d) = \int_{\mathbb{D}_s} d^3\mathbf{x}\, G_H^{\pm}(\mathbf{x}_d,\mathbf{x}) s^{\pm}(\mathbf{x}) + \int_{\mathbb{D}_p} d^3\mathbf{x}\, G_H^{\pm}(\mathbf{x}_d,\mathbf{x}) \delta\mathcal{L}(\mathbf{x}) \{p^+(\mathbf{x}) + p^-(\mathbf{x})\}, \tag{2.45}$$

which we refer to as Lippmann-Schwinger equation for directional wavefields.

We summarize some of the results we obtained so far in Table 2.2.

Table 2.2 *A table summarizing some of the domain-based representations.*

	Model-based	Operator-based
Directional	$p^{\pm}(\mathbf{x}_d) = \int_{\mathbb{D}_s} d^3\mathbf{x}\, G_H^{\pm}(\mathbf{x}_d,\mathbf{x})\, s^{\pm}(\mathbf{x}) + \int_{\mathbb{D}_p} d^3\mathbf{x}\, \omega^2 G_H^{\pm}(\mathbf{x}_d,\mathbf{x})\delta\kappa(\mathbf{x})\{p^+(\mathbf{x}) + p^-(\mathbf{x})\} + \int_{\mathbb{D}_p} d^3\mathbf{x}\, \partial_k G_H^{\pm}(\mathbf{x}_d,\mathbf{x})\delta l(\mathbf{x})\partial_k\{p^+(\mathbf{x}) + p^-(\mathbf{x})\}$	$\mathbf{p}(\mathbf{x}_d) = \int_{\mathbb{D}_s} d^3\mathbf{x}\, \mathbf{G}_F(\mathbf{x}_d,\mathbf{x})\mathbf{s}(\mathbf{x}) + \int_{\mathbb{D}_p} d^3\mathbf{x}\, \mathbf{G}_F(\mathbf{x}_d,\mathbf{x})\delta\mathbf{B}(\mathbf{x})\mathbf{p}(\mathbf{x})$ $p^{\pm}(\mathbf{x}_d) = \int_{\mathbb{D}_s} d^3\mathbf{x}\, G_H^{\pm}(\mathbf{x}_d,\mathbf{x})\, s^{\pm}(\mathbf{x}) + \int_{\mathbb{D}_p} d^3\mathbf{x}\, G_H^{\pm}(\mathbf{x}_d,\mathbf{x})\delta\mathcal{L}(\mathbf{x})\{p^+(\mathbf{x}) + p^-(\mathbf{x})\}$
Non-directional	$p(\mathbf{x}_d) = \int_{\mathbb{D}_s} d^3\mathbf{x}\, G_H(\mathbf{x}_d,\mathbf{x})\, s(\mathbf{x}) + \int_{\mathbb{D}_p} d^3\mathbf{x}\, \omega^2 G_H(\mathbf{x}_d,\mathbf{x})\delta\kappa(\mathbf{x})\, p(\mathbf{x}) - \int_{\mathbb{D}_p} d^3\mathbf{x}\, \partial_k G_H(\mathbf{x}_d,\mathbf{x})\delta l(\mathbf{x})\partial_k p(\mathbf{x})$	$\mathbf{q}(\mathbf{x}_d) = \int_{\mathbb{D}_s} d^3\mathbf{x}\, \mathbf{G}_A(\mathbf{x}_d,\mathbf{x})\mathbf{d}(\mathbf{x}) + \int_{\mathbb{D}_p} d^3\mathbf{x}\, \mathbf{G}_A(\mathbf{x}_d,\mathbf{x})\delta\mathbf{A}(\mathbf{x})\mathbf{q}(\mathbf{x})$ $p(\mathbf{x}_d) = \int_{\mathbb{D}_s} d^3\mathbf{x}\, G_H(\mathbf{x}_d,\mathbf{x})\, s(\mathbf{x}) + \int_{\mathbb{D}_p} d^3\mathbf{x}\, G_H(\mathbf{x}_d,\mathbf{x})\delta\mathcal{L}p(\mathbf{x})$

2.6. VARIOUS FORMS OF OPERATOR-BASED DIRECTIONAL REPRESENTATION

In this section we consider different forms of the directional operator-based representations. All Green's functions of the next presentations are thoroughly discussed and compared in Appendix A, while the states (state A and state B) in each situation are defined in Tables 2.3-2.5. As we will see, we have more flexibility in choosing the background or reference state for this kind of representation. This results in several representations that physically represent different ordering or distribution of the wavefields between the two states.

2.6.1. REPRESENTATION OF TYPE I

For clarity, we start by recasting Equation 2.44 with $\delta\mathbf{B}(\mathbf{x})$ written explicitly such that

$$\mathbf{p}(\mathbf{x}_d) = \int_{\mathbb{D}_s} d^3\mathbf{x}\, \mathbf{G}_f^0(\mathbf{x}_d,\mathbf{x})\mathbf{s}(\mathbf{x}) + \int_{\mathbb{D}_p} d^3\mathbf{x}\, \mathbf{G}_f^0(\mathbf{x}_d,\mathbf{x})\{-j\omega\delta\mathbf{\Lambda}(\mathbf{x}) + \delta\mathbf{T}(\mathbf{x}) + \delta\mathbf{R}(\mathbf{x})\}\mathbf{p}(\mathbf{x}), \quad (2.46)$$

where $\delta\mathbf{R} = \begin{pmatrix} 0 & \delta R^- \\ \delta R^+ & 0 \end{pmatrix}$, $\delta\mathbf{T} = \begin{pmatrix} \delta T^+ & 0 \\ 0 & \delta T^- \end{pmatrix}$ and $\delta\mathbf{\Lambda} = \begin{pmatrix} \delta\Lambda^+ & 0 \\ 0 & \delta\Lambda^- \end{pmatrix}$. Note here that the reference or background state, A, is entirely different from the actual state, B. So, not only reflection but also the transmission and the vertical wavenumber operators are different. Note also that the Green function $\mathbf{G}_f^0$ is the full Green function that encompasses both reflection and transmission of the background medium. It has the following form [10]

$$\mathbf{G}_f^0(\mathbf{x}_d,\mathbf{x}) = \begin{pmatrix} G_f^{0\,+,+}(\mathbf{x}_d,\mathbf{x}) & G_f^{0\,+,-}(\mathbf{x}_d,\mathbf{x}) \\ G_f^{0\,-,+}(\mathbf{x}_d,\mathbf{x}) & G_f^{0\,-,-}(\mathbf{x}_d,\mathbf{x}) \end{pmatrix}, \quad (2.47)$$

where the superscripts $(\pm,\pm)$ refer to the propagation direction at the detector, at location $\mathbf{x}_d$, and at the source, at location $\mathbf{x}$, respectively. We refer to Equation 2.46 as directional operator-based representation of Type-I. This representation can be used for inversion since the two states are entirely different. However, we derive a simpler version with simpler Green's functions in the next representation.

Table 2.3 *States A and B for deriving the directional representation theorem of type-I.*

	State A	State B
Wavefield	$\mathbf{G}_f^0(\mathbf{x},\mathbf{x}')$	$\mathbf{p}(\mathbf{x})$
Source	$\mathbf{I}\delta(\mathbf{x}-\mathbf{x}')$	$\mathbf{s}(\mathbf{x})$
Operators Type-I	$-j\omega\mathbf{\Lambda}_A + \mathbf{\Theta}_A$	$-j\omega\mathbf{\Lambda}_B + \mathbf{\Theta}_B$

2.6.2. REPRESENTATION OF TYPE II

Another choice that one could make is by assuming that the reflection operator of the background state (state A) vanishes (i.e. $\mathbf{R}_A = 0$) in order to derive another version (Type-

II), which states that

$$\mathbf{p}(\mathbf{x}_d) = \int_{\mathbb{D}_s} d^3\mathbf{x}\, \mathbf{G}_t^0(\mathbf{x}_d,\mathbf{x})\mathbf{s}(\mathbf{x}) + \int_{\mathbb{D}_p} d^3\mathbf{x}\, \mathbf{G}_t^0(\mathbf{x}_d,\mathbf{x})\{-j\omega\delta\mathbf{\Lambda}(\mathbf{x}) + \delta\mathbf{T}(\mathbf{x}) + \mathbf{R}(\mathbf{x})\}\mathbf{p}(\mathbf{x}). \tag{2.48}$$

The Green function for this representation is

$$\mathbf{G}_t(\mathbf{x},\mathbf{x}_s) = \begin{pmatrix} H(x_3 - x_{s,3})V^+(\mathbf{x},\mathbf{x}_s) & 0 \\ 0 & -H(x_{s,3} - x_3)V^-(\mathbf{x},\mathbf{x}_s) \end{pmatrix}, \tag{2.49}$$

where H is the Heaviside function and V is the propagator that includes transmission, unlike the W operator which we will encounter next.

Note that the Green function $\mathbf{G}_t^0$ includes transmission of the background medium but does not include reflection of the background medium and therefore Equation 2.48 has the term $\mathbf{R}(x)$, while Equation 2.46 uses $\delta\mathbf{R}(\mathbf{x})$. Table 2.4 lists the sources, wavefields and set of operators in state A and B.

Table 2.4 *States A and B for deriving the directional representation theorems of type-II and type-VII.*

	State A	State B
Wavefield Type-II	$\mathbf{G}_t^0(\mathbf{x},\mathbf{x}')$	$\mathbf{p}(\mathbf{x})$
Wavefield Type-VII	$\mathbf{G}_t(\mathbf{x},\mathbf{x}')$	$\mathbf{p}(\mathbf{x})$
Source	$\mathbf{I}\delta(\mathbf{x}-\mathbf{x}')$	$\mathbf{s}(\mathbf{x})$
Operators Type-II	$-j\omega\mathbf{\Lambda}_A + \mathbf{T}_A$	$-j\omega\mathbf{\Lambda}_B + \mathbf{\Theta}_B$
Operators Type-VII	$-j\omega\mathbf{\Lambda} + \mathbf{T}$	$-j\omega\mathbf{\Lambda} + \mathbf{\Theta}$

2.6.3. REPRESENTATION OF TYPE III

We can also assume that the transmission operator of the background state (state A) vanishes (i.e. $\mathbf{T}_A = 0$), in order to derive another form, Type-III (see Table 2.5), which results in

$$\mathbf{p}(\mathbf{x}_d) = \int_{\mathbb{D}_s} d^3\mathbf{x}\, \mathbf{G}_r^0(\mathbf{x}_d,\mathbf{x})\mathbf{s}(\mathbf{x}) + \int_{\mathbb{D}_p} d^3\mathbf{x}\, \mathbf{G}_r^0(\mathbf{x}_d,\mathbf{x})\{-j\omega\delta\mathbf{\Lambda}(\mathbf{x}) + \delta\mathbf{R}(\mathbf{x}) + \mathbf{T}(\mathbf{x})\}\mathbf{p}(\mathbf{x}). \tag{2.50}$$

Here the Green function does not include transmission but it contains the reflection of the background state, State A. It does contain, however, primary and multiple interactions of wavefields. The Green function in this situation is

$$\mathbf{G}_r(x,x_s) = \begin{pmatrix} G_r^{+,+}(x,x_s) & G_r^{+,-}(x,x_s) \\ G_r^{-,+}(x,x_s) & G_r^{-,-}(x,x_s) \end{pmatrix}, \tag{2.51}$$

where it contains four constituents; rather than two constituents since they contain the reflection operator of background medium.

Table 2.5 *States A and B for deriving the directional representation theorems of type-III and type-VI.*

	State A	State B
Wavefield Type-III	$\mathbf{G}^0_r(\mathbf{x},\mathbf{x}')$	$\mathbf{p}(\mathbf{x})$
Wavefield Type-VI	$\mathbf{G}_r(\mathbf{x},\mathbf{x}')$	$\mathbf{p}(\mathbf{x})$
Source	$\mathbf{I}\delta(\mathbf{x}-\mathbf{x}')$	$\mathbf{s}(\mathbf{x})$
Operators Type-III	$-j\omega\boldsymbol{\Lambda}_A+\mathbf{R}_A$	$-j\omega\boldsymbol{\Lambda}_B+\boldsymbol{\Theta}_B$
Operators Type-VI	$-j\omega\boldsymbol{\Lambda}+\mathbf{R}$	$-j\omega\boldsymbol{\Lambda}+\boldsymbol{\Theta}$

2.6.4. REPRESENTATION OF TYPE IV

In order to obtain another distinct representation, one could assume that $\mathbf{T}_A=0$ and $\mathbf{R}_A=0$ (see Table 3), while keeping the perturbation in the vertical slowness intact, to derive another version (Type-IV) that states

$$\mathbf{p}(\mathbf{x}_d)=\int_{\mathbb{D}_s} d^3\mathbf{x}\,\mathbf{G}^0_p(\mathbf{x}_d,\mathbf{x})\mathbf{s}(\mathbf{x})+\int_{\mathbb{D}_p} d^3\mathbf{x}\,\mathbf{G}^0_p(\mathbf{x}_d,\mathbf{x})\{-j\omega\delta\boldsymbol{\Lambda}(\mathbf{x})+\mathbf{R}(\mathbf{x})+\mathbf{T}(\mathbf{x})\}\mathbf{p}(\mathbf{x}), \tag{2.52}$$

which is the basis for Model-Independent Joint Migration Inversion (MI-JMI), derived by Hammad and Verschuur [12] and further discussed in Chapter 8. It can also be written as

$$\mathbf{p}(\mathbf{x}_d)=\int_{\mathbb{D}_s} d^3\mathbf{x}\,\mathbf{G}^0_p(\mathbf{x}_d,\mathbf{x})\mathbf{s}(\mathbf{x})+\int_{\mathbb{D}_p} d^3\mathbf{x}\,\mathbf{G}^0_p(\mathbf{x}_d,\mathbf{x})\boldsymbol{\Omega}(\mathbf{x})\mathbf{p}(\mathbf{x}), \tag{2.53}$$

where $\boldsymbol{\Omega}(\mathbf{x})=-j\omega\delta\boldsymbol{\Lambda}(\mathbf{x})+\mathbf{R}(\mathbf{x})+\mathbf{T}(\mathbf{x})$. In this situation, the Green function is

$$\mathbf{G}^0_p(\mathbf{x}_d,\mathbf{x})=\begin{pmatrix} H(x_{d,3}-x_3)W_0^+(\mathbf{x}_d,\mathbf{x}) & 0 \\ 0 & -H(x_3-x_{d,3})W_0^-(\mathbf{x}_d,\mathbf{x})\end{pmatrix}, \tag{2.54}$$

where W_0 is propagator [10], which does not include the transmission, but rather it belongs to a medium that is transparent of any reflection or transmission scattering and contains only direct arrivals [10].

Table 2.6 *States A and B for deriving the directional representation theorems of type-IV and type-V.*

	State A	State B
Wavefield Type-IV	$\mathbf{G}^0_p(\mathbf{x},\mathbf{x}')$	$\mathbf{p}(\mathbf{x})$
Wavefield Type-V	$\mathbf{G}_p(\mathbf{x},\mathbf{x}')$	$\mathbf{p}(\mathbf{x})$
Source	$\mathbf{I}\delta(\mathbf{x}-\mathbf{x}')$	$\mathbf{s}(\mathbf{x})$
Operators Type-IV	$-j\omega\boldsymbol{\Lambda}_A$	$-j\omega\boldsymbol{\Lambda}_B+\boldsymbol{\Theta}$
Operators Type-V	$-j\omega\boldsymbol{\Lambda}$	$-j\omega\boldsymbol{\Lambda}+\boldsymbol{\Theta}$

2.6.5. REPRESENTATION OF TYPE V

Another representation can by obtained by assuming that $\mathbf{T}_A = 0$ and $\mathbf{R}_B = 0$ (see Table 3), while keeping vertical slowness the same for both states. Then we then arrive at another version, (Type-V), which states

$$\mathbf{p}(\mathbf{x}_d) = \int_{\mathbb{D}_s} d^3\mathbf{x}\, \mathbf{G}_p(\mathbf{x}_d,\mathbf{x})\mathbf{s}(\mathbf{x}) + \int_{\mathbb{D}_p} d^3\mathbf{x}\, \mathbf{G}_p(\mathbf{x}_d,\mathbf{x})\{\mathbf{R}(\mathbf{x}) + \mathbf{T}(\mathbf{x})\}\mathbf{p}(\mathbf{x}), \tag{2.55}$$

which is derived by Wapenaar [10] and de Hoop [8] and which can also be written as

$$\mathbf{p}(\mathbf{x}_d) = \int_{\mathbb{D}_s} d^3\mathbf{x}\, \mathbf{G}_p(\mathbf{x}_d,\mathbf{x})\mathbf{s}(\mathbf{x}) + \int_{\mathbb{D}_p} d^3\mathbf{x}\, \mathbf{G}_p(\mathbf{x}_d,\mathbf{x})\boldsymbol{\Theta}(\mathbf{x})\mathbf{p}(\mathbf{x}). \tag{2.56}$$

A similar form is presented by Berkhout [13], being referred to as full wavefield modeling (FWMod) and its inverse, which is full wavefield migration (FWM) [14]. Note that with such modeling scheme, iterations are needed even for the primary wavefield as transmission effects are not included in the Green function. We will discuss the implementation of this equation in the next chapters.

2.6.6. REPRESENTATION OF TYPE VI

We can also let the propagator include transmission (see Table 4) to arrive at

$$\mathbf{p}(\mathbf{x}_d) = \int_{\mathbb{D}_s} d^3\mathbf{x}\, \mathbf{G}_t(\mathbf{x}_d,\mathbf{x})\mathbf{s}(\mathbf{x}) + \int_{\mathbb{D}_p} d^3\mathbf{x}\, \mathbf{G}_t(\mathbf{x}_d,\mathbf{x})\mathbf{R}(\mathbf{x})\mathbf{p}(\mathbf{x}), \tag{2.57}$$

which was derived by Hammad and Verschuur [15], but was also previously derived by Corones [16] yet using a different derivation scheme. This form is the basis for the generalization of the so-called Bremmer series [17] since the propagator includes transmission. Using the so-called Neumann series, one can model wavefields scattering order by scattering order, and therefore the iterative process is not purely mathematical but rather physical. Hence, it provides insight into the scattering process in terms of the multiple orders of primaries. Another method to achieve such objective, but only for surface multiples, is the so-called scattering order decomposition [18]. However, it is based on a boundary integral and assumes the full wavefield is readily available.

2.6.7. REPRESENTATION OF TYPE VII

A distinct final representation can also be obtained by including the reflection operator in the propagator, while the transmission operator is not included, (see Table 2.5) to arrive at

$$\mathbf{p}(\mathbf{x}_d) = \int_{\mathbb{D}_s} d^3\mathbf{x}\, \mathbf{G}_r(\mathbf{x}_d,\mathbf{x})\mathbf{s}(\mathbf{x}) + \int_{\mathbb{D}_p} d^3\mathbf{x}\, \mathbf{G}_r(\mathbf{x}_d,\mathbf{x})\mathbf{T}(\mathbf{x})\mathbf{p}(\mathbf{x}), \tag{2.58}$$

which could be used to model the transmission scattering rather than the reflection scattering as we was used in the previous representation 2.57. Such approach could be useful for tomographic experiments.

2.7. CONCLUSION

We have reviewed and derived various integral representations forms. We can classify them into four categories whether they are model-based or operator-based, directional or non-directional. The various forms are then readily available for different applications such as model-independent JMI, as well as operator-based non-directional inversion.

Alternative representations of the so-called Lippmann-Schwinger equation are discussed in this chapter. While the Lippmann-Schwinger equation invokes model-perturbations and non-directional wavefields, other representations invoke operator perturbations and/or directional wavefields. In fact four categories of representations are discussed in this chapter, which are summarized in Table 2.1. Although each category is represented by one or two equations, one category (operator-based directional representation) provides various forms of which seven are shown in this chapter. It is the most versatile representation. Those representations can be the basis for different modeling and inversion methods.

REFERENCES

[1] B. Jowett, *The Dialogues of Plato: Republic. Timaeus. Critias*, The Dialogues of Plato (Macmillan, 1892).

[2] D. Colton and R. Kress, *Integral equation methods in scattering theory*, Vol. 72 (SIAM, 2013).

[3] A. Tarantola, *Inversion of seismic reflection data in the acoustic approximation*, Geophysics **49**, 1259 (1984).

[4] P. M. Van Den Berg and R. E. Kleinman, *A contrast source inversion method*, Inverse problems **13**, 1607 (1997).

[5] C. P. A. Wapenaar and A. J. Berkhout, *Elastic Wave Field Extrapolation: Redatuming of Single- and Multi-component Seismic Data* (Elsevier Science Publishers B.V., Amsterdam, The Netherlands, 1989).

[6] J. Fokkema and P. van den Berg, *Seismic Applications of Acoustic Reciprocity* (Elsevier Science Publishers B.V., Amsterdam, The Netherlands, 1993).

[7] C. P. A. Wapenaar and J. L. T. Grimbergen, *Reciprocity theorems for one-way wavefields*, Geophysical Journal International **127**, 169 (1996).

[8] M. V. de Hoop, *Generalization of the bremmer coupling series*, Journal of Mathematical Physics **37**, 3246 (1996).

[9] A. T. de Hoop, *Handbook of radiation and scattering of waves: Acoustic waves in fluids, elastic waves in solids, electromagnetic waves* (Academic Press Limited, London, U.K., 1995).

[10] C. P. A. Wapenaar, *One-way representations of seismic data*, Geophysical Journal International **127**, 178 (1996).

[11] M. W. P. Dillen, J. T. Fokkema, and C. P. A. Wapenaar, *Recovering acoustic reflectivity using dirichlet-to-neumann maps and left-and right-operating adjoint propagators*, Geophysical Journal International **163**, 106 (2005).

[12] H. I. Hammad and D. J. Verschuur, *Nonlinear model-independent joint migration inversion*, in *SEG Technical Program Expanded Abstracts* (2017) pp. 5556–5560.

[13] A. J. Berkhout, *Review paper: An outlook on the future of seismic imaging, part I: forward and reverse modeling*, Geophysical Prospecting **62**, 911 (2014).

[14] A. J. Berkhout, *Review paper: An outlook on the future of seismic imaging, part II: Full-wavefield migration*, Geophysical Prospecting **62**, 931 (2014).

[15] H. I. Hammad and D. J. Verschuur, *Augmented full wavefield modeling: An iterative directional modeling scheme for inhomogeneous media*, in *79th EAGE Conference and Exhibition 2017* (2017).

[16] J. Corones, *Bremmer series that correct parabolic approximations,* Journal of Mathematical Analysis and Applications **50**, 361 (1975).

[17] H. Bremmer, *The W.K.B. approximation as the first term of a geometric-optical series,* Communications on Pure and Applied Mathematics **4**, 105 (1951).

[18] H. I. Hammad and D. J. Verschuur, *Scattering order decomposition-separating multiples by order of scattering,* in *79th EAGE Conference and Exhibition 2017* (2017).

3

MODELING AND ANALYSIS OF WAVENUMBER AND TRANSFER OPERATORS

"Nature does nothing without reason or in vain."

Aristotle [1, p. 480 (On the Heavens, 291b 13)]

Full wavefield modeling is a method that invokes the transfer operators in order to model wave propagation. However, generalized transfer operators, which are more general than those that are equivalent to Zoeppritz' equations in acoustic media, are needed in order to model waves in such media. We compute those generalized transfer coefficients and invoke them into the full wavefield modeling method, which models multiples along with primaries. We compute those coefficients using a formulation that allows discontinuous media to be modeled. A comparison between the conventional approach of using the acoustic equivalent of Zoeppritz' equations and our proposed method shows a pronounced difference. In one example, it is shown that neighboring sand channels have a clear impact on the reflection coefficient at a single sand channel. This work sets the stage to an elastic formulation that has the potential to replace the commonly used Zoeppritz' equations for laterally varying elastic media.

3.1. INTRODUCTION

In Chapter 2, we have presented several representations that invoke operators which, in turn, are generated using model parameters. In this chapter we pick a single representation and we start implementing and analyzing it, first through its operators. In Chapter 4, we go beyond generating those operators to generating the end product of such a modeling method, which is the full wavefield. As shown in Figure 3.1, we first map the model parameters into operators and in the next chapter we map those operators into wavefields. Although we address the acoustic situation in this chapter, we address the anisotropic situation in Chapter 6 and the elastodynamic situation in Chapter 7.

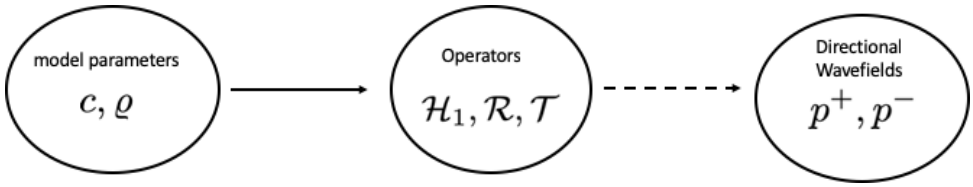

Figure 3.1 *A schematic showing the mapping discussed in this chapter, where model parameters are mapped to operators. The next chapter is concerned with mapping the operators to directional wavefields.*

3.2. GENERAL EQUATION FOR MODELING

Our aim is to implement an integral equation that takes operators as input and produces wavefields as output. Although we have discussed the underlying theory in Chapter 2, we state the equation to be implemented and discuss it in detail in this chapter. The equation states [e.g. 2, 3] that

$$\mathbf{p}(\mathbf{x}_d) = \int_{\mathbb{R}^3} d^3\mathbf{x}\, \mathbf{G}_p(\mathbf{x}_d,\mathbf{x})\mathbf{s}(\mathbf{x}) + \int_{\mathbb{R}^3} d^3\mathbf{x}\, \mathbf{G}_p(\mathbf{x}_d,\mathbf{x})\boldsymbol{\Theta}(\mathbf{x})\mathbf{p}(\mathbf{x}), \tag{3.1}$$

where the wavefield, $\boldsymbol{p}$, is composed of downgoing and upgoing components such that $\mathbf{p} = \begin{pmatrix} p^+ \\ p^- \end{pmatrix}$, the source $\mathbf{s} = \begin{pmatrix} s^+ \\ s^- \end{pmatrix}$, is, likewise, composed of downgoing, s^+, and upgoing, s^-, components and $\boldsymbol{\Theta} = -\begin{pmatrix} \mathcal{T}^+ & \mathcal{R}^- \\ \mathcal{R}^+ & \mathcal{T}^- \end{pmatrix}$ is the set of transfer operators, where $\mathcal{R}^\pm$ is the reflection operator and $\mathcal{T}^\pm$ is transmission operator from above and below. The Green's function is defined as

$$\mathbf{G}_p(\mathbf{x},\mathbf{x}') = \begin{pmatrix} H(x_3 - x_3')W^+(\mathbf{x},\mathbf{x}') & 0 \\ 0 & -H(x_3' - x_3)W^-(\mathbf{x},\mathbf{x}') \end{pmatrix}, \tag{3.2}$$

where, $H(x_3 - x_3')$ is the Heaviside function, and $W^+(\mathbf{x},\mathbf{x}')$ is the propagator, which is obtained using the generalized wavenumber operator, $\tilde{\mathcal{H}}_1$, such that

$$W^{\pm}(\mathbf{x},\mathbf{x}') = exp[\mp j(x_3 - x_3')\tilde{\mathcal{H}}_1(\mathbf{x})]. \tag{3.3}$$

In addition, the initial solution is obtained via the Green's functions such that

$$\mathbf{p}_0(\mathbf{x}') = \int_{\mathbb{R}^3} d^3\mathbf{x}\ \mathbf{G}_p(\mathbf{x}',\mathbf{x})\mathbf{s}(\mathbf{x}). \tag{3.4}$$

Now that we have stated the general representation, we can then dive deeper into those operators and how they are modeled.

3.3. HELMHOLTZ AND WAVENUMBER OPERATORS

In this section, we first begin by stating the main equations that allow for medium heterogeneity starting with the Helmholtz operator, from which the generalized vertical wavenumber operator can be derived. Subsequently, a generalized slowness operator can then be derived and used to investigate the kinematics. The dynamics can then be studied using a formulation that includes this generalised slowness operator. We follow the notation and equations given by Wapenaar and Grimbergen [4] throughout this section.

The Helmholtz operator in the constant density situation[e.g. 3, 4] is given by

$$\hat{\mathcal{H}}_2(\mathbf{x}) = \left(\frac{\omega}{c'(\mathbf{x})}\right)^2 + \partial_\alpha\partial_\alpha, \tag{3.5}$$

where ω is the angular frequency, $c'(\mathbf{x})$ is the velocity and α takes on the values of 1 and 2 for the lateral axes (i.e. x_1 and x_2), where the summation convention is implied. The Helmholtz kernel operator $\mathcal{H}_2(\mathbf{x}_h;\mathbf{x}_H')$ is defined as [4]

$$\hat{\mathcal{H}}_2(\mathbf{x}_H)F(\mathbf{x}_H) = \int_{IR^2} d^2\mathbf{x}_H'\ \mathcal{H}_2(\mathbf{x}_H;\mathbf{x}_H')F(\mathbf{x}_H'), \tag{3.6}$$

where F is any arbitrary function. Modal expansion of the Helmholtz kernel operator can be carried out such that [4]

$$\mathcal{H}_2(\mathbf{x}_H;\mathbf{x}_H') = \int_{IR^2} d^2\boldsymbol{\kappa}\ \phi(\mathbf{x}_H,\boldsymbol{\kappa})\lambda(\boldsymbol{\kappa})\phi^*(\mathbf{x}_H',\boldsymbol{\kappa}) + \sum_{\lambda_i\in\,\text{discr}} \phi^{(i)}(\mathbf{x}_H)\lambda_i\phi^{(i)}(\mathbf{x}_H'), \tag{3.7}$$

where ϕ are eigenfunctions and λ are eigenvalues and where the expansion results in discrete and continuous parts. The wavenumber operator can then be obtained by taking the square root of the eigenvalues such that [4]

$$\mathcal{H}_1(\mathbf{x}_H;\mathbf{x}_H') = \int_{IR^2} d^2\boldsymbol{\kappa}\ \phi(\mathbf{x}_H,\boldsymbol{\kappa})\lambda^{1/2}(\boldsymbol{\kappa})\phi^*(\mathbf{x}_H',\boldsymbol{\kappa}) + \sum_{\lambda_i\in\,\text{discr}} \phi^{(i)}(\mathbf{x}_H)\lambda_i^{1/2}\phi^{(i)}(\mathbf{x}_H'). \tag{3.8}$$

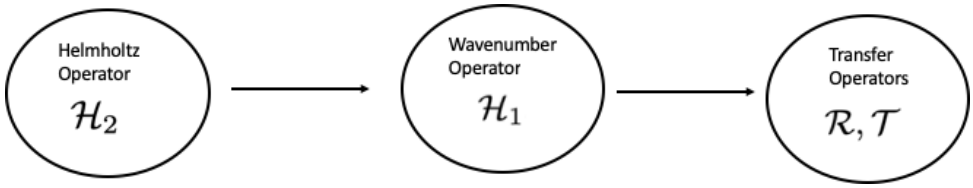

Figure 3.2 *A schematic showing the order of which the operators are obtained; first the Helmholtz operator, $\mathcal{H}_2$, from which the wavenumber operator, $\mathcal{H}_1$, is obtained and finally the transfer operators, $\mathcal{R}$ and $\mathcal{T}$, are obtained.*

3.4. SLOWNESS AND COSINE OPERATORS

Note that the wavenumber operator is defined in both space and local offset, $\mathbf{x}'_H$, the integration dummy variable. In order to obtain the wavenumber operator in space and local wavenumber ($\mathbf{k}'_H$), i.e. $\mathcal{H}_1(\mathbf{x}_H;\mathbf{k}'_H)$, we need to apply the spatial Fourier transformation, yielding

$$\mathcal{H}_1(\mathbf{x}_H;\mathbf{k}'_H) = \frac{1}{4\pi^2}\int_{IR^2} d^2\mathbf{x}'_H\, \mathcal{H}_1(\mathbf{x}_H;\mathbf{x}'_H)\, e^{j\mathbf{k}'_H\mathbf{x}'_H}. \tag{3.9}$$

One could obtain such result directly from the modal decomposition, but we limit the discussion to this form in this chapter. Similarly, one can also obtain slowness operator $\Lambda_1(\mathbf{x}_H;\mathbf{x}'_H) = \omega^{-1}\mathcal{H}_1(\mathbf{x}_H;\mathbf{x}'_H)$, in the local slowness domain, $\mathbf{p}'_H$, resulting in

$$\Lambda_1(\mathbf{x}_H;\mathbf{p}'_H) = \frac{1}{4\pi^2}\int_{IR^2} d^2\mathbf{x}'_H\, \Lambda_1(\mathbf{x}_H;\mathbf{x}'_H)\, e^{j\omega\mathbf{p}'_H\mathbf{x}'_H}. \tag{3.10}$$

Since velocity varies spatially, one would need to normalized the slowness operator by velocity so that a reasonable comparison can be achieved between different slowness curves at different locations.Thus, we then normalize by velocity in order to obtain a velocity-normalized slowness or cosine-sine curves, where the generalized cosine operator, $\Pi_1(\mathbf{x}_H;\mathbf{x}'_H) = c'\omega^{-1}\mathcal{H}_1(\mathbf{x}_H;\mathbf{x}'_H)$, is given by

$$\Pi_1(\mathbf{x}_H;\boldsymbol{\gamma}'_H) = \frac{1}{4\pi^2}\int_{IR^2} d^2\mathbf{x}'_H\, \Pi_1(\mathbf{x}_H;\mathbf{x}'_H)\, e^{j\omega c'^{-1}\gamma'\mathbf{x}'_H}, \tag{3.11}$$

where $\boldsymbol{\gamma}'$ is the sine of the scattering angle. Similarly, one can obtain the reflection operator $\mathcal{R}(\mathbf{x}_H;\boldsymbol{\gamma}'_H)$ using the formulas of the flux-normalized operator for vertically piecewise continuous media given, whose details are given by Hammad and Verschuur [5].

3.5. TRANSFER OPERATORS

Transfer coefficients can be computed using two methods [6]. The first method assumes smoothly varying media, where they are assumed to be infinitely differentiable. The second method allows discontinuous media where the vertical derivative may not exist. For instance, a situation of relevance to seismic prospecting is the case where a jump of the velocity happens when transitioning from clastics to top halite and back to clastics again at the base of halite. We refer to the transmission coefficient generated by the

first method and second method as the transfer coefficient of the first and second kinds, respectively.

The first method's advantage is that the vertical interaction of the wave with the medium is captured, whereas the second method does not capture such interaction. It assumes that a discontinuity separates two half spaces. Nevertheless the second method can model transfer coefficient in situations where the first methods cannot unless a smoothing operator is applied to the model.

3.5.1. TRANSFER COEFFICIENTS OF THE FIRST KIND

We can express the transfer coefficients in operator form similar to that of [7] and [6] as follows, the power-flux normalized reflection coeffcient [4] is

$$\hat{\mathcal{R}}_1^{\pm} = (\hat{\mathcal{Z}}_1 - \hat{\mathcal{Z}}_2), \tag{3.12}$$

where $\hat{\mathcal{Z}}_1$ is the impedance ratio per unit depth along the distance direction and $\hat{\mathcal{Z}}_2$ is the impedance ratio per unit depth along the local offset direction.

Similarly for the transmission coefficient we arrive at

$$\hat{\mathcal{T}}_1^{\pm} = (\hat{\mathcal{Z}}_1 + \hat{\mathcal{Z}}_2). \tag{3.13}$$

The impedance ratio per unit depth is expressed as

$$\hat{\mathcal{Z}}_1 = \frac{1}{2}\hat{\mathcal{H}}_1^{\frac{1}{2}}\hat{\varrho}^{-\frac{1}{2}}\partial_3(\hat{\varrho}^{\frac{1}{2}}\hat{\mathcal{H}}_1^{-\frac{1}{2}}) \tag{3.14}$$

and

$$\hat{\mathcal{Z}}_2 = \frac{1}{2}\hat{\mathcal{H}}_1^{-\frac{1}{2}}\hat{\varrho}^{\frac{1}{2}}\partial_3(\hat{\varrho}^{-\frac{1}{2}}\hat{\mathcal{H}}_1^{\frac{1}{2}}), \tag{3.15}$$

where $\hat{\varrho}$ is mass density and $\hat{\mathcal{H}}_1^{\frac{1}{2}}$ is the vertical wavenumber square-root operator, which can be determined from the eigen decomposition of the Helmholtz operator.

3.5.2. TRANSFER COEFFICIENTS OF THE SECOND KIND

For the situation where the vertical derivative of the wavenumber operator of the medium does not exist (i.e., discontinuous medium properties), there is an alternative way to compute the transfer coefficient operators. We derive expressions similar to those derived for the pressure normalized situation in [6]. After such derivation, the reflection coefficient operator is

$$\hat{\mathcal{R}}_2^{\pm} = (\hat{\mathcal{Z}}'_1 - \hat{\mathcal{Z}}'_2)(\hat{\mathcal{Z}}'_1 + \hat{\mathcal{Z}}'_2)^{-1} \tag{3.16}$$

and the transmission coefficient is

$$\hat{\mathcal{T}}_2^{\pm} = (\hat{\mathcal{Z}}'_1 + \hat{\mathcal{Z}}'_2)^{-1}, \tag{3.17}$$

where the impedance ratio along the x direction is

$$\hat{\mathcal{Z}}'_1 = \frac{1}{2}\hat{\mathcal{H}}_{1,u}^{\frac{1}{2}}\hat{\varrho}_u^{-\frac{1}{2}}\hat{\varrho}_l^{\frac{1}{2}}\hat{\mathcal{H}}_{1,l}^{-\frac{1}{2}} \tag{3.18}$$

and the impedance ratio along the local offset direction is

$$\hat{\mathcal{Z}}'_2 = \frac{1}{2}\hat{\mathcal{H}}_{1,u}^{-\frac{1}{2}}\hat{\varrho}_u^{\frac{1}{2}}\hat{\varrho}_l^{-\frac{1}{2}}\hat{\mathcal{H}}_{1,l}^{\frac{1}{2}}. \tag{3.19}$$

The subscripts u and l refers to the operators for the upper layer and the lower layers respectively.

We can arrive at those results by assuming a welded contact where vertical particle velocity and pressure are continuous, which results in equating

$$\begin{pmatrix} L_{1,u} & L_{1,u} \\ L_{2,u} & -L_{2,u} \end{pmatrix}\begin{pmatrix} p_u^+ \\ p_u^- \end{pmatrix} = \begin{pmatrix} L_{1,l} & L_{1,l} \\ L_{2,l} & -L_{2,l} \end{pmatrix}\begin{pmatrix} p_l^+ \\ p_l^- \end{pmatrix}, \tag{3.20}$$

where the subscripts u and l refer to upper and lower layers. Then we can derive the coefficients from above by equating [e.g. 6, p. 98]

$$\begin{pmatrix} L_{1,u} & L_{1,u} \\ L_{2,u} & -L_{2,u} \end{pmatrix}\begin{pmatrix} I \\ \mathcal{R}_2^+ \end{pmatrix} = \begin{pmatrix} L_{1,l} & L_{1,l} \\ L_{2,l} & -L_{2,l} \end{pmatrix}\begin{pmatrix} \mathcal{T}_2^+ \\ 0 \end{pmatrix}. \tag{3.21}$$

Similarly, we can derive those coefficients from below such that

$$\begin{pmatrix} L_{1,u} & L_{1,u} \\ L_{2,u} & -L_{2,u} \end{pmatrix}\begin{pmatrix} 0 \\ \mathcal{T}_2^- \end{pmatrix} = \begin{pmatrix} L_{1,l} & L_{1,l} \\ L_{2,l} & -L_{2,l} \end{pmatrix}\begin{pmatrix} \mathcal{R}_2^- \\ I \end{pmatrix}, \tag{3.22}$$

where

$$L_{1,u} = L_{1,l} = (\frac{\omega\,\varrho}{2})^{1/2}\mathcal{H}_1^{-1/2} \tag{3.23}$$

and

$$L_{2,u} = L_{1,l} = (2\omega\,\varrho)^{-1/2}\mathcal{H}_1^{1/2}. \tag{3.24}$$

Solving the linear system of equations 3.21 and 3.22 results in equations 3.16 and 3.17. Note that we derive the flux-normalized transfer operators in this situation. For pressure-normalized transfer operators, one could refer to Wapenaar and Berkhout [e.g. 6, p. 98].

3.6. ASPECTS OF NUMERICAL IMPLEMENTATION

3.6.1. STRETCHED-COORDINATE PML

For implementing such a scheme, an absorbing boundary condition needs to be incorporated in order to avoid the undesired back-scattered energy off the boundaries. We implement for this purpose a stretched-coordinate perfectly-matched layer (PML). Applying a stretched-coordinate PML is also commonly used for solving Maxwell equations. It can be interpreted physically as introducing a lossy layer at the desired boundaries, but it can also be interpreted mathematically as transforming the spatial coordinates into stretched ones [e.g. 8] such that

$$\tilde{x}_\alpha := x_\alpha + j\frac{1}{\omega}\int_0^{x_\alpha}\xi_\alpha(x)dx, \tag{3.25}$$

where $\tilde{x}_\alpha$ is the transformed coordinate and x_α is the original coordinate, where the subscript α takes on values of 1 and 2 and ξ_α is the relaxation function. Note that the PML is not needed along the preferred extrapolation direction unlike the case for conventional modeling with the two-way wave equation.

This transformation results in

$$\frac{\partial}{\partial x_\alpha} := \eta_\alpha \frac{\partial}{\partial \tilde{x}_\alpha}, \tag{3.26}$$

where η_α is the stretch factor determined using the relaxation function such that

$$\eta_\alpha = \frac{1}{1 + j\xi_\alpha/\omega}, \tag{3.27}$$

where ω is the angular frequency. Applying such transformation to the Helmholtz operator, $\mathcal{H}_2$ [e.g. 4, 5], results in

$$\tilde{\mathcal{H}}_2 = \frac{\omega^2}{\hat{c}^2} + \eta_\alpha \partial_\alpha \left(\eta_\alpha \partial_\alpha\right) + \tilde{\mathcal{J}}, \tag{3.28}$$

where

$$\tilde{\mathcal{J}} = -\frac{3(\eta_\alpha \partial_\alpha \hat{\varrho})(\eta_\alpha \partial_\alpha \hat{\varrho})}{4\hat{\varrho}^2} + \frac{\eta_\alpha \partial_\alpha \left(\eta_\alpha \partial_\alpha \hat{\varrho}\right)}{2\hat{\varrho}}, \tag{3.29}$$

in which $\hat{\varrho}$ is the density and $\hat{c}$ is the velocity. We choose a relaxation function, which is also used in [8], such that

$$\xi_\alpha(x_\alpha) = \begin{cases} 0, & \text{if } |x_\alpha| < a_\alpha \\ \bar{\xi}_\alpha \left(\frac{|x_\alpha - a_\alpha|}{L_\alpha} - \frac{\sin\left(\frac{2\pi |x_\alpha - a_\alpha|}{L_\alpha}\right)}{2\pi} \right), & \text{if } a_\alpha \le |x_\alpha| \le a_\alpha + L_\alpha, \end{cases} \tag{3.30}$$

where L_α is the PML width, α takes on the values 1 and 2 (i.e. the lateral spatial coordinates), a_α and $\bar{\xi}_\alpha$ are spatial and relaxation reference values, respectively. Those equations are discretized using finite differences in the next section.

We also note that the resulting transformed Helmholtz operator is not self-adjoint, unlike the case for purely lossless media. This also results in complex eigenvalues and eigenfunctions, whose combined effect gives the desired solutions. The Helmholtz operator is decomposed into different modes such that $\tilde{\mathcal{H}}_2 = \tilde{\mathcal{Y}}\tilde{\Sigma}\tilde{\mathcal{Y}}^{-1}$, where $\tilde{\mathcal{Y}}$ are the eigenfunctions and $\tilde{\Sigma}$ are the eigenvalues. The generalized wavenumber operator, $\tilde{\mathcal{H}}_1$, is then obtained using $\tilde{\mathcal{H}}_1 = \tilde{\mathcal{Y}}\tilde{\Sigma}^{1/2}\tilde{\mathcal{Y}}^{-1}$. Note that the inverse rather than the transpose of the eigenfunctions is used since the medium is essentially lossy, unlike the lossless situation assumed by Grimbergen *et al.* [9].

3.6.2. FINITE DIFFERENCE DISCRETIZATION

We can discretize the Helmholtz operator using a staggered-grid central finite difference discretization scheme with second-order accuracy. Using such a scheme yields

$$\tilde{\mathcal{H}}_{2,j,l}u_{j,l} = \frac{\omega^2}{\hat{c}^2_{j,l}} + \tilde{\mathcal{J}}_{j,l} + \eta_{1,j,l}\frac{1}{\Delta x_1^2}\left[\eta_{1,j+\frac{1}{2},l}u_{j+1,l} - (\eta_{1,j+\frac{1}{2},l} + \eta_{1,j-\frac{1}{2},l})u_{j,l} + \eta_{2,j-\frac{1}{2},l}u_{j-1,l}\right] + \eta_{2,j,l}\frac{1}{\Delta x_2^2}\left[\eta_{2,j,l+\frac{1}{2}}u_{j,l+1} - (\eta_{2,j,l+\frac{1}{2}} + \eta_{2,j,l-\frac{1}{2}})u_{j,l} + \eta_{2,j,l-\frac{1}{2}}u_{j,l-1}\right], \tag{3.31}$$

where $\tilde{\mathcal{J}}_{j,l} = \tilde{\mathcal{J}}'_{j,l} + \tilde{\mathcal{J}}''_{j,l}$, which each, in turn, is discretized as

$$\tilde{\mathcal{J}}'_{j,l} = -\frac{3}{4\hat{\varrho}^2_{j,l}}\left[\left[\eta_1(-\frac{1}{2}\hat{\varrho}_{j-1,l} + \frac{1}{2}\hat{\varrho}_{j+1,l})\right]^2 + \left[\eta_2(-\frac{1}{2}\hat{\varrho}_{j,l-1} + \frac{1}{2}\hat{\varrho}_{j,l+1})\right]^2\right] \tag{3.32}$$

and

$$\tilde{\mathcal{J}}''_{j,l} = \frac{\eta_{1,j,l}\left(\eta_{1,j+\frac{1}{2},l}\hat{\rho}_{j+1,l} - (\eta_{1,j+\frac{1}{2},l} + \eta_{1,j-\frac{1}{2},l})\hat{\rho}_{j,l} + \eta_{1,j-\frac{1}{2},l}\hat{\rho}_{j-1,l}\right)}{2\Delta x_1^2\hat{\rho}_{j,l}} + \frac{\eta_{2,j,l}\left(\eta_{2,j,l+\frac{1}{2}}\hat{\rho}_{j,l+1} - (\eta_{2,j,l+\frac{1}{2}} + \eta_{2,j,l-\frac{1}{2}})\hat{\rho}_{j,l} + \eta_{2,j,l-\frac{1}{2}}\hat{\rho}_{j,l-1}\right)}{2\Delta x_2^2\hat{\rho}_{j,l}}.$$

3.6.3. TOP AND BOTTOM BOUNDARY CONDITIONS

For the top and bottom boundaries, one can apply Sommerfeld radiation condition if the medium is assumed unbounded and that results in $\mathcal{R} = 0$ and $\mathcal{T} = 0$. For implementing a free surface, we can then let $\mathcal{R} = -\mathcal{I}$ and $\mathcal{T} = 0$. For further details the reader is referred to [6, p. 142] .

3.7. NUMERICAL EXAMPLES AND APPLICATIONS

In this section, we present three numerical examples. The first example compares the propagation operator for a locally heterogeneous medium, i.e. the conventional approach, to the more accurate operator for generally heterogeneous media. The second example presents the slowness curves for a heterogeneous model, and finally the third example shows the scattering operators in a fully heterogeneous realistic model of clastic alluvial channels.

3.7.1. PROPAGATION OPERATOR IN GENERALLY HETEROGENEOUS VS. LOCALLY HETEROGENEOUS MEDIA: A COMPARISON

In this first numerical example, the effect of inhomogeneity on the propagation operator, W, is illustrated. This example compares two methods, the method used in this chapter and the conventional method which is often used for one-way wavefield extrapolation [e.g. 10], which is based on the pressure-normalized formulation.

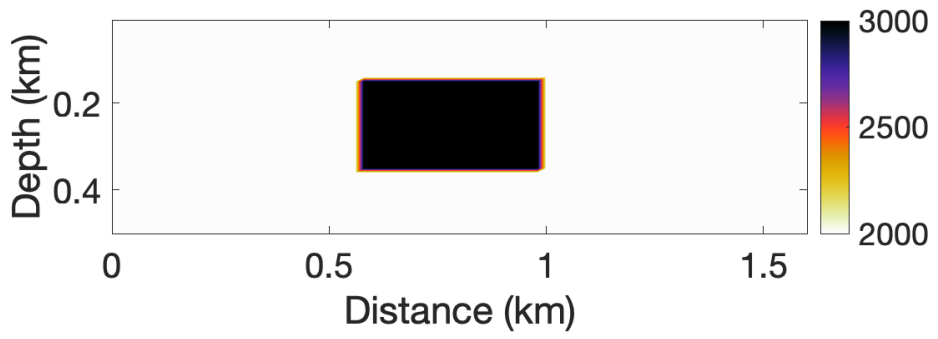

Figure 3.3 *Velocity model with laterally heterogeneity used to demonstrate the difference between the formulation involving locally homogeneous media and that of generally heterogeneous media.*

We use the velocity model shown in Figure 3.3, where the embedded velocity in this example is 3000 m/s and the other background velocity is 2000 m/s with a modeling frequency of 10 Hz. The W for fully inhomogeneous media is shown in Figure 3.4(b) and that for locally homogeneous media is shown in Figure 3.4(a). Note that in Figure 3.4(a), the analytical form of the k_z operator is used to populate the rows of the matrix and, hence, only the rows carry the lateral velocity information. However, the other operator shown in Figure 3.4(b) carries the full lateral velocity information in both rows and columns while its edges are directly tapered using the PML boundary conditions.

3.7.2. SLOWNESS AND REFLECTION OPERATOR CURVES IN LATERALLY HETEROGENEOUS MEDIA

Next, we examine the effects of lateral heterogeneity using the velocity model given in Figure 3.5, which contains a lateral velocity change with a slight smoothing of the vertical discontinuity. Since the lateral differentiability of the medium is assumed, a lateral mild smoothing ensures the existence of such derivatives. We then compute the velocity-normalized slowness operator for the laterally homogeneous part of the model, where the resulting curve, Figure 3.6(a), is nothing but a circle, as expected in this homogeneous isotropic region.

We then compute the vertical-velocity-normalized slowness curves for the laterally heterogeneous part of the model (at 3941 m lateral distance, 200 m depth and a frequency of 20 Hz), see Figure 3.6(b). Note that the deviation from a circle occurs more to the right hand side of the curve but not to the left hand side of the curve, which indicates that heterogeneity exists only on one side but not on the other. We then change the frequency to 50 Hz, see Figure 3.6(c). Note that changes occur from Figure 3.6(b) especially at higher angles. The deviation from a circle occurs after a certain angle after which both curves in Figure 3.6(b) and Figure 3.6(c) look different for different frequencies and, hence, those curves are dispersive for laterally heterogeneous media unlike their counterparts for homogeneous media.

We then compute the negative power-flux normalised reflection coefficient curves,

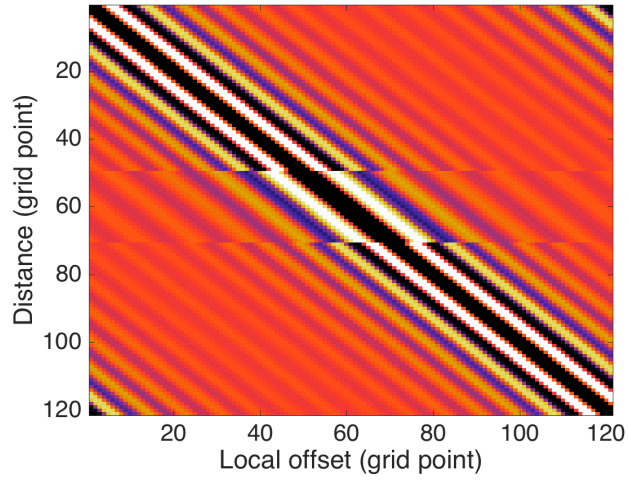

(a)

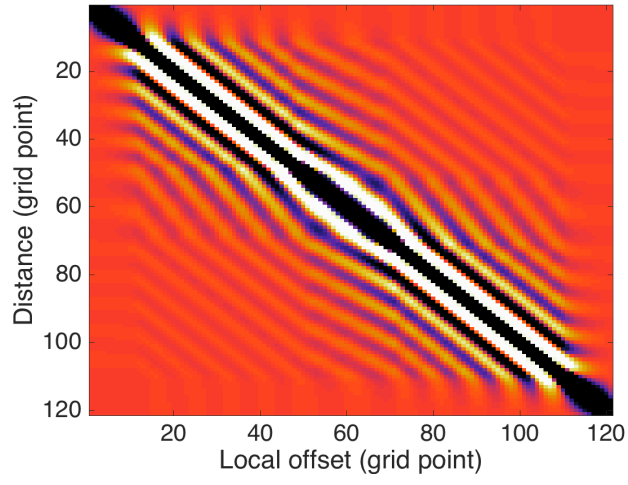

(b)

Figure 3.4 *The propagator, W, for locally homogeneous (a) and fully inhomogeneous formulation (b). The propagator belongs to a constant depth level at the middle of the velocity model in Figure 3.3. Note how the presence of the velocity anomaly impacts the middle part of the rows and column of each operator differently.*

Figure 3.7, at a constant depth level (180m) but at different lateral locations equally spaced from 3566 m to 3941 m. The curve at 3566 m is the one closest to zero amplitude since no vertical heterogeneity exists at this location. The curve at 3941 m is the one with the highest amplitude and the one closest in shape to the well-known classical situation that involves no lateral heterogeneity. The rest of the curves are between those

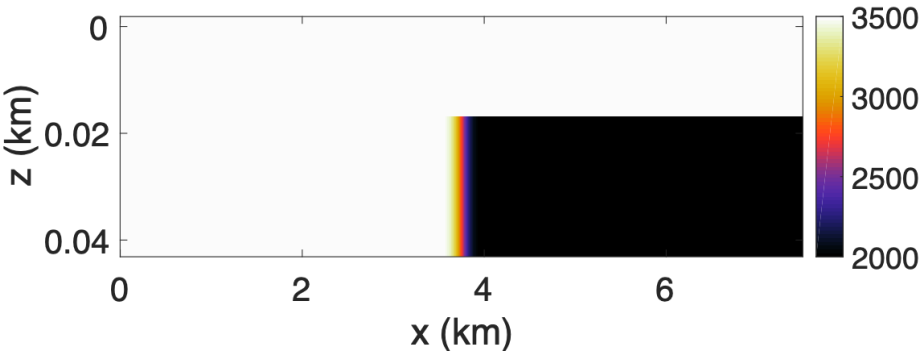

Figure 3.5 *The velocity model used to demonstrate the role of lateral heterogeneity. The model consists of two velocities with a slight smoothing at the vertical discontinuity.*

two extremes. Note that the amplitudes of the reflection coefficients, at different lateral locations, vary differently at both vertical incidence angle and at the rest of the angles. This variation could have impact on AVO/AVA methodologies that are based on laterally invariant media.

We note that the power flux-normalization entails not a scalar normalization but rather angle dependent scaling as it ensures that the reflection coefficients from above and from below are the same and, hence, reciprocity holds. For details the reader is referred to [4].

3.7.3. SCATTERING IN A MODEL OF CLASTIC ALLUVIAL CHANNELS

In the next example, the effect of inhomogeneity is illustrated using the Book Cliffs model [11]. The location of investigation is at a lateral location 11800 m and at a depth of 12.8 m. Figure 3.8 shows part of the Book Cliffs model. The white line indicates the depth level at which the reflection coefficient operator is computed. The model shown in Figure 3.8(a) is the interface separating two homogeneous interfaces, an assumption used for the acoustic equivalent of Zoeppritz equations.

The monochromatic reflection coefficient operators are computed, for those models, for a frequency of 8 Hz, and the result is shown in Figures 3.9(a) and 3.9(b), respectively. The operator shown in Figure 3.9(a) is a diagonal symmetric matrix. The operator shown in Figure 3.9(b) is symmetric but not diagonal. It contains the response of the neighboring sand channels. In fact, the anomalies in this operator correspond to the neighboring sand channels. A thresholding of the amplitudes is applied, visually, in order to see the details of the operator.

3.8. CONCLUSION

We have shown and implemented the modeling of vertical wavenumber and transfer operators, a step towards full implementation of full wavefield modeling. In order to avoid boundary artifacts, the implementation requires absorbing boundary conditions, which can be implemented using the so called stretched coordinate PML using a stag-

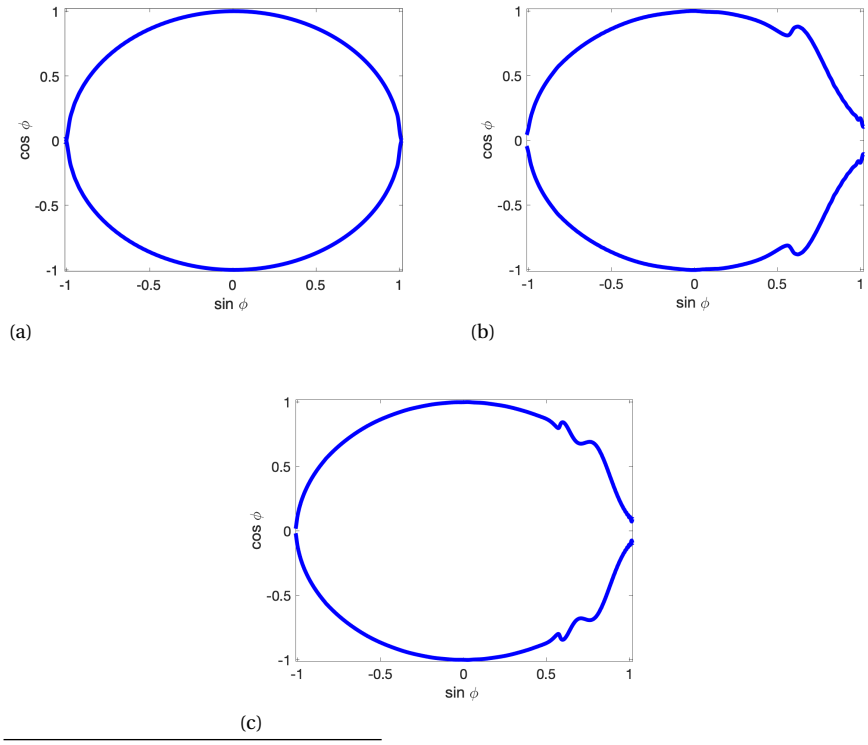

Figure 3.6 *Velocity-normalized slowness curves or cosine-sine curves of the scattering angle, (a) for the laterally homogeneous part of the model with a velocity of 3500 m/s; (b) for the laterally heterogeneous part of the model at depth level 200 m and lateral distance of 3754 m with frequency of 20 Hz. (c) The same as (b) but with a frequency of 50 Hz. Note that the normalized slowness curves (b) and (c) are different for different frequencies and hence are dispersive for the laterally heterogeneous part of the model unlike that of the laterally homogeneous one.*

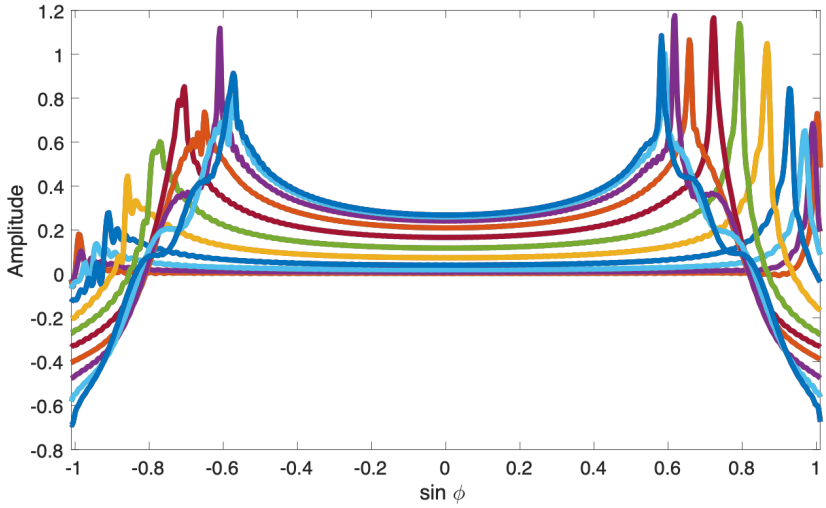

Figure 3.7 *The negative power-flux normalized reflection coefficient curves at different, equally spaced lateral locations between 3566 m and 3941 m with a depth of 180 m in the velocity model. The curves closest to zero in amplitude is at 3566 m and the one furthest away is at 3941m in lateral distance. Note that the upper blue curve is the closest to the classical situation that involves two homogeneous half spaces, while the rest are in between this curve and the on with zero amplitude. Also note that not only the value at vertical incidence angle is different for each curve, but also at the other angles.*

gered finite difference stencil. The impact of heterogeneity on slowness curves can then be assessed and we found that it is dispersive and hence changes from one frequency to another with larger impact on slowness curves of higher frequency, as one would intuitively expect. We can then see the impact of heterogeneity on reflection coefficient curves and what we find is that those curves, depending on their lateral position from the heterogeneity, exhibit deviation from the classical curve which involves two homogeneous half spaces — the situation assumed in Zoeppritz equations. We then compare the reflection operator of a fully heterogeneous medium and that of a Zoeppritz situation that involves two homogeneous half spaces. What we found is that the impact of heterogeneity represented by alluvial channels is clear and global on the operator involving heterogeneous media, whereas the influence of those channels is not present in the operators belonging to the Zoeppritz situation.

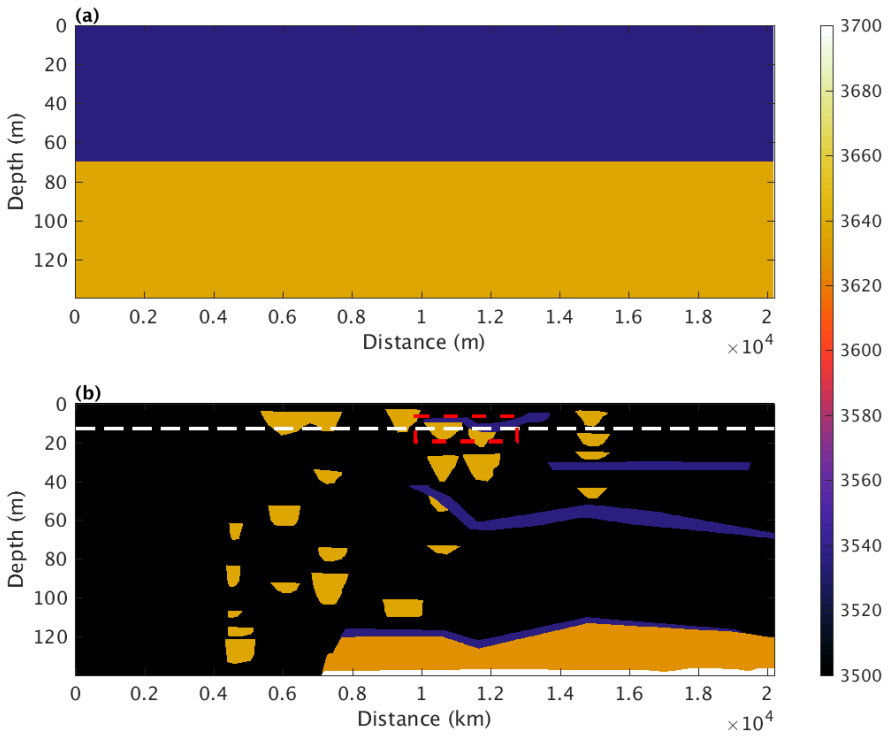

Figure 3.8 *A portion of the Book Cliffs model (b) and a zoomed-in laterally locally homogeneous part (a).*

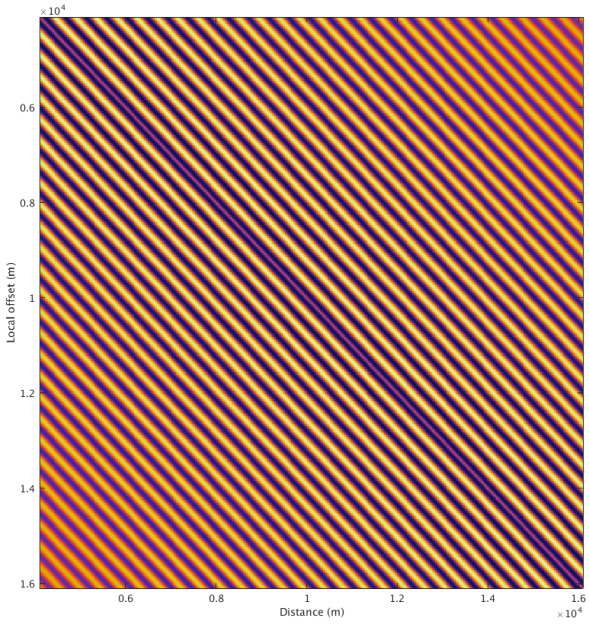

(a)

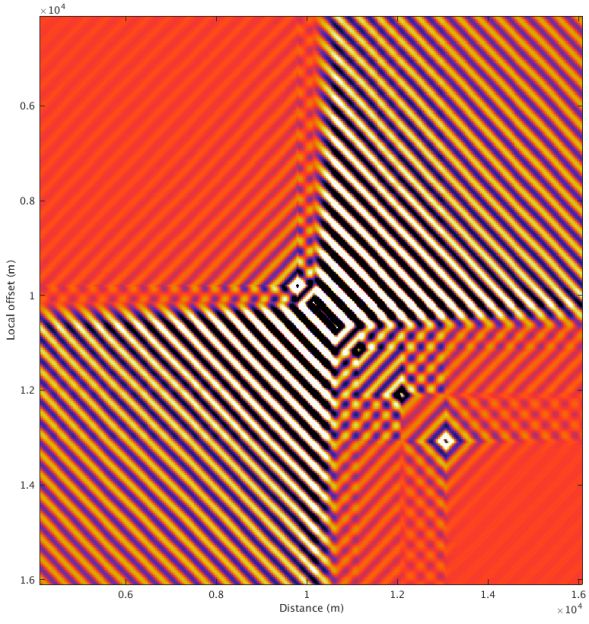

(b)

Figure 3.9 *Monochromatic reflection and transmission operators for a frequency 8 Hz computed using a) the acoustic equivalent of Zoeppritz equations and b) using the fully inhomogeneous formulation.*

REFERENCES

[1] Aristotle, *Complete Works of Aristotle, Volume 1: The Revised Oxford Translation*, edited by J. Barnes, Bollingen Series (General) (Princeton University Press, 2014).

[2] C. P. A. Wapenaar, *One-way representations of seismic data,* Geophysical Journal International **127**, 178 (1996).

[3] M. V. de Hoop, *Generalization of the Bremmer coupling series,* Journal of Mathematical Physics **37**, 3246 (1996).

[4] C. P. A. Wapenaar and J. L. T. Grimbergen, *Reciprocity theorems for one-way wavefields,* Geophysical Journal International **127**, 169 (1996).

[5] H. I. Hammad and D. J. Verschuur, *Towards forward modeling beyond zoeppritz's: Full-wavefield modeling for inhomogeneous media,* in *SEG Technical Program Expanded Abstracts 2016* (Society of Exploration Geophysicists, 2016) pp. 3960–3965.

[6] C. P. A. Wapenaar and A. J. Berkhout, *Elastic Wave Field Extrapolation: Redatuming of Single- and Multi-component Seismic Data* (Elsevier Science Publishers B.V., Amsterdam, The Netherlands, 1989).

[7] A. J. Berkhout, *Seismic migration, imaging of acoustic energy by wave field extrapolation: A. Theoretical Aspects* (Elsevier Science Publishers B.V., Amsterdam, The Netherlands, 1984).

[8] M. J. Grote and I. Sim, *Efficient PML for the wave equation,* ArXiv e-prints (2010).

[9] J. L. T. Grimbergen, F. J. Dessing, and K. Wapenaar, *Modal expansion of one-way operators in laterally varying media,* GEOPHYSICS **63**, 995 (1998).

[10] J. W. Thorbecke, K. Wapenaar, and G. Swinnen, *Design of one-way wavefield extrapolation operators, using smooth functions in wlsq optimization,* GEOPHYSICS **69**, 1037 (2004).

[11] D. Tetyukhina, S. Luthi, and A. Gisolf, *Acoustic nonlinear full-waveform inversion on an outcrop-based detailed geological and petrophysical model (Book Cliffs, Utah),* AAPG Bulletin **98**, 119 (2014).

4

MODELING WAVEFIELDS

"One may conceive light to spread successively, by spherical waves."

Christiaan Huygens [1, p. 171]

Full wavefield modeling is divided into two steps: operator generation and wavefield generation. In this chapter, we generate wavefields first using a homogeneous model where we benchmark the solution with the analytical one and we find good agreement. We then model diving waves using the x-direction as a direction of preference, and, as it turns out, a single iteration is sufficient using such configuration in order to model the diving wave for a model that changes linearly with depth. We then use a more complex model and we model approximately each scattering order using a Neuman's iterative scheme. We show the evolution of the wavefield in terms of the scattering orders in both frequency and time domains. This example shows that this method is useful for such cases where one is interested in understating the wavefield in terms of its scattering orders.

4.1. INTRODUCTION

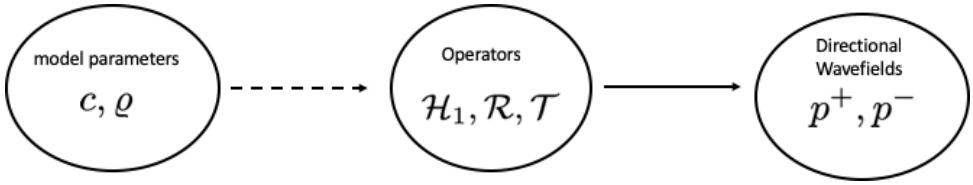

Figure 4.1 *A schematic diagram showing the mapping discussed in this chapter, where operators are mapped to directional wavefields.*

Full wavefield modeling is a method that incorporates transfer operators: reflection and transmission operators. It also utilizes propagation operators in order to simulate wave propagation[2–4]. We have presented in Chapter 3 those operators and we have compared the propagation operators to the ones obtained for locally inhomogeneous media. In this chapter, we proceed to the next step of full wavefield modeling: generating the wavefields using those operators, as shown in Figure 4.1.

So, we start his chapter by discussing the theory including the Neuman's series which is used to generate the wavefields iteratively. We then show three examples: one for homogeneous media where we benchmark the method against the analytical one, another example where we examine diving waves, and a third example where we generate the wavefields for an inhomogeneous medium.

Full wavefield modeling is a method that incorporates transfer operators, reflection and transmission operators, as well as, propagation operators, in order to model wave propagation [2–4]. [5] have implemented full wavefield modeling for homogeneous media and have also shown the transfer operators for such media [6]. They have also shown propagation operators and compared them to the ones obtained for locally inhomogeneous media. However, handling strongly inhomogeneous media requires the physical direct arrival rather than an approximate and consequently one would expect an improved convergence rate.

This chapter shows the derivation of a representation theorem that can handle such media. The representation theorem is similar to that derived by Corones [7]. A Neumann, as well as, a generalized Neumann expansion is also presented. Some examples illustrate the implementation aspects of the theorem.

4.2. MODELING USING THE NEUMANN ITERATIVE SCHEME

Now that we have modeled the operators in Chapter 3, we turn our attention to modeling wavefields using the following equation, by combining Equations 3.1 and 3.4:

$$\mathbf{p}(\mathbf{x}') = \mathbf{p}_0(\mathbf{x}') + \int_{\mathbb{R}^3} d^3\mathbf{x}\ \mathbf{G}_p(\mathbf{x}',\mathbf{x})\boldsymbol{\Theta}(\mathbf{x})\mathbf{p}(\mathbf{x}). \tag{4.1}$$

In order to demonstrate how this equation can be solved, let's first express it in symbolic form such that

$$\mathbf{p} = \mathbf{p}_0 + \mathbf{G}_p \boldsymbol{\Theta} \mathbf{p}. \tag{4.2}$$

Letting

$$\mathbf{L} = \mathbf{I} - \mathbf{G}_p \boldsymbol{\Theta}, \tag{4.3}$$

we can then express the equation as a typical inverse problem such that

$$\mathbf{L}\mathbf{p} = \mathbf{p}_0. \tag{4.4}$$

The most straight-forward solution to this equation is by using a direct solver. However, such a solution is only practical for small-scale problems. Therefore, we seek an iterative solution, and the simplest and perhaps the most straight forward method, as we will see in Chapter 5, is that of Neumann. Such a method results in the following iterative scheme:

$$\mathbf{p}_k = \mathbf{p}_0 + \mathbf{G}_p \boldsymbol{\Theta} \mathbf{p}_{k-1}, \tag{4.5}$$

where k is the iteration number. Hence, we recursively obtain the solution using previous solutions, and we start with the direct arrival such that

$$\mathbf{p}_0 = \mathbf{G}_p \mathbf{s}. \tag{4.6}$$

4.3. NUMERICAL EXAMPLES

4.3.1. VALIDATION AND SIMPLE EXAMPLE

In order to validate the numerical implementation and assess the accuracy of the modeling algorithm, a comparison is performed between a Green's function obtained using the proposed algorithm and a Green's function obtained via an analytical solution using the Hankel transform. The 2D Green's function for a homogeneous medium can be represented as [8]

$$G_{2D}(x, z, x_s, z_s, \omega) = -jH_0^{(2)}(rk), \tag{4.7}$$

where $H_0^{(2)}$ is the zeroth order Hankel function of the second kind, r is the radius, where $r = \sqrt{(x-x_s)^2 + (z-z_s)^2}$ and k is the wave-number such that $k = \frac{\omega}{c}$.

Since the two approaches are different in their numerical implementation, they need to be calibrated with a scale factor. Figure 4.2 shows the results of such comparison using a velocity model of 2000 m/s and a frequency of 15 Hz. A good fit is achieved especially in the far field with a slight mismatch in the near field due to the fact that the PML is not perfect.

We also show the full 2D wavefield in Figure 4.3 , where we model a wavefield for a using the same homogeneous model and the same monopole source. We place the source inside the medium and extrapolate the wavefield from the surface all the way downward first. Once the propagation operator encounters the source the wavefield is

emitted downward. When the propagation operator returns to finish a roundtrip, it encounters the source again and emits the wavefield upward. Note that this process occurs not only for the induced sources, which are often placed on the surface, but also for the secondary sources within the subsurface. This example also shows that the extrapolation operator is able to propagate the wavefield without any significant limitation on the propagation angles even in the simple Cartesian coordinate system.

The white boundaries on both the left and the right hand sides represent the PML layer. The wavefield energy on these boundaries is absorbed by this layer without the need to taper the propagation operator. The quality of the PML result depends on both the width and the slope of the relaxation function. Those parameters control the cost of the computation. In this example we only used a width of almost 250 meters on both sides.

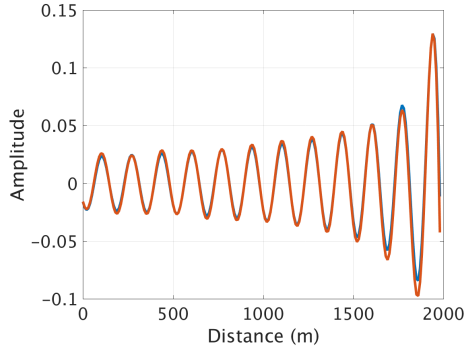

(a)

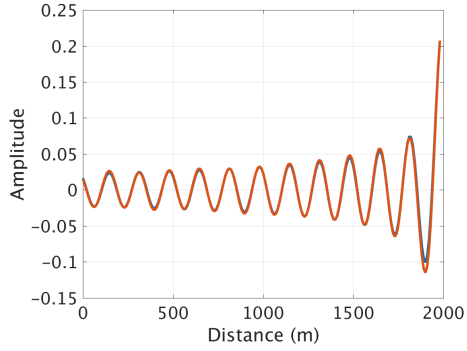

(b)

Figure 4.2 *Comparison between an analytical and a numerical Green's function in a homogeneous medium with a velocity of 2000 m/s and for a frequency of 10 Hz ; real (a) and imaginary parts (b).*

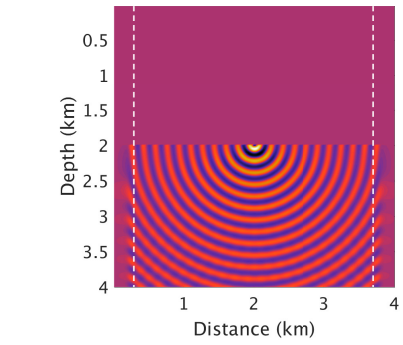

(a)

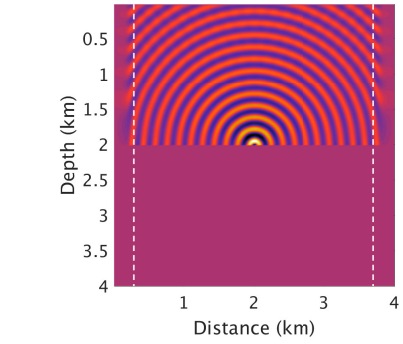

(b)

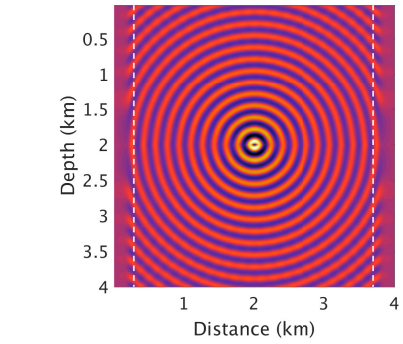

(c)

Figure 4.3 *The extrapolated wavefield for a monopole source of 15 Hz embedded in a homogeneous medium with a velocity of 2000 m/s. The wavefield in a) is generated when the downward component of the source is encountered while extrapolating the wavefield downward. Similarly for the upward propagating wavefield in b). c) shows the sum of both wavefields in a) and b). The dashed white lines, in all figures, show the extent of the PML. Note that finally the full angles of the wavefield are constructed.*

4.3.2. DIVING WAVES

Although the proposed method can handle generally inhomogeneous media, it is important to investigate a particularly important case of horizontally propagating waves, which is referred to as diving wave, whose exact solution in two-dimensions for a linear velocity gradient is given by Kuvshinov and Mulder [9]. For simplicity, we choose the x-direction as the direction of preference. Figure 4.5a shows the time domain shot record modeled for linearly increasing velocity model. The first arrival in this case is the direct wave along the short offsets and turns into a diving wave at large offset, where the first arrival time becomes curved rather than linear. The dotted red line shows the solution of the eikonal equation obtained using the method of [10]. Note the consistency between the two solutions.

Figure 4.5b shows a monochromatic wavefield of 15 Hz. The dotted black lines show the eikonal solution. Note once again the consistency between the two solutions. We also note the desired effect of the PML shown above and below, where the wavefield is gently tapered and absorbed with minimal back-scattering off the top and bottom boundaries.

Although we flip the coordinates and we model a diving wave in this example, we need to point out that the wave is not strictly horizontally propagating with respect to the flipped coordinates. In Chapter 5, we model diving waves using the z-direction as a direction or preference but, as we will see, we have to iterate several times unlike modeling with the x-direction as a direction of preference. So, in this situation, it is more computationally efficient to model diving waves using the x-direction as a direction of preference since no further iterations are necessary beyond the initial one.

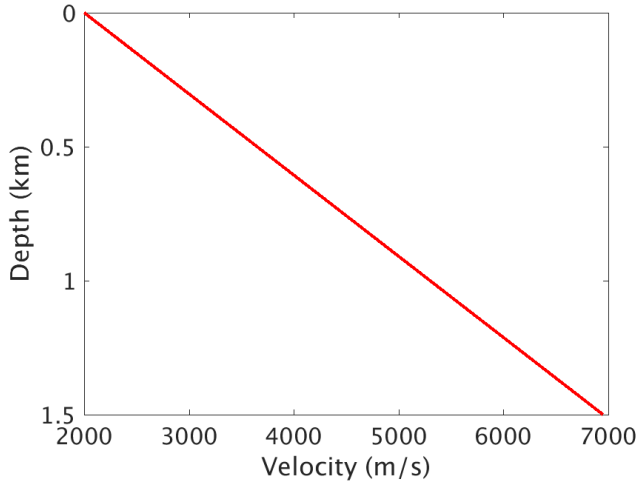

Figure 4.4 *A linearly-increasing velocity model used for modeling diving waves.*

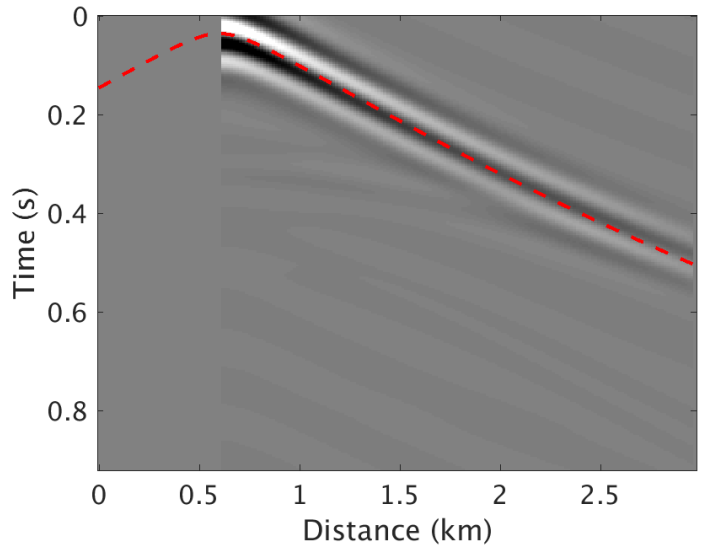

(a)

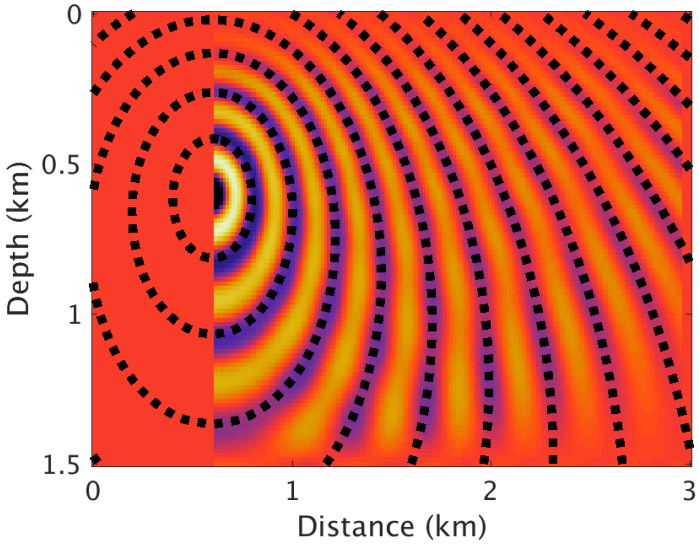

(b)

Figure 4.5 *(a) Shot gather modeled in a linearly increasing velocity model, Figure 4.4, with the red-dashed line representing the first-arrival time modeled using the eikonal equation. The receiver line is at 0.6 km. (b) A monochromatic wavefield of frequency 15 Hz with black-dashed lines representing the solution of the eikonal equation. Only the right-going wavefield is shown in both figures. Notice the consistency between the wavefield solution and the arrival times modeled using the eikonal equation.*

4.3.3. INHOMOGENEOUS MODEL

Next, we demonstrate the full wavefield modeling method using the model shown in Figure 4.6. In this example, we assume the absence of a free surface, in addition to the absence of an upgoing component of the source. Figure 4.7 shows the downgoing wavefields and upgoing wavefields for different orders of scattering. Figure 4.7a shows the downgoing direct arrival, Equation 4.6, used to initiate further iterations.

The upgoing primary is shown in Figure 4.7b. The downgoing, as well as, the upgoing multiples are shown in the rest of the plots (Figure 4.7c-4.7f). Since this example does not include a free surface, nor does it include an upgoing component of the source, the multiples, $\mathbf{m}_n$ for a scattering order $n > 0$ can be computed from the difference between the even and odd-numbered wavefieds such that $\mathbf{m}_n^+ = \mathbf{p}_{2n}^+ - \mathbf{p}_{2n-2}^+$ and $\mathbf{m}_n^- = \mathbf{p}_{2n+1}^- - \mathbf{p}_{2n-1}^-$, as demonstrated in the original work of [11]. The time-domain shot records are shown in Figure 4.8 for each scattering order. Note that the amplitudes are thresholded so that later multiples are also visible.

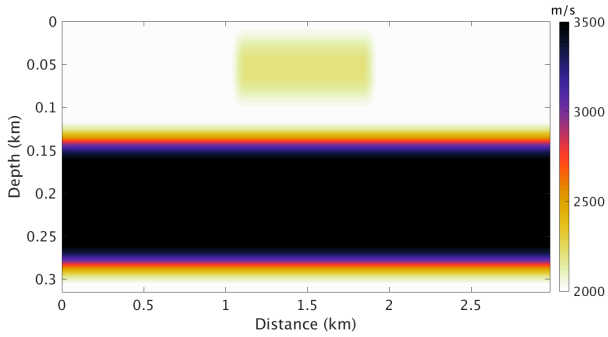

Figure 4.6 *A laterally-inhomogeneous velocity model used for modeling. Although the method can handle strongly inhomogeneous media, the model is kept relativity simple for illustration purposes.*

4.4. CONCLUSION

We have implemented the wavefield generation phase of full wavefield modeling. We implemented the Neumann iterative series, which represents one of the simplest iterative methods. We first benchmarked the method with the analytical solution for a homogeneous medium and we found good agreement between the two solutions. We then modeled diving waves using the x-direction as the direction of preference and one iteration seems to be sufficient to model such wavefields using such configuration. We also benchmarked the diving wave solution kinematically with the solution of the eikonal equation and also found good agreement between the two solutions. We then turned to modeling the wavefield using a more complex heterogeneous model and we found that each iteration corresponds approximately to an order of scattering and hence this method seems to attractive in modeling such wavefields where one is interested in the evolution of the wavefield in terms scattering orders.

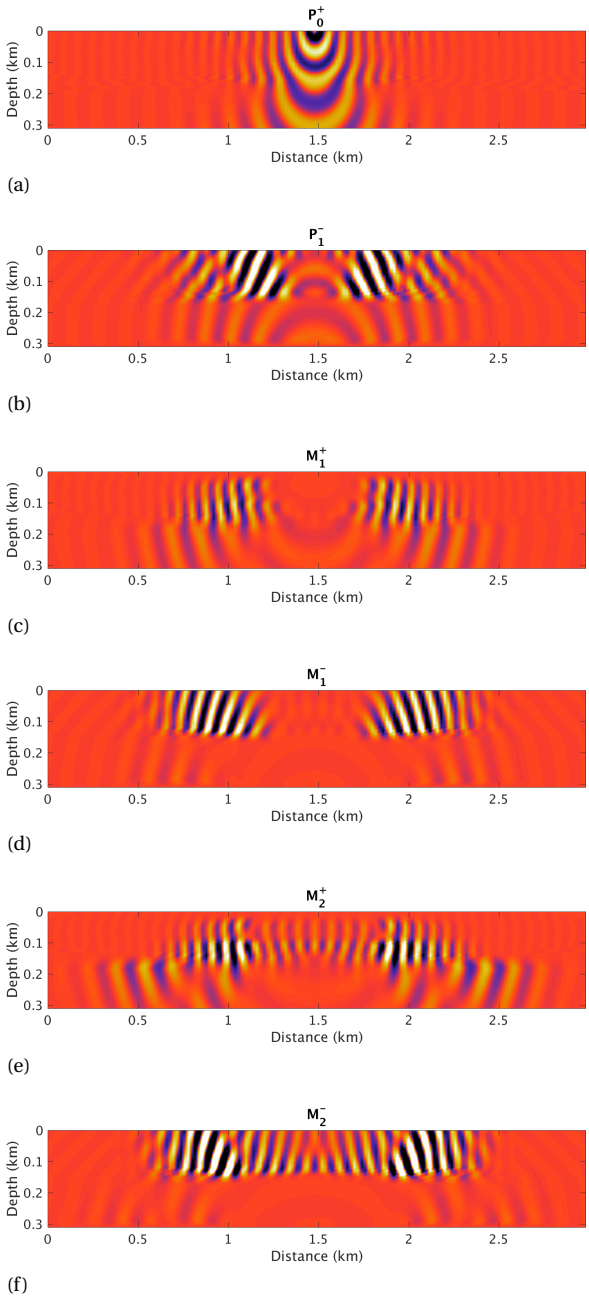

Figure 4.7 *The real part of monochromatic wavefields, 15 Hz, for different scattering orders. (a) The downgoing direct arrival. (b) The upgoing primary. (c,d) The downgoing and upgoing first-order multiples, respectively, as well as, (e,f) the upgoing and downgoing second order multiples. Note that not only the upgoing and downgoing wavefields are obtained, but also the ones for each scattering order.*

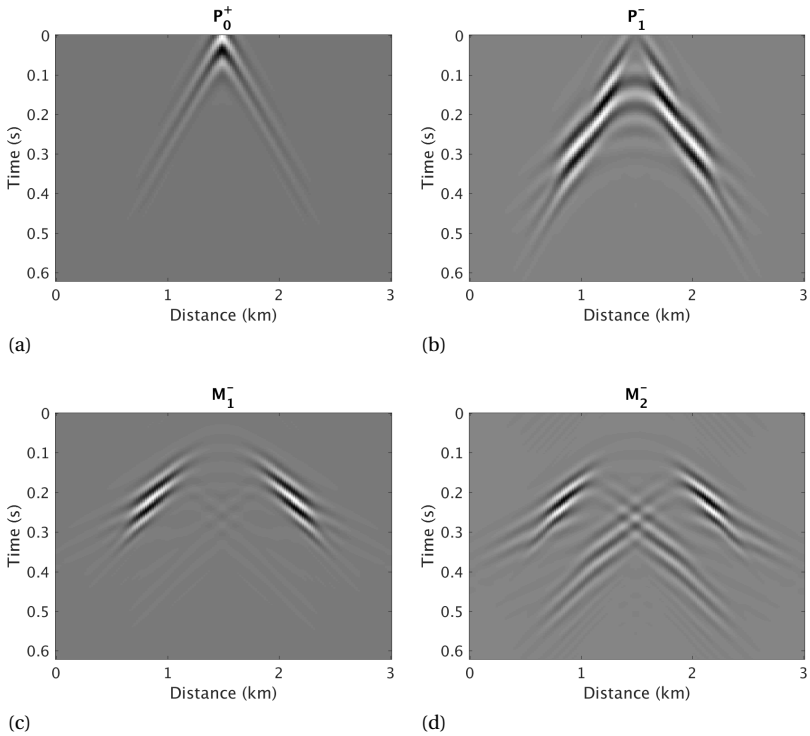

Figure 4.8 *A time-domain shot record for different scattering orders measured at depth level 0.02 km for the model in Figure 4.6. (a) Direct arrival. (b) Primary wavefield. (c) First-order multiples. (d) Second-order multiples.*

REFERENCES

[1] K. Kuehn, *A Student's Guide Through the Great Physics Texts: Volume III: Electricity, Magnetism and Light,* Undergraduate Lecture Notes in Physics (Springer International Publishing, 2015).

[2] C. P. A. Wapenaar, *One-way representations of seismic data,* Geophysical Journal International **127**, 178 (1996).

[3] M. V. de Hoop, *Generalization of the Bremmer coupling series,* Journal of Mathematical Physics **37**, 3246 (1996).

[4] A. J. Berkhout, *Review paper: An outlook on the future of seismic imaging, part I: forward and reverse modeling,* Geophysical Prospecting **62**, 911 (2014).

[5] H. I. Hammad and D. J. Verschuur, *Joint migration inversion for laterally varying media,* in *78th EAGE Conference and Exhibition 2016* (2016).

[6] H. I. Hammad and D. J. Verschuur, *Towards forward modeling beyond zoeppritz's: Full-wavefield modeling for inhomogeneous media,* in *SEG Technical Program Expanded Abstracts 2016* (Society of Exploration Geophysicists, 2016) pp. 3960–3965.

[7] J. Corones, *Bremmer series that correct parabolic approximations,* Journal of Mathematical Analysis and Applications **50**, 361 (1975).

[8] A. J. Berkhout, *Seismic migration, imaging of acoustic energy by wave field extrapolation: A. Theoretical Aspects* (Elsevier Science Publishers B.V., Amsterdam, The Netherlands, 1984).

[9] B. N. Kuvshinov and W. A. Mulder, *The exact solution of the time-harmonic wave equation for a linear velocity profile,* Geophysical Journal International **167**, 659 (2006).

[10] F. Qin, Y. Luo, K. B. Olsen, W. Cai, and G. T. Schuster, *Finite-difference solution of the eikonal equation along expanding wavefronts,* Geophysics **57**, 478 (1992).

[11] H. Bremmer, *The W.K.B. approximation as the first term of a geometric-optical series,* Communications on Pure and Applied Mathematics **4**, 105 (1951).

5

ITERATIVE SOLUTIONS TO MODELING WAVEFIELDS

"to be learning something is the greatest of pleasures not only to the philosopher but also to the rest of mankind."

Aristotle [Poetics, 1448b]

Full Wavefield Modeling is a directional modeling method, which simulates wavefields such as upgoing and downgoing wavefields. The most straightforward implementation of such a method is to employ the Neumann's iterative method, which is, nonetheless, well-known not to be necessarily convergent for all situations. Thus, we use three different methods that represent a generalization of the Neumann's solution; one is a preconditioned overrelaxation, and the other two are preconditioned conjugate gradient and a truncated Krylov method, the so-called GMRes. We compare the convergence of all those methods, as well as, stationary and successive overrelaxation methods without preconditioning. We find that such truncated Krylov method, i.e., GMRes, is overall faster to converge and requires no preconditioning to ensure convergence. We show two examples, one using a velocity model linearly increasing with depth and one using a complex salt model adapted from the SEG SEAM model. In the first model, full wavefield modeling provides the upgoing and downing diving waves including the horizontally propagating constituents, while in the second model, it provides the evolution of the scattering process with different iterations, providing insight into the actual scattering process.

5.1. INTRODUCTION

In the previous chapter (Chapter 4), we used a simple iterative method, Neumann's method, to solve our modeling problem. In this chapter we investigate the convergence of this iterative method and we compare its convergence to other methods. As we will discuss in detail, the Neumann's series— as a general iterative method for solving integral equations — is known not be unconditionally convergent [1]. For example, using the nondirectional counterpart of our problem, the Lippmann-Schwinger equation, it has been demonstrated that the Neumann series is not always convergent and its convergence depends on how strong the perturbation is relative to the background model [2]. So, one would legitimately wonder if similar behavior could be encountered in our problem.

However, de Hoop [3] has shown that the Neumann series is theoretically convergent in the time domain when applied to the directional modeling method. Nevertheless, it has not been shown to be convergent in the frequency domain, which is of interest to us since it reduces the computation cost by transforming the more expensive convolutions into simple multiplications. Therefore, it is important to investigate if indeed the full wavefield modeling method is convergent in the frequency domain when Neumann's series is used and whether it is indeed convergent in practice rather than in theory.

Throughout this chapter, we use the Neumann series as well as some of its generalizations. Because of the similarity between our problem and that of the Lippman-Schwinger equation, we use the generalizations presented by Kleinman and van den Berg [2] and Fokkema and Van Den Berg [1]. Such generalizations have been utilized in different papers such as [4] and [5].

5.2. NEUMANN SOLUTION

We state here the Neumann solution as a point of reference since all other solutions are generalized forms of this fundamental solution. As we have discussed in Chapter 4, our modeling equation is

$$\mathbf{p}(\mathbf{x}') = \mathbf{p}_0(\mathbf{x}') + \int_{\mathbb{R}^3} d^3\mathbf{x}\ \mathbf{G}_p(\mathbf{x}',\mathbf{x})\boldsymbol{\Theta}(\mathbf{x})\mathbf{p}(\mathbf{x}), \tag{5.1}$$

where

$$\mathbf{p}_0 = \int_{\mathbb{R}^3} d^3\mathbf{x}\ \mathbf{G}_p(\mathbf{x}',\mathbf{x})\mathbf{s}(\mathbf{x}). \tag{5.2}$$

Stating Equation 5.1 in symbolic form — as we did in Chapter 4 — but replacing $\mathbf{G}_p$ with $\mathbf{G}$ for simplicity , results in

$$\mathbf{p} = \mathbf{p}_0 + \mathbf{G}\boldsymbol{\Theta}\mathbf{p}, \tag{5.3}$$

where $\mathbf{p}_0 = \mathbf{G}\mathbf{s}$. Letting

$$\mathbf{L} = \mathbf{I} - \mathbf{G}\boldsymbol{\Theta}, \tag{5.4}$$

our linear inverse problem becomes

$$\mathbf{L}\mathbf{p} = \mathbf{p}_0. \tag{5.5}$$

That is, the wavefield could be obtained by directly inverting the operator $\mathbf{L}$ such that

$$\mathbf{p} = \mathbf{L}^{-1}\mathbf{p}_0, \tag{5.6}$$

but as we discussed in Chapter 4, a direct solution is impractical for the size of problems we typically encounter in exploration seismology and, hence, an iterative solution is necessary and one of the simplest solutions is that of Neumann where the iterative solution is given by

$$\mathbf{p}_k = \mathbf{p}_0 + \mathbf{G\Theta p}_{k-1}. \tag{5.7}$$

Although, we have discussed some aspects of the Neumann series in Chapter 4, we have not discussed how this method reduces the residual with each iteration. As it turns out (see [2] for details), Neumann's method reduces an l_2 norm, $\|\mathbf{r}\|$, with each subsequent iteration, k, such that

$$\mathbf{r}_k = \mathbf{G\Theta r}_{k-1}, \tag{5.8}$$

starting from the initial residual, which encompasses the direct arrival such that

$$\mathbf{r}_0 = \mathbf{G\Theta p}_0. \tag{5.9}$$

The iterative solution then becomes

$$\mathbf{p}_k = \mathbf{p}_{k-1} + \mathbf{r}_{k-1}. \tag{5.10}$$

Knowing this residual is essential for convergence comparison analysis and in cases where Neumann's series diverges. As it turns out, in order for Neumann's series to converge — and hence for the residual not to blow up — the norm, $\|\mathbf{G\Theta}\|$, needs to be always less than one so that the operator $\mathbf{L}$ stays positive. Otherwise the residual increases with each iteration rather than decreases. For such situations, one would need to look for generalizations of the Neumann series, which we investigate next.

5.3. BEYOND NEUMANN VIA OVERRELAXATION METHOD

We present two solutions beyond that of Neumann using the so-called stationary and successive overrelaxation methods [e.g. 2], which were used for the non-directional domain integral problem. Using those methods, we can generalize the Neumann solution by simply choosing a scalar, α, such that it forms a cap over the residual and attempts to prevent if from growing such that

$$\mathbf{p}_k = \mathbf{p}_{k-1} + \alpha\mathbf{r}_{k-1}. \tag{5.11}$$

We can immediately see that if $\alpha = 1$ then we get the exact Neumann solution, (i.e. Equation 5.10). Therefore, the Neumann method is essentially a special case of those methods and that's why those methods are, in turn, mere generalizations of the Neumann method. The same observation can be pointed out when the residual is derived such that

$$\mathbf{r}_k = [\mathbf{I} - \alpha\mathbf{I} + \alpha\mathbf{G\Theta}]\mathbf{r}_{k-1}, \tag{5.12}$$

while the initial residual is kept the same as that of Neumann, i.e. $\mathbf{r}_0 = \mathbf{G\Theta p}_0$. Substituting the residuals one can obtain the iterative wavefield solution in terms of previous iterations of wavefields such that

$$\mathbf{p}_k = \alpha \mathbf{p}_0 + [\mathbf{I} - \alpha \mathbf{I} + \alpha \mathbf{G\Theta}]\mathbf{p}_{k-1}. \tag{5.13}$$

We can observe from Equation 5.13 that the scalar α suppresses not only subsequent iterations of wavefields but even the initial solution, i.e the direct arrival. Compare that to Neumann's method (Equation 5.10), where no scalars are used but rather all wavefields are left without any caps.

What remains now is only the value of the scalar α that can be derived using different ways (see [2] for details) and we pick α such that

$$\alpha = \frac{\mathbf{r}_0^\dagger (\mathbf{I} - \mathbf{G\Theta})\mathbf{r}_0}{\| (\mathbf{I} - \mathbf{G\Theta})\mathbf{r}_0 \|}, \tag{5.14}$$

where the dagger refers to conjugate transpose. Then we come to the question: Why keep α constant? Why could it not change with iterations so that it adapts to how large the residual is in each iteration? Such method is called the successive overrelaxation method [2]. Then the scalar step length α becomes

$$\alpha_k = \frac{\mathbf{r}_k^\dagger (\mathbf{I} - \mathbf{G\Theta})\mathbf{r}_k}{\| (\mathbf{I} - \mathbf{G\Theta})\mathbf{r}_k \|}, \tag{5.15}$$

and hence the residual is

$$\mathbf{r}_k = [\mathbf{I} - \alpha_k \mathbf{I} + \alpha_k \mathbf{G\Theta}]\mathbf{r}_{k-1}. \tag{5.16}$$

For implementation purposes, one can always start by implementing the first method, stationary overrelaxation, and then progress by varying the scalar, α, for subsequent iterations. Thus, from theoretical and practical point of view, it is beneficial to consider both methods.

5.4. PRECONDITIONED SUCCESSIVE OVERRELAXATION

We can now state even more generalized forms of the Neumann series, which were applied to the non-directional form of our integral equation (i.e. the Lippmann-Schwinger equation) by Kleinman and van den Berg [2] . One such form is the preconditioned successive overrelaxation method, which is almost always convergent. Such a method introduces an preconditioning operator, $\mathbf{T}$, such that

$$\mathbf{p}_k = \mathbf{p}_{k-1} + \alpha_k \mathbf{T}\mathbf{r}_{k-1}. \tag{5.17}$$

One could choose $\mathbf{T} = \mathbf{L}^\dagger = (\mathbf{I} - \mathbf{G\Theta})^\dagger$, where the dagger refers to the adjoint operation (the conjugate transpose of the operator), which results in

$$\mathbf{r}_k = [\mathbf{I} - \alpha_k (\mathbf{I} - \mathbf{G\Theta})^\dagger (\mathbf{I} - \mathbf{G\Theta})]\mathbf{r}_{k-1}. \tag{5.18}$$

Notice that the resulting operator $\mathbf{L}^\dagger\mathbf{L} = (\mathbf{I} - \mathbf{G\Theta})^\dagger (\mathbf{I} - \mathbf{G\Theta})$ is always positive and hence this method is always convergent unlike the previous ones. However, its main problem,

as we will see in the examples, is that it is slow. Also, notice that if $\mathbf{T} = \mathbf{I}$ and $\alpha = 1$ then we are back to the Neumann solution, (i.e. Equation 5.10).

Consequently, we can get the form that includes the wavefields such that

$$\mathbf{p}_k = \mathbf{p}_{k-1} + \alpha_k (\mathbf{I} - \mathbf{G}\boldsymbol{\Theta})^\dagger \mathbf{r}_{k-1}, \tag{5.19}$$

or equivalently

$$\mathbf{p}_k = \alpha_k (\mathbf{I} - \mathbf{G}\boldsymbol{\Theta})^\dagger \mathbf{p}_0 + [\mathbf{I} - \alpha_k (\mathbf{I} - \mathbf{G}\boldsymbol{\Theta})^\dagger (\mathbf{I} - \mathbf{G}\boldsymbol{\Theta})]\mathbf{p}_{k-1}. \tag{5.20}$$

The step length is then

$$\alpha_k = \frac{\left\| (\mathbf{I} - \mathbf{G}\boldsymbol{\Theta})^\dagger \mathbf{r}_{k-1} \right\|^2}{\left\| (\mathbf{I} - \mathbf{G}\boldsymbol{\Theta})^\dagger (\mathbf{I} - \mathbf{G}\boldsymbol{\Theta}) \mathbf{r}_{k-1} \right\|^2}. \tag{5.21}$$

5.5. PRECONDITIONED CONJUGATE GRADIENT METHOD

Now, we attempt to solve the slow convergence of the previous method with the preconditioned conjugate gradient method. This method uses not only one step length but two and hence we have α and β.

While the conjugate gradient method is convergent for only positive operators, the operator can be made positive by preconditioning with the adjoint. For our problem the wavefields are updated such that (see [2])

$$\mathbf{p}_k = \mathbf{p}_{k-1} + \alpha_k \mathbf{q}_k, \tag{5.22}$$

where

$$\mathbf{q}_k = (\mathbf{I} - \mathbf{G}\boldsymbol{\Theta})^\dagger \mathbf{r}_{k-1} + \beta_{k-1} \mathbf{q}_{k-1}, \tag{5.23}$$

and

$$\mathbf{r}_k = \mathbf{r}_{k-1} - \alpha_k (\mathbf{I} - \mathbf{G}\boldsymbol{\Theta}) \mathbf{q}_k, \tag{5.24}$$

but $\mathbf{q}_1 = \mathbf{r}_o$. The step lengths are then

$$\alpha_k = \frac{\left\| (\mathbf{I} - \mathbf{G}\boldsymbol{\Theta})^\dagger \mathbf{r}_{k-1} \right\|^2}{\left\| (\mathbf{I} - \mathbf{G}\boldsymbol{\Theta}) \mathbf{q}_k \right\|^2}, \tag{5.25}$$

and

$$\beta_{k-1} = \frac{\left\| (\mathbf{I} - \mathbf{G}\boldsymbol{\Theta})^\dagger \mathbf{r}_{k-1} \right\|^2}{\left\| (\mathbf{I} - \mathbf{G}\boldsymbol{\Theta})^\dagger \mathbf{q}_{k-2} \right\|^2}. \tag{5.26}$$

5.6. TRUNCATED KRYLOV METHODS

Considering the preceding extension to the Neumann's method, we can also consider more step length values rather using than only two, as in the conjugate gradient method. This brings us the Krylov method. So, the solution is obtained using a series such that

$$\mathbf{p}_k = \mathbf{p}_{k-1} - \alpha_k \mathbf{q}_k \tag{5.27}$$

where

$$\mathbf{q}_k = \mathbf{r}_{k-1} + \sum_{j=1}^{k-1} \gamma_{k,j} \mathbf{q}_j. \tag{5.28}$$

and $\mathbf{q}_1 = \mathbf{r}_o$. Consequently, for every single solution, all previous iterations are involved but with different scalars, $\gamma_{k,j}$.

While the conjugate gradient method uses two previous iterations, the full Krylov method [2] uses all the previous iterations in order to scale the wavefields properly. The series can be truncated, however, to a few previous iterations — five previous iterations for instance (i.e. $j = 1$ to $j = k-1$ if $k < 6$, and $j = k-5$ to $j = k-1$ if $k > 6$).

Another method is the one by Saad and Schultz [6], the so-called GMRes, generalized minimal residual method, which uses so-called Arnoldi orthogonalization to compute the step lengths, while the one by Kleinman and van den Berg [2] computes them explicitly. So, we use GMRes method, which is more widely available.

The only drawback of any truncated Krylov method is that the previous intermediate solutions are needed instead of only one or two as in all previous methods. As a consequence, one would trade off memory for CPU as we will point out in the numerical examples.

5.7. MODELING DIVING WAVES

We apply full wavefield modeling to the velocity model shown in 5.1a in order to model diving waves. Figure 5.2 shows the diving waves for both upgoing and downgoing wavefields for a single frequency of 15 Hz. The initial downgoing and upgoing solutions are shown in Figure 5.2a and 5.2b with a zero upgoing source. The intermediate solutions for the first two iterations are shown in Figure 5.2c-5.2f. Note how the intermediate solutions reveal the horizontally propagating constituents of the diving waves, thus providing an insight into the scattering process. The solutions were computed using the GMRes method, whose convergence plot is compared to other methods in Figure 5.3. Note that all preconditioned methods, i.e., preconditioned stationary, preconditioned successive overrelaxation and preconditioned conjugate gradient, are slower than the other methods, with the fastest convergence provided by GMRes. The reason is that the condition number of the resulting operator is higher when the adjoint operator, $L^\dagger$, is used as a preconditioner and the convergence is slower as a result. Note that the purpose of the so-called preconditioning, in this situation, is not necessarily to speed up the convergence but rather to guarantee it by making the resulting operator positive. We also note the Neumann solution is convergent for this model. It remains to see if the Neumann solution is indeed convergent for a more complex model, which is next.

5.8. MODELING IN COMPLEX MEDIA: SALT

We also model the wavefields using the velocity model shown in Figure 5.1b. The wavefields modeled for a frequency of 6 Hz and are shown in Figure 5.4. Note that in Figure 5.4c the update of the wavefield is mostly surrounding the wavefield passing through the salt. The reason for such an update is that transmission effects are not included in the propagator but added with subsequent iterations. The wavefields are computed with GMRes, whose convergence is compared with other methods in Figure 5.5. We note that

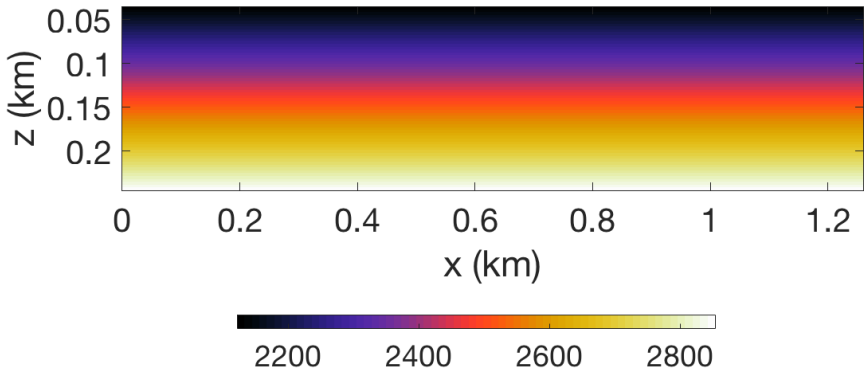

(a)

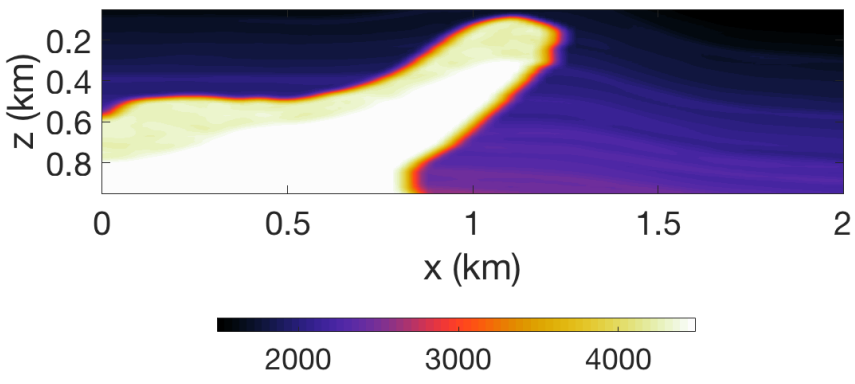

(b)

Figure 5.1 *Velocity models used to demonstrate the modeling method. (a) Velocity model (Model A) containing only linearly increasing velocity for modeling diving waves. (b) Velocity model (Model B) adapted form the SEG SEAM model, with the shallow position of the mobile salt body.*

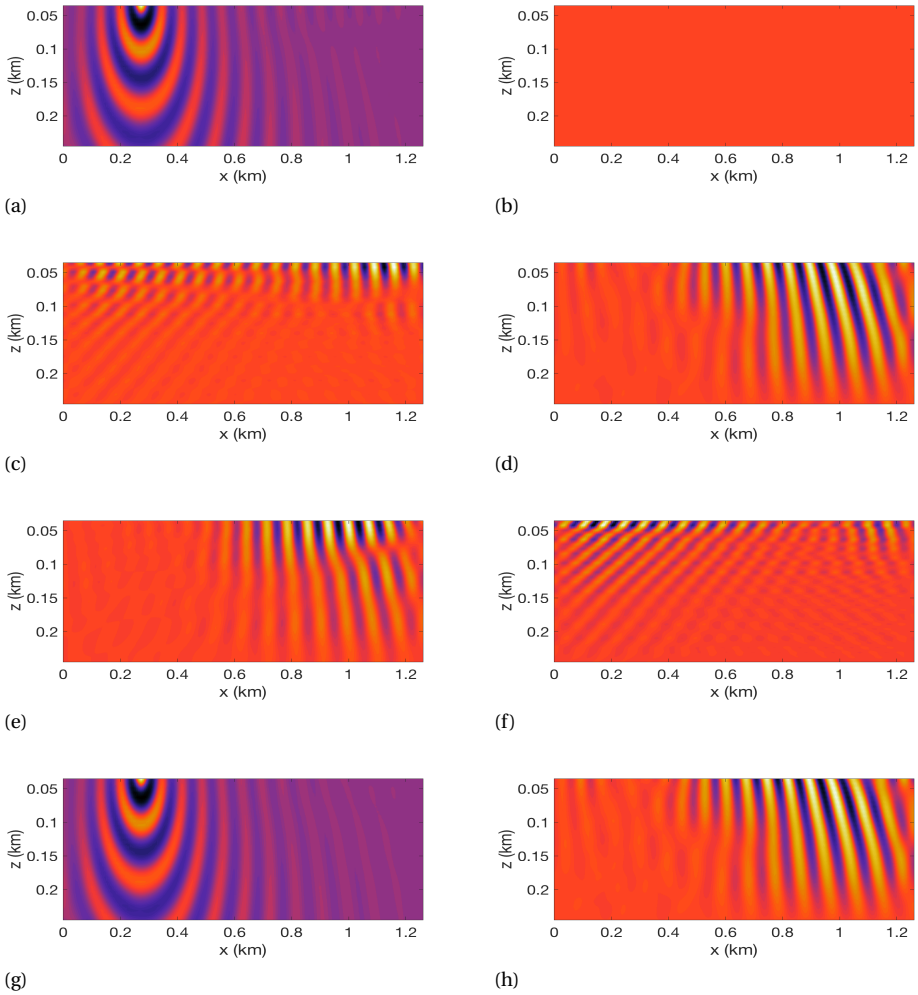

Figure 5.2 *Wavefields modeled for the linearly increasing velocity model, Model A (Figure 5.1a). The updates are shown to demonstrate how the wavefield evolves with iterations. (a) The downgoing direct arrival, p_0^+. (b) The upgoing direct arrival, p_0^+, which is set to zero. (c) The first downgoing residual, r_1^+ (d) The first upgoing residual, r_1^-. (e) The second downgoing residual, r_2^+ . (f) The second upgoing residual, r_2^-. (g) The final downgoing wavefield, p_{30}^+ and (h) the final upgoing total wavefield, p_{30}^+.*

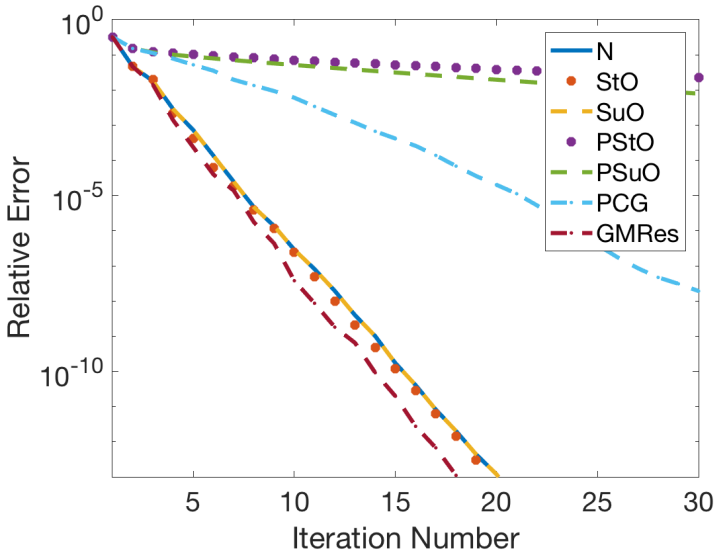

Figure 5.3 *Convergence plot for the first model A with comparison between Neumann's method (N), stationary overrelaxation (StO), successive overelaxation (SuO), precondition stationary overrelaxation (PStO), preconditioned successive overrelaxation (PSuO), preconditioned conjugate gradient (PCG) and GMRes.*

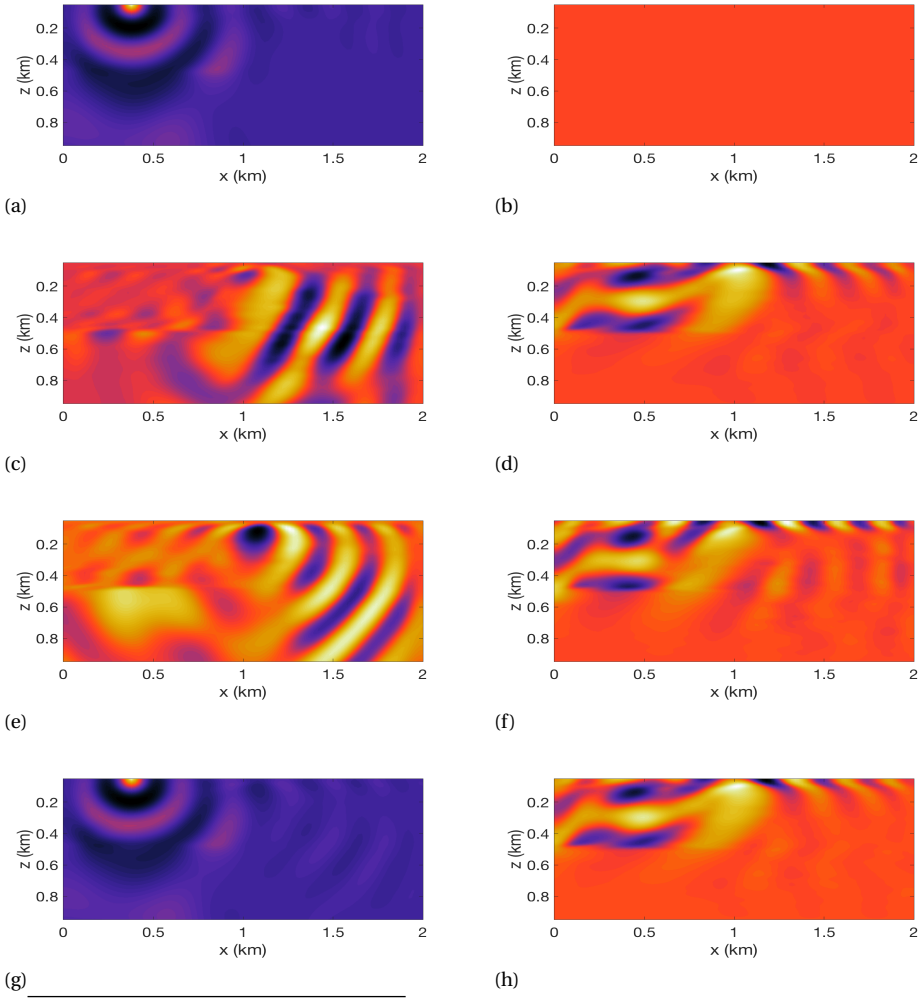

Figure 5.4 *Wavefields modeled for the salt model, Model B (Figure 5.1b). (a) The downgoing direct arrival, p_0^+. (b) The upgoing direct arrival, p_0^+, which is set to zero. (c) The first downgoing residual, r_1^+. (d) The first upgoing residual, r_1^-. (e) The second downgoing residual, r_2^+ . (f) The second upgoing residual, r_2^-. (g) The final downgoing wavefield, p_{30}^+ and (h) the final upgoing total wavefield, p_{30}^+.*

the fastest convergence is provided with GMRes, while the slowest is provided with preconditioned conjugate gradient method, due to the preconditioning with the adjoint, as mentioned in the previous section. We also note that the Neumann solution is convergent even for this more complex model.

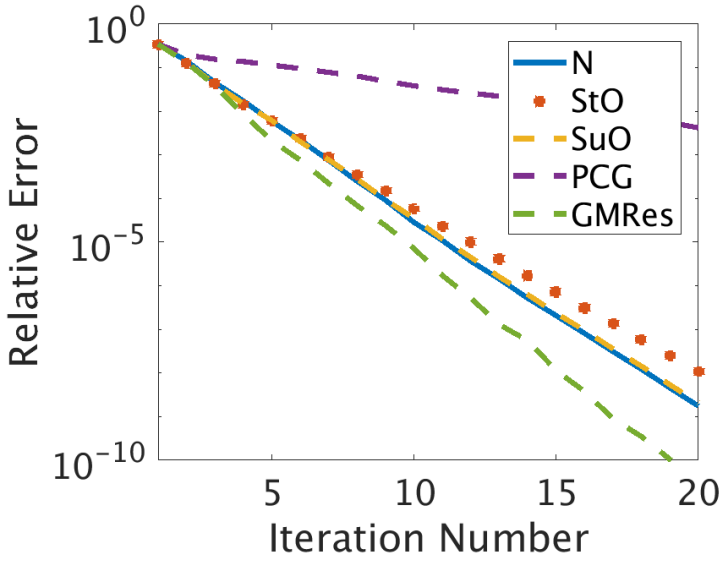

Figure 5.5 *Convergence plot for the wavefield modeled in the SEAM-based salt model shown in model B (Figure 5.1b).*

5.9. CONCLUSIONS

We have extended the solutions of the full wavefield modeling method beyond those of Neumann. We have presented three generalizations applied to this modeling problem; preconditioned successive overelaxation, preconditioned conjugate gradient and a truncated Krylov method, the so-called GMRes method. We have also compared the solutions and found that a truncated Krylov method, GMRes, provides faster convergence and requires no preconditioning to assure convergence, unlike the preconditioned methods, which suffer from slower convergence due to the preconditioning with the adjoint operator. We have shown two examples; one using a model which is linearly increasing with depth, to demonstrate diving waves. Full wavefield modeling shows clearly the upgoing and the downgoing waves, including the horizontally propagating constituents of the diving waves. We have also shown an example using a salt model, which shows the full evolution of the wavefields with iterations, thus providing insight into scattering in such a complex medium. The Neumann solutions are convergent for both models, and hence the Neumann solution might be unconditionally convergent in the frequency domain, similar to its time-domain counterpart, as known theoretically.

REFERENCES

[1] J. Fokkema and P. Van Den Berg, *Seismic applications of acoustic reciprocity* (Elsevier, 1993).

[2] R. E. Kleinman and P. M. van den Berg, *Iterative methods for solving integral equations,* Radio Science **26**, 175 (1991).

[3] M. V. de Hoop, *Generalization of the Bremmer coupling series,* Journal of Mathematical Physics **37**, 3246 (1996).

[4] G. Osnabrugge, S. Leedumrongwatthanakun, and I. M. Vellekoop, *A convergent born series for solving the inhomogeneous helmholtz equation in arbitrarily large media,* Journal of computational physics **322**, 113 (2016).

[5] M. Jakobsen and R.-S. Wu, *Renormalized scattering series for frequency-domain waveform modelling of strong velocity contrasts,* Geophysical Journal International **206**, 880 (2016).

[6] Y. Saad and M. H. Schultz, *GMRES: A generalized minimal residual algorithm for solving nonsymmetric linear systems,* SIAM J. Sci. Stat. Comput. **7**, 856 (1986).

6

MODELING OPERATORS AND WAVEFIELDS IN QUASI-ELASTIC TRANSVERSELY ISOTROPIC MEDIA

"What, then, impels us to devise theory after theory? Why do we devise theories at all? The answer ... is simply: because we enjoy "comprehending," i.e., reducing phenomena by the process of logic to something already known or (apparently) evident."

Albert Einstein [1]

Full wavefield modeling is a modeling process that utilizes reflection and transmission operators for inhomogeneous media in order to produce the wavefields. We extend this modeling process to the quasi-elastic anisotropic situation, where the elastodynamic generalized vertical wavenumber operator for P-waves is embedded in the acoustic formulation, assuming transversely isotropic media. Two examples are presented; one for a homogeneous and the other for an inhomogeneous medium. The wavefields generated exhibit the typical angular distortion behavior introduced by anisotropy. While useful on its own, this extension of generalized full wavefield modeling paves the road to the inversion process, model-independent joint migration inversion.

6.1. INTRODUCTION

We have investigated in detail the full wavefield modeling method in the previous chapters. In this chapter we extend this method to the anisotropic situation. One of the simplest but realistic anisotropic situations used in exploration seismology is that of transverse isotropic media although the simplest situation, elliptic anisotropy, is known not to be realistic for exploration seismology [2]. Hence, we adopt transverse anisotropy with vertically axis of symmetry (TIV) in this chapter.

Although the locally laterally homogeneous situation has been considered previously [e.g., 3], we extend in this chapter the method to laterally heterogeneous TIV media and we use the full P-wave vertical wavenumber operator rather than an approximation of it that assumes weak anisotropy [4]. So, it is derived from the full elastodynamic situation, but since we embed it in the acoustic situation that models solely P-wave, we refer to such configuration as quasi-elastic.

Hence, this chapter extends the modeling process to the quasi-elastic situation where only P-waves are modeled using their full elastodynamic generalized vertical wavenumber operator and for the TIV situation. This chapter first starts by stating the differential system of equations, so that we are clear on the starting configuration. Then, we derive the generalized vertical wavenumber for P-waves from the elastodynamic situation and use it for our modeling integral equations. We then show a simple example for a homogeneous medium followed by an example for an inhomogeneous medium.

6

6.2. DIFFERENTIAL SYSTEM OF EQUATIONS

We first state the two-way wave equation and the one-way wave equations similar to those presented by Wapenaar and Grimbergen [5] and Wapenaar and Berkhout [6]. Then we show how a key component, the generalized vertical wavenumber operator, is used to generalize the formulation to the quasi-elastic situation. The two-way acoustic wave equation states that (see also section 2.2.3)

$$\frac{\partial \mathbf{q}}{\partial x_3} = \mathbf{A}\mathbf{q} + \mathbf{d}, \tag{6.1}$$

where

$$\mathbf{q} = \begin{pmatrix} p \\ v_3 \end{pmatrix}, \tag{6.2}$$

which encompasses the vertical particle velocity, v_3, and pressure p. The operator

$$\mathbf{A} = \begin{pmatrix} 0 & -j\omega\rho \\ \frac{1}{j\omega\rho} H_2 & 0 \end{pmatrix}, \tag{6.3}$$

where H_2 is the vertical Helmholtz operator, ρ is the density and ω is the angular frequency. The source term is expressed as

$$\mathbf{d} = \begin{pmatrix} f_3 \\ q' - \frac{1}{j\omega}\partial_\alpha(\frac{1}{\rho} f_\alpha) \end{pmatrix}, \tag{6.4}$$

where f is the force component and q is the pressure source. Equation 6.1 can be decomposed into directional wavefields, e.g. upgoing and downgiong wavefields, by applying eigen decomposition to the operator $\mathbf{A} = -j\omega\mathbf{L}\Lambda\mathbf{L}$, which results in the equations

$$\frac{\partial \mathbf{p}}{\partial x_3} = \mathbf{B}\mathbf{p} + \mathbf{s}, \tag{6.5}$$

where the operator

$$\mathbf{B} = -j\omega\mathbf{\Lambda} + \mathbf{\Theta}, \tag{6.6}$$

such that the scattering operator

$$\mathbf{\Theta} = -\mathbf{L}^{-1}\partial_3\mathbf{L}. \tag{6.7}$$

Opting for the so-called power-flux normalization [7] of the wavefields results in the operator

$$\mathcal{H}_2 = \rho^{-1/2}(H_2\rho^{1/2}\cdot). \tag{6.8}$$

Modal decomposition can then be carried out in order to obtain the generalized wavenumber operator such that

$$\mathcal{H}_1 = \mathcal{H}_2^{1/2} = YQ^{1/2}Y^{-1}. \tag{6.9}$$

One can obtain the directional wavefield using the composition operator such that

$$\mathbf{p} = \mathbf{L}\mathbf{q}. \tag{6.10}$$

Thus, we have presented the basic differential system of equations, which will be extended to the quasi-elastic anisotropic situation next.

6.3. GENERALIZATION TO THE QUASI-ELASTIC ANISOTROPIC SITUATION

Although we have presented the equations for the acoustic situation, the equations for the elastodynamic situation are also known [e.g 6]. However, our objective is to extract an expression for the Helmholtz operator from the elastodynamic situation and insert it into the equations of the acoustic situation. Thus, we ultimately arrive at a situation that is in between the acoustic and fully elastodynamic anisotropic situation, and hence the name quasi-elastodynamic situation. This allows modeling of P-wave reflections according to the elastodynamic anisotropy, which can play an important role in inverting P-wave data. The vertical slowness, s_3, for the TIV situation can be expressed [e.g 6, 8] as

$$s_3^2 = \frac{1}{2c_{33}c_{44}}(d - (d^2 - 4e)^{1/2}), \tag{6.11}$$

where

$$e = c_{33}c_{44}(\rho - c_{11}s_\alpha s_\alpha)(\rho - c_{44}s_\alpha s_\alpha) \tag{6.12}$$

and

$$d = (c_{33} + c_{44})\rho - [c_{11}c_{33} - (c_{13} + c_{44})^2 + c_{44}^2]s_\alpha s_\alpha, \tag{6.13}$$

where, for instance, c_{33} and c_{44} are the vertical compression and shear stiffness, respectively. Transforming Equation 6.11 to the wavenumber and then to the spatial domain

and using the same Fourier sign convention as that used by Wapenaar and Berkhout [6], yields

$$H_2 = \frac{1}{2c_{33}c_{44}}[\mathcal{D} - (\mathcal{D}\cdot\mathcal{D} - 4\mathcal{E})^{1/2}], \tag{6.14}$$

where

$$\mathcal{E} = c_{33}c_{44}\left(\omega^2\rho + c_{11}\partial_\alpha\partial_\alpha\right)\left(\omega^2\rho + c_{44}\partial_\alpha\partial_\alpha\right) \tag{6.15}$$

and

$$\mathcal{D} = \omega^2(c_{33}+c_{44})\rho + [c_{11}c_{33} - (c_{13}+c_{44})^2 + c_{44}^2]\partial_\alpha\partial_\alpha. \tag{6.16}$$

We can derive the H_1 operator from the Helmholtz operator using modal decomposition, as is done in the isotropic acoustic situation.

The solution to the wavefield can then be obtained using the same integral solution used in Chapter 3. Although we have defined our model in terms of stiffness parameters, the so-called Thomsen parameters [2] can also be used and we show our example models using those parameters.

The integral solution is then given by

$$\mathbf{p}_k(\mathbf{x}_d) = \int_{\mathbb{R}^3} d^3\mathbf{x}\,\mathbf{G}_p(\mathbf{x}_d,\mathbf{x})\mathbf{s}(\mathbf{x}) + \int_{\mathbb{R}^3} d^3\mathbf{x}\,\mathbf{G}_p(\mathbf{x}_d,\mathbf{x})\boldsymbol{\Theta}(\mathbf{x})\mathbf{p}_{k-1}(\mathbf{x}), \tag{6.17}$$

which is the same solutions used for the acoustic situation, where k is the iteration number of the Neumann iteration scheme.

6.4. NUMERICAL EXAMPLES

We present two numerical examples to illustrate the method; one for a homogeneous model, and the other for an inhomogeneous model. Figure 6.1 shows the wavefields for the homogeneous isotropic situation, Figure 6.1a, and the homogeneous anisotropic situation, Figure 6.1b, where vertical velocity $v_p = 2000$ m/s, vertical shear velocity $v_s = v_p/2$, $\epsilon = 0.2$ and $\delta = 0.2$. Note that the wavefield for the isotropic situation differs from that of the anisotropic situation. The wavefields for the anisotropic situation shows a clear lateral and near vertical stretch. In the vertical direction, however, both wavefields are kinematically the same since the vertical velocities are the same — a behavior that is expected in such a situation.

We then consider the wavefields for the inhomogeneous situation. Figure 6.2 shows the models used for v_p, ϵ and δ. The model for the vertical shear velocity is half that of the vertical compressional velocity. We note again the clear kinematic differences/distortion of the anisotropic situation relative to that of the isotropic case for both the incident and the scattered wavefields, see Figure 6.3.

6.5. CONCLUSION

We have introduced anisotropy to the full wavefield modeling method that is valid for inhomogeneous media. By considering a quasi-elastodynamic formulation where

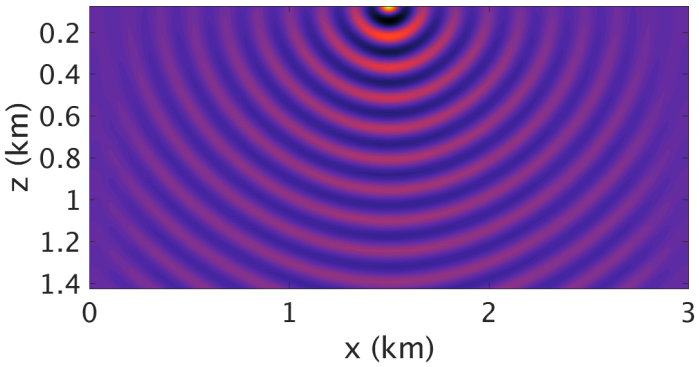

(a)

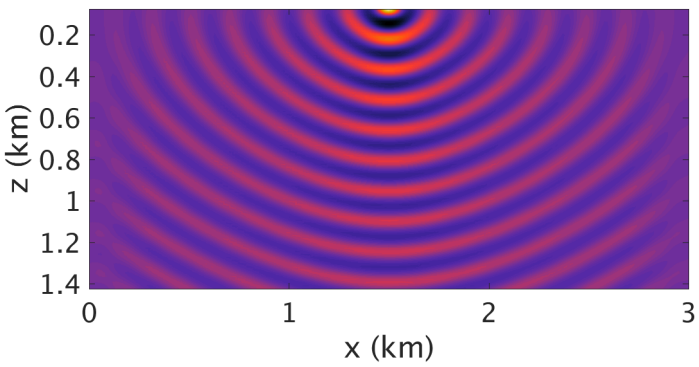

(b)

Figure 6.1 *Monochromatic wavefield for a homogeneous isotropic model. (b) Monochromatic wavefield for a homogeneous anisotropic medium. Note how stretched the wavefield is in the horizontal and near vertical directions, as expected, compared to the isotropic case.*

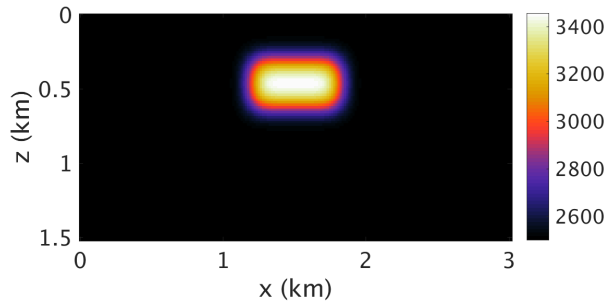

(a)

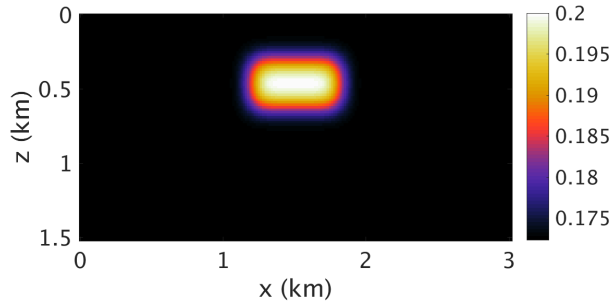

(b)

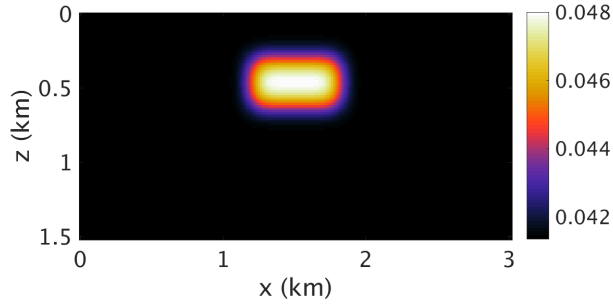

(c)

Figure 6.2 *(a) Vertical compressional velocity model used for modeling the wavefields shown in Figure 6.3. (b) ϵ model (c) δ model. The velocity model is inhomogeneous with respect to vertical velocities and anisotropic parameters and features an anomaly in the middle of the model.*

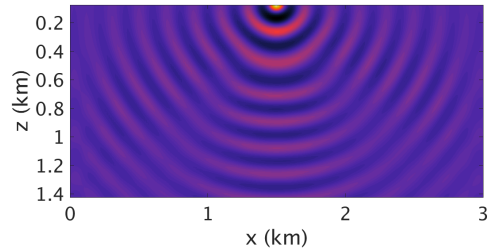

(a)

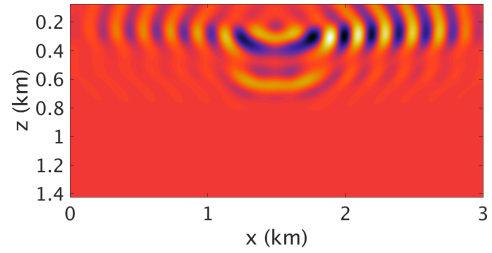

(b)

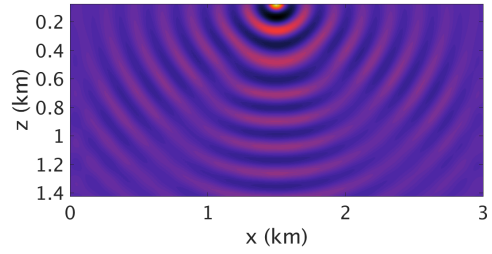

(c)

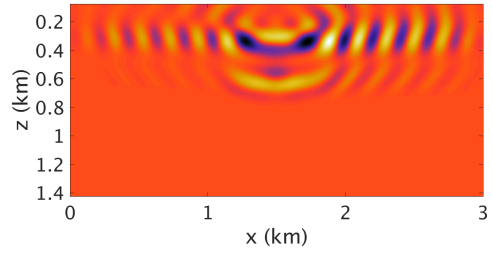

(d)

Figure 6.3 *Monochromatic incident wavefield, p^+, (a) and scattered wavefield, p^-, (b) for the isotropic situation and (c,d) for the anisotropic situation, showing p^+ and p^-, respectively. Note that the incident as well as the scattered wavefields in the anisotropic situation exhibit kinematic distortions and, therefore, the curvature of the two wavefields are clearly different.*

the elastodynamic generalized vertical wavenumber operator for P-waves is embedded in the acoustic formulation, we introduced anisotropy to the full wavefield modeling method. We have implemented the method, and we have shown two examples. One example shows the typical behavior of anisotropy in the homogeneous situation, whereas the other one shows both the incident and the scattered wavefields in an anisotropic inhomogeneous medium. The anisotropy examples show clear kinematic and curvature differences compared to the isotropic situation. This development paves the road to not only understanding different phenomena, such as multiples, in anisotropic media but also (and more importantly) to understanding the so-called Model-Independent Joint Migration Inversion process, whose goal is to obtain operators rather than model parameters from the measured data.

REFERENCES

[1] A. Einstein, *On the generalized theory of gravitation,* Scientific American **182**, 13 (1950).

[2] L. Thomsen, *Weak elastic anisotropy,* Geophysics **51**, 1954 (1986).

[3] A. A. Alshuhail, *Anisotropic Joint Migration Inversion: Automatic estimation of reflectivities and anisotropic velocities*, Ph.D. thesis, Delft University of Technology, Delft, The Netherlands (2017).

[4] T. Alkhalifah, *An acoustic wave equation for anisotropic media,* Geophysics **65**, 1239 (2000).

[5] C. P. A. Wapenaar and J. L. T. Grimbergen, *Reciprocity theorems for one-way wavefields,* Geophysical Journal International **127**, 169 (1996).

[6] C. P. A. Wapenaar and A. J. Berkhout, *Elastic Wave Field Extrapolation: Redatuming of Single- and Multi-component Seismic Data* (Elsevier Science Publishers B.V., Amsterdam, The Netherlands, 1989).

[7] M. V. de Hoop, *Generalization of the bremmer coupling series,* Journal of Mathematical Physics **37**, 3246 (1996).

[8] M. Musgrave, *Crystal Acoustics: Introduction to the Study of Elastic Waves and Vibrations in Crystals*, Holden-Day series in mathematical physics (Holden-Day, 1970).

7

ELASTODYNAMIC MODELING

"A man becomes a person thanks to the intellect."

Al-Farabi

We extend in this chapter the full wavefield modeling method to the elastodynamic case. While the acoustic case encompasses directional decomposition — where upgoing and dowing wavefields are modeled in addition to modal decomposition, through which heterogeneity is properly handled — the elastodynamic case encompasses three types of decomposition: directional, polarizational and modal. The polarizational decomposition separates the wavefields into its constituent polarizations: quasi-P, quasi-SV, and quasi-SH waves. We present two formulations: one is simpler to implement yet it contains no polarizational decomposition while the other one handles all three types of decomposition. Although we begin with the most general equations for anisotropic inhomogeneous media, we reduce those equations to the isotropic case, and we consider only P-SV waves for simplicity. We implement only the square wavenumber operator, whose implementation closely resembles that of the acoustic case.

7.1. INTRODUCTION

We have presented previously the acoustic version of full wavefield modeling, which can accommodate inhomogeneous media, with various formulations, see Chapters [3-6]. We extend in this chapter our analysis to the elastodynamic situation, which is considerably more involved than the acoustic case.

The elastodynamic version of full wavefield modeling is not as well developed as the acoustic one. The theory is thoroughly discussed by various authors [e.g. 1–4] with generalizations to anisotropic media. The elastodynamic version encompasses operators that are generalizations of the Zoeppritz equations — the basis for seismic AVO analysis [e.g. 5] — to heterogeneous media. Different aspects of elastodynamic in seismology, as well as, the Zoeppritz equations are discussed in various references[e.g. 6].

We start by stating the general equations of motion for anisotropic inhomogeneous media. We then show how three distinct types of decomposition are applied to the equations. The first decomposition is directional where wavefields are decomposed into upgoing and downgoing wavefields or for that matter left-going or right-going wavefields. The second decomposition is polarizational where different polarizations of the directional wavefields are obtained in the form of quasi-P, quasi-SV, and quasi-SH waves. The third and final decomposition is the lateral modal decomposition, through which laterally heterogeneity is accounted for in the modeling process. One can also work with directional decomposition alone without the polarizational one. The resulting equations are easier to normalize, manipulate and implement. However, they contain no polarizational decomposition. We show the details of such approach in Appendix B.

7

7.2. GENERAL EQUATIONS FOR ELASTODYNAMICS IN INHOMOGENEOUS ANISOTROPIC MEDIA

Throughout this chapter, we follow the formulations presented by de Hoop and de Hoop [2], Wapenaar and Berkhout [3], de Hoop [7] and some of the notation used by Wapenaar *et al.* [8]. We start by stating the equations for elastodynamics in inhomogeneous anisotropic media. The equation states that

$$\partial_3 \mathbf{q}^o = \mathbf{A}^o \mathbf{q}^o + \mathbf{d}^o, \tag{7.1}$$

where

$$\mathbf{q}^o = \begin{pmatrix} \mathbf{v} \\ \boldsymbol{\tau}_3 \end{pmatrix}, \tag{7.2}$$

such that $\mathbf{v}$ is the particle velocity consisting of $(v_1,\ v_2\ ,\ v_3)$ and $\boldsymbol{\tau}_3$ is vertical traction consisting of τ_{31}, τ_{32}, and τ_{33}. The source is defined as

$$\mathbf{d}^o = \begin{pmatrix} \mathbf{d}_1 \\ \mathbf{d}_2 \end{pmatrix}, \tag{7.3}$$

where

$$\mathbf{d}_1 = j\omega \mathbf{C}_{33}^{-1} \boldsymbol{\sigma}_3 \tag{7.4}$$

and

$$\mathbf{d}_2 = -\partial_\alpha(\mathbf{C}_{\alpha 3}\mathbf{C}_{33}^{-1}\boldsymbol{\sigma}_3 - \boldsymbol{\sigma}_\alpha) - \mathbf{f}, \tag{7.5}$$

where $\mathbf{f}$ is the force and $\boldsymbol{\sigma}_3$ contains the deformation sources. The stiffness matrices are those indicated by $\mathbf{C}_{ij}$. The operator $\mathbf{A}^o$ is a matrix that consists of the following elements:

$$\mathbf{A}^o = \begin{pmatrix} \mathbf{A}_{11}^o & \mathbf{A}_{12}^o \\ \mathbf{A}_{21}^o & \mathbf{A}_{22}^o \end{pmatrix}, \tag{7.6}$$

where

$$\mathbf{A}_{11}^o = -\mathbf{C}_{33}^{-1}\mathbf{C}_{3\beta}\partial_\beta, \tag{7.7}$$

$$\mathbf{A}_{12}^o = j\omega\mathbf{C}_{33}^{-1}, \tag{7.8}$$

$$\mathbf{A}_{21}^o = j\omega\rho\mathbf{I}_3 - \frac{1}{j\omega}\partial_\alpha(\mathbf{U}_{\alpha\beta}\partial_\beta\cdot), \tag{7.9}$$

and

$$\mathbf{A}_{22}^o = -\partial_\alpha(\mathbf{C}_{\alpha 3}\mathbf{C}_{33}^{-1}\cdot). \tag{7.10}$$

Also, the matrix $\mathbf{U}_{\alpha l}$ consists of a combination of stiffness parameters such that

$$\mathbf{U}_{\alpha l} = \mathbf{C}_{\alpha l} - \mathbf{C}_{\alpha 3}\mathbf{C}_{33}^{-1}\mathbf{C}_{3l}. \tag{7.11}$$

Note again that we use the summation convention where the subscripts α and β take on the values 1, 2 and 3.

7.2.1. ANTI-DIAGONAL SYSTEM

In order to simplify the operator $\mathbf{A}$, it can be made into an anti-diagonal matrix, by shuffling the rows and columns [2]. The system can be anti-diagonal up to the mono-clinic symmetry. The operator A then becomes

$$\mathbf{A} = \begin{pmatrix} 0 & \mathbf{A}_{12} \\ \mathbf{A}_{21} & 0 \end{pmatrix}. \tag{7.12}$$

One can also permute the system, as demonstrated by Wapenaar and Berkhout [3], for easier manipulation and permute it back. We will consider this permutation in detail later in the 2D situation.

7.3. DIRECTIONAL DECOMPOSITION

Equation 7.1 can be decomposed into directional wavefields, e.g. upgoing and downgiong wavefields, by applying eigen decomposition to the operator

$$\mathbf{A} = -j\omega\mathbf{L}\boldsymbol{\Lambda}\mathbf{L}, = \mathbf{L}\mathbf{N}\mathbf{L}, \tag{7.13}$$

i.e. $\mathbf{N} = -j\omega\mathbf{\Lambda}$, which results in the equations

$$\frac{\partial \mathbf{p}_d}{\partial x_3} = \mathbf{B}_d \mathbf{p}_d + \mathbf{s}_d, \tag{7.14}$$

where

$$\mathbf{B}_d = -\mathbf{N} + \mathbf{\Theta}_d, \tag{7.15}$$

such that the scattering operator

$$\mathbf{\Theta}_d = -\mathbf{L}^{-1}\partial_3 \mathbf{L}, \tag{7.16}$$

and with the resulting wavefield $\mathbf{p}_d = \begin{pmatrix} \mathbf{p}_d^+ \\ \mathbf{p}_d^- \end{pmatrix}$ where

$$\mathbf{p}_d^{\pm} = \begin{pmatrix} \phi_1^{\pm} \\ \phi_2^{\pm} \\ \phi_3^{\pm} \end{pmatrix}. \tag{7.17}$$

The resulting wavefields $\phi_i^{\pm}$ are decomposed by direction but not by polarizational decomposition. One can obtain the directional wavefields using the composition operator such that

$$\mathbf{p}_d = \mathbf{L}\mathbf{q}. \tag{7.18}$$

The composition operators (eigenvectors) can be defined as

$$\mathbf{L} = \begin{pmatrix} \mathbf{L}_1 & \mathbf{L}_1 \\ \mathbf{L}_2 & -\mathbf{L}_2 \end{pmatrix}, \tag{7.19}$$

with the inverse

$$\mathbf{L}^{-1} = \frac{1}{2}\begin{pmatrix} \mathbf{L}_1^{-1} & \mathbf{L}_2^{-1} \\ \mathbf{L}_1^{-1} & -\mathbf{L}_2^{-1} \end{pmatrix}, \tag{7.20}$$

where $\mathbf{L}_1 = \mathbf{A}_{12}, x\, \mathbf{L}_2 = \mathbf{N}$. The normalization of the eigenvectors is similar to the pressure-normalization in the acoustic situation, as proposed by de Hoop and de Hoop [2] and de Hoop [7].

7.4. POLARIZATIONAL DECOMPOSITION

One can also perform further decomposition of the matrix operator $\mathbf{A}$ such that we go from the directional decomposition, which is

$$\mathbf{A} = \mathbf{L}\mathbf{N}\mathbf{L}^{-1}, \tag{7.21}$$

to further polarizational decomposition of the operator $\mathbf{N}$ so that

$$\mathbf{N} = \mathbf{M}\mathbf{H}\mathbf{M}^{-1}. \tag{7.22}$$

Then $\mathbf{A}$ becomes

$$\mathbf{A} = \mathbf{L}\mathbf{M}\mathbf{H}\mathbf{M}^{-1}\mathbf{L}^{-1}, \tag{7.23}$$

or equivalently

$$\mathbf{A} = \mathbf{L}_c \mathbf{H} \mathbf{L}_c^{-1}, \tag{7.24}$$

where $\mathbf{L}_c = \mathbf{L}\mathbf{M}$ and

$$\mathbf{M} = \begin{pmatrix} \mathbf{M}_b & 0 \\ 0 & \mathbf{M}_b \end{pmatrix}. \tag{7.25}$$

The resulting directional wave equation then becomes

$$\partial_3 \mathbf{p} = \mathbf{B}\mathbf{p} + \mathbf{s}, \tag{7.26}$$

where

$$\mathbf{B} = -\mathbf{H} + \boldsymbol{\Theta}, \tag{7.27}$$

and

$$\mathbf{p} = \begin{pmatrix} \mathbf{p}^+ \\ \mathbf{p}^- \end{pmatrix}. \tag{7.28}$$

The resulting wavefields are then fully decomposed into their respective polarizations yet they are also directional, such that

$$\mathbf{p}^\pm = \begin{pmatrix} \psi^\pm_{qP} \\ \psi^\pm_{qSV} \\ \psi^\pm_{qSH} \end{pmatrix}. \tag{7.29}$$

Note that $\mathbf{p}_d = \mathbf{L}_c \mathbf{p}$. The scattering operator, then, becomes

$$\boldsymbol{\Theta} = -(\mathbf{M}^{-1}\partial_3 \mathbf{M} + \mathbf{M}^{-1}\boldsymbol{\Theta}_d \mathbf{M}) \tag{7.30}$$

or equivalently

$$\boldsymbol{\Theta} = -\mathbf{L}_c^{-1}\partial_3 \mathbf{L}_c. \tag{7.31}$$

The source term is

$$\mathbf{s} = \mathbf{M}^{-1}\mathbf{L}^{-1}\mathbf{d} \tag{7.32}$$

Unlike $\mathbf{N}$, which mixes different polarizations, the operator $\mathbf{H}$ is defined clearly as

$$\mathbf{H} = \begin{pmatrix} j\mathbf{H}_1^+ & 0 \\ 0 & -j\mathbf{H}_1^- \end{pmatrix}, \tag{7.33}$$

where

$$\mathbf{H}_1^\pm = \begin{pmatrix} \mathcal{H}^\pm_{1,qP} & 0 & 0 \\ 0 & \mathcal{H}^\pm_{1,qSV} & 0 \\ 0 & 0 & \mathcal{H}^\pm_{1,qSH} \end{pmatrix}. \tag{7.34}$$

7.5. MODAL DECOMPOSITION

In order to include lateral heterogeneity, the medium can be treated as a waveguide with different radiating modes. Decomposing the operators into different modes can be carried out through eigen decomposition [e.g. 2, 9]. The generalized Helmholtz slowness operator is

$$\mathbf{H}_2 = \mathbf{H}\mathbf{H} = \mathbf{Y}\boldsymbol{\Xi}\mathbf{Y}^{-1}, \tag{7.35}$$

and the generalized vertical wavenumber operator can be obtained by

$$\mathbf{H} = \mathbf{Y}\boldsymbol{\Xi}^{1/2}\mathbf{Y}^{-1}. \tag{7.36}$$

Including directional, polarizational and modal decomposition into $\mathbf{A}$ results in

$$\mathbf{A} = \mathbf{L}\mathbf{M}\mathbf{Y}\boldsymbol{\Xi}^{1/2}\mathbf{Y}^{-1}\mathbf{M}^{-1}\mathbf{L}^{-1} \tag{7.37}$$

or equivalently

$$\mathbf{A} = \mathbf{L}_c\mathbf{Y}\boldsymbol{\Xi}^{1/2}\mathbf{Y}^{-1}\mathbf{L}_c^{-1}. \tag{7.38}$$

7.6. TWO-DIMENSIONAL ELASTODYNAMIC ISOTROPIC SITUATION

7.6.1. NON-DIRECTIONAL EQUATIONS

We can reduce Equation 7.65 to the simple two-dimensional isotropic situation where P-SV and SH wavefields decouple and we can consider only the P-SV waves. The operator $\mathbf{A}$ in the wavenumber domain [e.g. 10] then becomes

$$\tilde{\mathbf{A}}^o = \begin{pmatrix} 0 & jk_x & j\frac{\omega}{\mu} & 0 \\ jk_x\frac{\lambda}{\lambda+2\mu} & 0 & 0 & \frac{j\omega}{\lambda+2\mu} \\ j\omega\rho + \frac{1}{j\omega}\eta k_x^2 & 0 & 0 & \frac{jk_x\lambda}{\lambda+2\mu} \\ 0 & j\omega\rho & jk_x & 0 \end{pmatrix}, \tag{7.39}$$

where

$$\eta = \frac{4\mu(\lambda+\mu)}{\lambda+2\mu}, \tag{7.40}$$

and

$$\mathbf{q}^o = \begin{pmatrix} v_1 \\ v_3 \\ \tau_{13} \\ \tau_{33} \end{pmatrix}, \tag{7.41}$$

where λ and μ are the compressional and shear stiffness. We can then re-arrange the matrix similar the that done by de Hoop and de Hoop [2], such that

$$\mathbf{q} = \begin{pmatrix} v_1 \\ \tau_{33} \\ \tau_{13} \\ v_3 \end{pmatrix}, \tag{7.42}$$

leading to

$$\tilde{\mathbf{A}} = \begin{pmatrix} 0 & 0 & j\frac{\omega}{\mu} & jk_x \\ 0 & 0 & jk_x & j\omega\rho \\ j\omega\rho + \frac{1}{j\omega}\eta k_x^2 & jk_x\frac{\lambda}{\lambda+2\mu} & 0 & 0 \\ jk_x\frac{\lambda}{\lambda+2\mu} & \frac{j\omega}{\lambda+2\mu} & 0 & 0 \end{pmatrix}. \tag{7.43}$$

Therefore, we now have two sub-matrices

$$\tilde{\mathbf{A}}_{21} = \begin{pmatrix} j\omega\rho + \frac{1}{j\omega}\eta k_x^2 & jk_x\frac{\lambda}{\lambda+2\mu} \\ jk_x\frac{\lambda}{\lambda+2\mu} & \frac{j\omega}{\lambda+2\mu} \end{pmatrix}, \tag{7.44}$$

and

$$\tilde{\mathbf{A}}_{12} = \begin{pmatrix} j\frac{\omega}{\mu} & jk_x \\ jk_x & j\omega\rho \end{pmatrix}, \tag{7.45}$$

which we can then transform to the spatial domain such that

$$\mathbf{A}_{12} = \begin{pmatrix} j\frac{\omega}{\mu} & -\partial_x \\ -\partial_x & j\omega\rho \end{pmatrix} \tag{7.46}$$

and for inhomogeneous media

$$\mathbf{A}_{21} = \begin{pmatrix} j\omega\rho - \frac{1}{j\omega}\partial_x\left(\eta\partial_x\cdot\right) & \partial_x\left(\frac{-\lambda}{\lambda+2\mu}\cdot\right) \\ -\frac{\lambda}{\lambda+2\mu}\partial_x & \frac{j\omega}{\lambda+2\mu} \end{pmatrix}. \tag{7.47}$$

7.6.2. DIRECTIONAL, POLARIZATIONAL AND MODAL DECOMPOSITION

Performing both directional and polarizational decomposition results in

$$\partial_3\mathbf{p} = \mathbf{B}\mathbf{p}+ = \mathbf{s}, \tag{7.48}$$

where

$$\mathbf{p} = \begin{pmatrix} \psi^+_{qP} \\ \psi^+_{qSV} \\ \psi^-_{qP} \\ \psi^-_{qSV} \end{pmatrix}. \tag{7.49}$$

Also,

$$\mathbf{B} = -\mathbf{H} + \boldsymbol{\Theta}, \tag{7.50}$$

where the scattering operator is

$$\boldsymbol{\Theta} = -\mathbf{L}_c^{-1}\partial_3\mathbf{L}_c = -(\mathbf{M}^{-1}\partial_3\mathbf{M} + \mathbf{M}^{-1}\boldsymbol{\Theta}_d\mathbf{M}), \tag{7.51}$$

and the source term is

$$\mathbf{s} = \mathbf{M}^{-1}\mathbf{L}^{-1}\mathbf{d}, \tag{7.52}$$

and the generalized vertical wavenumber operator is

$$\mathbf{H} = \begin{pmatrix} -j\mathbf{H}_1 & 0 \\ 0 & +j\mathbf{H}_1 \end{pmatrix}, \tag{7.53}$$

where

$$\mathbf{H}_1 = \begin{pmatrix} \mathcal{H}_{1,p} & 0 \\ 0 & \mathcal{H}_{1,s} \end{pmatrix}. \tag{7.54}$$

In the wavenumber domain, the square vertical wavenumber operators then become

$$\tilde{\mathcal{H}}_{2,s} = \frac{\rho\omega^2}{\mu} - k_x^2 \tag{7.55}$$

and

$$\tilde{\mathcal{H}}_{2,p} = \frac{\rho\omega^2}{\lambda+2\mu} - k_x^2, \tag{7.56}$$

which become

$$\mathcal{H}_{2,s} = \frac{\rho\omega^2}{\mu} + \partial_x^2 \tag{7.57}$$

and

$$\mathcal{H}_{2,p} = \frac{\rho\omega^2}{\lambda+2\mu} + \partial_x^2 \tag{7.58}$$

in the spatial domain. The composition and decomposition operators then become (in the wavenumber domain)

$$\tilde{\mathbf{L}} = \begin{pmatrix} \tilde{\mathbf{A}}_{12} & \tilde{\mathbf{A}}_{12} \\ \tilde{\mathbf{N}} & -\tilde{\mathbf{N}} \end{pmatrix} \tag{7.59}$$

and

$$\tilde{\mathbf{L}}^{-1} = \frac{1}{2}\begin{pmatrix} \tilde{\mathbf{A}}_{12}^{-1} & \tilde{\mathbf{N}}^{-1} \\ \tilde{\mathbf{A}}_{12}^{-1} & -\tilde{\mathbf{N}}-1 \end{pmatrix}, \tag{7.60}$$

where $\tilde{\mathbf{A}}_{12}$ is given in Equation 7.45, and its inverse is

$$\tilde{\mathbf{A}}_{12}^{-1} = \begin{pmatrix} -j\rho\omega\tilde{\mathcal{H}}_{2,s}^{-1} & jk_x\tilde{\mathcal{H}}_{2,s}^{-1} \\ jk_x\tilde{\mathcal{H}}_{2,s}^{-1} & -j\omega\mu^{-1}\tilde{\mathcal{H}}_{2,s}^{-1} \end{pmatrix}. \tag{7.61}$$

Analogous to the pressure-normalized analog, the generalized Helmholtz operator can be obtained such that

$$\tilde{\mathbf{N}}_2 = \tilde{\mathbf{A}}_{21}\tilde{\mathbf{A}}_{12}. \tag{7.62}$$

where

$$\begin{aligned} \tilde{\mathbf{N}} &= \tilde{\mathbf{N}}_2^{1/2} \\ &= (\tilde{\mathbf{A}}_{21}\tilde{\mathbf{A}}_{12})^{1/2} \\ &= \tilde{\mathbf{M}}\tilde{\mathbf{H}}_2^{1/2}\tilde{\mathbf{M}}^{-1} \\ &= \tilde{\mathbf{M}}\tilde{\mathbf{H}}\tilde{\mathbf{M}}^{-1}, \end{aligned}$$

where

$$\tilde{\mathbf{M}}_b = \begin{pmatrix} 1 & \frac{\rho\omega}{k_x} - \frac{2k_x\mu}{\omega} \\ 1 & -\frac{2k_x\mu}{\omega} \end{pmatrix}, \tag{7.63}$$

and

$$\tilde{\mathbf{M}}_b^{-1} = \begin{pmatrix} \alpha & 1-\alpha \\ \frac{k_x}{\rho\omega} & \frac{-k_x}{\rho\omega} \end{pmatrix}, \tag{7.64}$$

which have mixed-normalization.

7.7. INTEGRAL SOLUTION

The modeling or wavefield generation can be done similar to the acoustic situation that we covered in the previous chapters. A generalized integral can be used such that for iteration k the wavefield is given by

$$\mathbf{p}_k(\mathbf{x}_d) = \int_{\mathbb{R}^3} d^3\mathbf{x}\, \mathbf{G}_p(\mathbf{x}_d,\mathbf{x})\mathbf{s}(\mathbf{x}) + \int_{\mathbb{R}^3} d^3\mathbf{x}\, \mathbf{G}_p(\mathbf{x}_d,\mathbf{x})\boldsymbol{\Theta}(\mathbf{x})\mathbf{p}_{k-1}(\mathbf{x}), \tag{7.65}$$

with a the Green's functions, $\mathbf{G}_p$, such that

$$\boldsymbol{G}_p(\boldsymbol{x},\boldsymbol{x}') = \begin{pmatrix} H(x_3 - x_3')\mathbf{W}^+(\boldsymbol{x},\boldsymbol{x}') & 0 \\ 0 & -H(x_3' - x_3)\mathbf{W}^-(\boldsymbol{x},\boldsymbol{x}') \end{pmatrix}, \tag{7.66}$$

while the propagator is now different such that

$$\begin{aligned} \mathbf{W}^{\pm} &= \exp\{-j\Delta z\mathbf{H}\} \\ &= \mathbf{Y}\exp\{-j\Delta z\boldsymbol{\Xi}^{1/2}\}\mathbf{Y}^{-1}, \end{aligned}$$

where the elastodynamic wavenumber operator, $\mathbf{H}$, is invoked.

7.8. NUMERICAL EXAMPLE

We show a simple example for a homogeneous medium with compressional velocity, $vp = 3500$ m/s, and shear velocity, $v_s = 2300$ m/s with a v_s/v_p ratio of 0.66. A particularly useful feature of the modeling scheme is that it does not only provide decomposition of the wavefields into different directions, such as downgoing and upgoing, but also it decomposes the wavefields into different phases, compressional and shear. As expected, the wavelength of the shear wave is smaller than to the compressional wave due to the fact that shear velocity is lower—a fact that is s confirmed by this example.

7.9. CONCLUSION

Elastodynamic full wavefield modeling could encompass three types of decomposition: directional, polarizational and modal. If no polarizational decomposition is needed, one can implement a simpler version that can be easily normalized into the acoustic equivalent of pressure, particle-velocity, and power-flux normalization. We have implemented the vertical wavenumber operator and subsequently the propagator, through which we model the homogeneous situation. Those operators closely resemble their acoustic counterparts. Although we have derived the scattering operator which contains all the elastodynamic amplitude behavior, the implementation of such an operator is beyond the scope of the present chapter.

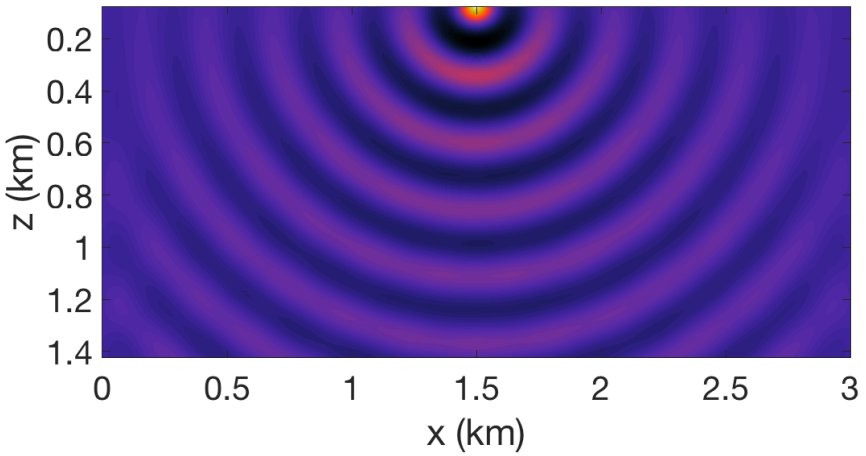

(a)

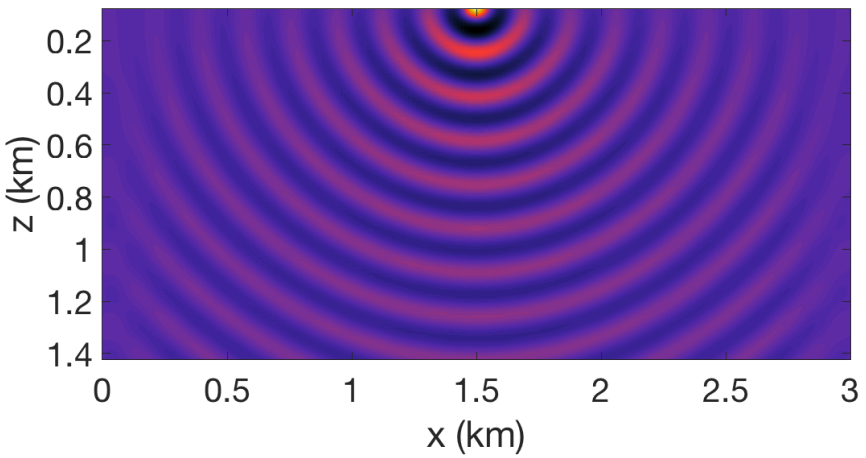

(b)

Figure 7.1 *(a) Compressional downgoing wavefield. (b) Shear downing wavefield. The velocity model is homogeneous with $v_p = 3500$ m/s and $v_s = 2300$ m/s.*

REFERENCES

[1] B. Ursin, *Review of elastic and electromagnetic wave propagation in horizontally layered media,* Geophysics **48**, 1063 (1983).

[2] M. de Hoop and A. T. de Hoop, *Elastic wave up/down decomposition in inhomogeneous and anisotropic media: an operator approach and its approximations,* Wave Motion **20**, 57 (1994).

[3] C. P. A. Wapenaar and A. J. Berkhout, *Elastic Wave Field Extrapolation: Redatuming of Single- and Multi-component Seismic Data* (Elsevier Science Publishers B.V., Amsterdam, The Netherlands, 1989).

[4] C. P. A. Wapenaar, *One-way representations of seismic data,* Geophysical Journal International **127**, 178 (1996).

[5] R. Simm, M. Bacon, and M. Bacon, *Seismic Amplitude: An interpreter's handbook* (Cambridge University Press, 2014).

[6] K. Aki and P. Richards, *Quantitative Seismology, 2^{nd} edition* (University Science Books, 2002).

[7] M. V. de Hoop, *Generalization of the bremmer coupling series,* Journal of Mathematical Physics **37**, 3246 (1996).

[8] K. Wapenaar, E. Slob, and R. Snieder, *Seismic and electromagnetic controlled-source interferometry in dissipative media,* Geophysical prospecting **56**, 419 (2008).

[9] J. L. T. Grimbergen, F. J. Dessing, and K. Wapenaar, *Modal expansion of one-way operators in laterally varying media,* GEOPHYSICS **63**, 995 (1998).

[10] C. Chapman, *Fundamentals of Seismic Wave Propagation* (Cambridge University Press, Cambridge, U.K., 2004).

8

TOWARDS MODEL-INDEPENDENT JOINT MIGRATION INVERSION

"We cannot define anything precisely. If we attempt to, we get into that paralysis of thought that comes to philosophers, who sit opposite each other, one saying to the other, "You don't know what you are talking about!". The second one says, "What do you mean by know? What do you mean by talking? What do you mean by you?"

Richard Feynman, [1, Sec. 8-2]

This chapter presents an operator-based inversion process, which is referred to as model-independent joint migration inversion (MI-JMI).The operators ultimately sought by the proposed JMI method are reflection and augmented transmission operators (the sum of slowness and transmission operators), yet the reference/background operators are only the simpler Green's primary-only operators. The proposed method is an operator-based model-independent approach to the inverse problem, in contrast with the model-dependent conventional approach of Full Waveform Inversion, which not only uses the physical model parameters, velocity and density in the acoustic situation, but also forces the data to obey a certain model, e.g. isotropic or anisotropic. Two frameworks are proposed in this chapter: one where those operators are inverted directly and another where those operators are inverted via what is referred to as phantom sources — a combination of operator contrasts and wavefields. An implementation of the direct framework shows that the method is capable of distinguishing between the relatively easy to obtain vertical heterogeneity, embedded in the reflection operator, and the more difficult to obtain lateral heterogeneity, embedded in the augmented transmission operator. This feature, among others, is expected to have a major influence on the inversion process, including its convergence properties.

8.1. INTRODUCTION

While we discussed modeling (i.e. the forward problem) in the previous chapters, we turn our attention in this chapter to the inverse problem, which encompasses the forward one. In other words, the inverse problem uses modeling iteratively to compare the observed data to the synthetic ones since ultimately a valid model or solution should be able to explain or reproduce the observations [e.g. 2, 3].

The seismic inverse problem of fitting the measured wavefields, has been traditionally addressed with the full waveform inversion (FWI) method [4, 5], as it is referred to in the geophysical literature. Other methods that are similar are those of the inverse scattering, which are developed perhaps in different disciplines but are treated coherently in applied mathematics [e.g. 6]. One such method is the so-called contrast source method [7]. However, all those methods have something in common; they solve for the actual physical parameters, such as velocity and density in the acoustic situation, for instance. While they attempt to match synthetic waveforms with the observed ones, they are fundamentally built on a core engine which is migration. In other words, they are based on migrating or backprojecting data residuals iteratively in order to match the waveforms [5].

Starting from migration, let us take a step back and attempt to look at the broader picture of this type of inverse problems. Those inverse problems can be classified into different categories. The first category is only simple qualitative imaging, i.e. migration. An assumption of migration is that a reasonable smooth model is given; that is, non-blocky with generally no sharp boundaries. The output of migration is a qualitative image that shows those boundaries. Because only smooth models are given, mainly primary events, i.e. the first order of scattering, that get migrated properly but not multiples, i.e. further orders of scattering. The book of Berkhout [8] among others [e.g. 9–11] talk about this basic process, upon which further methods are based.

The second category aims for quantitatively accurate images of reflectivity using primaries and/or multiples. The quantitatively accurate image can then be analyzed and used as an input to AVO/AVA analysis. If the primary wavefield is of concern, then linear iterative migration of the data is performed; a process referred to as a primary wavefield migration by Berkhout [12]. Another analogue methods are those of least-squares migration [13], or the more direct methods that are often referred to as true amplitude migration [e.g. 14, 15]. One could also aim for a migration of multiples (or one could argue removing them) by iterative non-linear migration, which is also refereed to as full wavefield migration [12, 16].

The third category aims for a model, in addition to a quantitatively accurate image using non-linear iterative migration. That is referred to as JMI [17, 18]. Another analogue to JMI is FWI yet no quantitative reflectivity image is produced in most FWI processes, although a qualitative one is used by some variants of FWI such as the so-called Tomographic FWI [19].

The fourth category, which is perhaps the most general one, aims for a data-adaptive inversion that let the data determine its physics model similar to the well-known process of SRME [20–22]. Therefore, rather than forcing a model on the data, we let the inversion adapt to the model provided by the actual data.

This chapter proposes an underlying representation — derived and discussed briefly

in Chapter 2 — which includes this type of data-adaptive inversion. It is so general that it compasses those basic methods such as JMI and FWM as special cases so we focus only on it.

We will look at the inverse problem. We also propose two different frameworks to solve this operator-based inversion method.

One framework inverts operators directly, that is, without using or inverting for any intermediate variables. Another method is akin to the so-called contrast source inversion method — mentioned previously — in such a way that it inverts the operators through intermediate variables referred to in this chapter as phantom sources. Another framework uses the full Green's functions rather than the primary-only Green's functions, used by the previous two methods. While using the primary Green's functions offers simplicity and computational efficiency, using the full Green's functions might have other advantages that have to do with multiples, but we leave this method to Appendix C.

We, then, analyze the problem for laterally homogeneous media. Finally, a numerical example is shown, revealing different key aspects of the method including its tendency to isolate vertical heterogeneity, which is easier to obtain, from lateral heterogeneity, which is harder to obtain.

8.2. THE UNDERLYING REPRESENTATION

As we have discussed briefly in Chapter 2, the purpose of those representations derived there is to ultimately utilize them for inversion; that is for inferring information about the medium from the recorded wavefield. One such representation — which we pointed out previously (Equation 2.53) — that could be used for such a purpose is repeated here as follows:

$$\mathbf{p}(\mathbf{x}_d) = \int_{\mathbb{D}_s} d^3\mathbf{x}\, \mathbf{G}_p^0(\mathbf{x}_d,\mathbf{x})\mathbf{s}(\mathbf{x}) + \int_{\mathbb{D}_p} d^3\mathbf{x}\, \mathbf{G}_p^0(\mathbf{x}_d,\mathbf{x})\boldsymbol{\Omega}(\mathbf{x})\mathbf{p}(\mathbf{x}), \tag{8.1}$$

or equivalently

$$\mathbf{p}(\mathbf{x}_d) = \mathbf{p}_{ref}(\mathbf{x}_d) + \int_{\mathbb{D}_p} d^3\mathbf{x}\, \mathbf{G}_p^0(\mathbf{x}_d,\mathbf{x})\boldsymbol{\Omega}(\mathbf{x})\mathbf{p}(\mathbf{x}), \tag{8.2}$$

by letting $\mathbf{p}_{ref}(\mathbf{x}_d) = \int_{\mathbb{D}_s} d^3\mathbf{x}\, \mathbf{G}_p^0(\mathbf{x}_d,\mathbf{x})\mathbf{s}(\mathbf{x})$.

However, one could rightfully ask that of all those representations given in Chapter 2, why would one pick Equation 8.1 in particular? In order to address this question, let us remind ourselves of what $\boldsymbol{\Omega}$ is composed of.

The operator $\boldsymbol{\Omega}$ in this situation is nothing but a composition of the operator R and T for the actual state and a slowness perturbation or a slowness contrast to the reference state, i.e. $j\omega\delta\Lambda$, and hence

$$\boldsymbol{\Omega}(\boldsymbol{x}) = \begin{pmatrix} \Gamma^+(\boldsymbol{x}) & R^-(\boldsymbol{x}) \\ R^+(\boldsymbol{x}) & \Gamma^-(\boldsymbol{x}) \end{pmatrix}, \tag{8.3}$$

where

$$\Gamma^\pm = \mp j\omega\delta\Lambda(\boldsymbol{x}) \pm T^\pm(\boldsymbol{x}). \tag{8.4}$$

It follows that this representation is suitable because it contains a difference between what is in inversion a known reference or starting state and an unknown actual state, unlike the other representations that contain perhaps a single reference state or that contain no contrast to the slowness operator, which is what is actually pursued in inversion. The other justification of using this representation — as opposed to Equation 2.44 — is that this representation contains the primary, $\mathbf{G}_p^0$, rather than the full Green's functions $\mathbf{G}_f^0$.

For clarity, we start by recasting Equation 2.44 with $\delta\mathbf{B}(\mathbf{x})$ written explicitly such that

$$\mathbf{p}(\mathbf{x}_d) = \int_{\mathbb{D}_s} d^3\mathbf{x}\, \mathbf{G}_f^0(\mathbf{x}_d,\mathbf{x})\mathbf{s}(\mathbf{x}) + \int_{\mathbb{D}_p} d^3\mathbf{x}\, \mathbf{G}_f^0(\mathbf{x}_d,\mathbf{x})\delta\mathbf{B}(\mathbf{x})\mathbf{p}(\mathbf{x}), \tag{8.5}$$

where

$$\mathbf{G}_f^0(\mathbf{x}_d,\mathbf{x}) = \begin{pmatrix} G_f^{0\,+,+}(\mathbf{x}_d,\mathbf{x}) & G_f^{0\,+,-}(\mathbf{x}_d,\mathbf{x}) \\ G_f^{0\,-,+}(\mathbf{x}_d,\mathbf{x}) & G_f^{0\,-,-}(\mathbf{x}_d,\mathbf{x}) \end{pmatrix}, \tag{8.6}$$

whereas

$$\mathbf{G}_p^0(\mathbf{x}_d,\mathbf{x}) = \begin{pmatrix} H(x_{d,3}-x_3)W_0^+(\mathbf{x}_d,\mathbf{x}) & 0 \\ 0 & -H(x_3-x_{d,3})W_0^-(\mathbf{x}_d,\mathbf{x}) \end{pmatrix}, \tag{8.7}$$

so the computational complexity is significantly reduced when using $\mathbf{G}_p^0$ as opposed to $\mathbf{G}_f^0$. It is reduced not only because two Green's functions are not computed in the antidiagonal of matrix in Equation 8.7, but also because the full Green's functions contain all orders of scattering and require further iterations for computing them, unlike the primary Green's function, which does not require any iteration — it can be derived directly from the wavenumber operator [see 23].

However, since all orders of scattering are contained in $\mathbf{G}_f^0$, it is not obvious what impact would it have on multiples and whether its computational complexity could result in any advantage at all. Thus, it is not wise to disregard it completely at this point, and hence, it is covered in Appendix C.

In the next two sections, we will look at two different frameworks of solving the inverse problem. One inverts the operator $\mathbf{\Omega}$ directly and the other one does so through intermediate solutions, which we refer to as phantom sources, akin to the ones used in the contrast source inversion method [7].

8.3. FIRST FRAMEWORK: OPERATOR INVERSION

Let us now look at the inversion scheme involving inversion of operators directly. The framework is described schematically in Figure 8.1.

Casting Equation 8.2 in symbolic form for easier subsequent mathematical manipulation yields

$$\mathbf{p} = \mathbf{p}_{ref} + \mathbf{G}_p\mathbf{\Omega}\mathbf{p}, \tag{8.8}$$

where we drop the superscript 0 of $\mathbf{G}_p^0$ for simplicity. We can then state the objective of the inversion scheme through the so-called objective functional

$$\phi_{mea} = \sum_i \|\mathbf{r}_i\|, \tag{8.9}$$

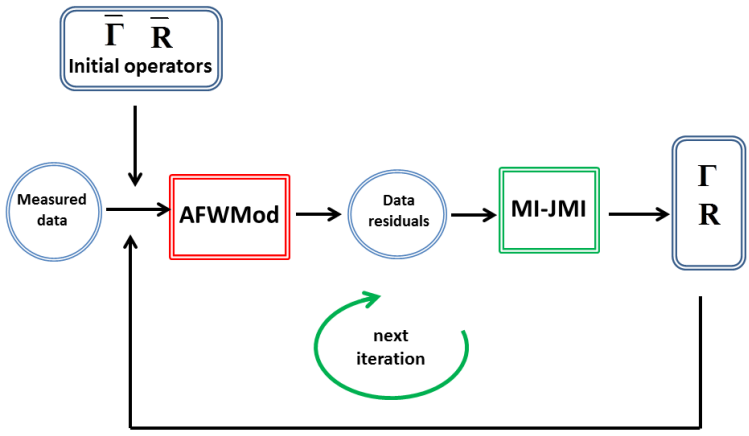

Figure 8.1 *A schematic diagram that shows the workflow of MI-JMI where the input is the measured data with initial reflection and augmented transmission operators. Those operators are then updated iteratively and represent the final output.*

which contains a residual to be reduced, summed over shot index, i. The residual can be expressed explicitly as

$$\mathbf{r} = \mathbf{p}_{mea} - (\mathbf{p}_{ref} + \mathbf{G}_p \mathbf{\Omega} \mathbf{p}), \tag{8.10}$$

which is a difference between measured wavefield, $\mathbf{p}_{mea}$ and synthetic or modeled one expressed by $(\mathbf{p}_{ref} + \mathbf{G}_p \mathbf{\Omega} \mathbf{p})$.

We are then interested to find the gradient of the objective functional, since a gradient-based optimization scheme is typically needed for such large-scale problems as ours. The gradient is then

$$\frac{\partial \phi_{mea,n}}{\partial \mathbf{\Omega}} = \delta \mathbf{\Omega}_n = 2\mathbf{G}^{\dagger}_{p,n} \mathbf{r}_{n-1} \mathbf{p}^{\dagger}_n, \tag{8.11}$$

where the dagger refers to the adjoint operation — the conjugate transpose of the operator. Finally, the iterative scheme becomes

$$\mathbf{\Omega}_n = \mathbf{\Omega}_{n-1} - \alpha_n \delta \mathbf{\Omega}_n. \tag{8.12}$$

where the step length α can be derived easily depending on the inversion scheme.

It is evident that when working with inverse problems, some sort of regularization is needed [e.g 3]. That is typically achieved by adding a term to the objective functional such that the norm of the model space is minimized after applying a regularization operator $\mathfrak{L}$, which is typically subject to empirical test (i.e. trial and error) and determined

by the user. In mathematical form

$$\phi_{reg,n} = \lambda_n \| \mathfrak{L}\, \mathbf{\Omega}_n \| , \tag{8.13}$$

where λ_n is typically chosen empirically or through for instance the so-called L-curve analysis [see e.g. 2, 3]. Since it adds some complexity fo the formulas above, the regularization term is kept separate.

8.4. SECOND FRAMEWORK: PHANTOM SOURCE INVERSION

We turn our attention to an alternative framework, which we propose in this section. Its advantage is that it uses even simpler Green functions. They are for homogeneous media, although they are not required to be. Choosing Green's functions for homogeneous media, as in the case of conventional contrast source inversion, provides us with the opportunity of turning the convolution with Green's functions, $\mathbf{G}_p^0(\mathbf{x},\mathbf{x}_s)$ into multiplication in the wavenumber domain. That is because the Green functions for homogeneous media is $\mathbf{G}_p^0(\mathbf{x}-\mathbf{x}_s)$; that is, the non-stationary convolution is converted into a stationary one [see 24] and in the wavenumber domain it turns into scalar multiplication with $\tilde{\mathbf{G}}_p^0(\mathbf{k})$. That was realized by Stolt [25] and that's the basis of the so-called Stolt migration. Hence, at the core of this method is the simple yet powerful Stolt migration when applied in the wavenumber domain.

Let us now define those phantom sources upon which this method is based. We can define the phantom sources as

$$\hat{\mathbf{s}}(\mathbf{x}) = \mathbf{\Omega}(\mathbf{x})\mathbf{p}(\mathbf{x}). \tag{8.14}$$

Then, substituting Equation 8.14 into Equation 8.2 results in

$$\mathbf{p}(\mathbf{x}_d) = \mathbf{p}_{ref}(\mathbf{x}_d) + \int_{\mathbb{D}_p} d^3\mathbf{x}\, \mathbf{G}_p^0(\mathbf{x}_d,\mathbf{x})\hat{\mathbf{s}}(\mathbf{x}). \tag{8.15}$$

The objective functional of this method is then the same as Equation 8.9, but the residual now is expressed in terms of the phantom sources such that

$$\mathbf{r} = \mathbf{p}_{mea} - (\mathbf{p}_{ref} + \mathbf{G}_p\hat{\mathbf{s}}). \tag{8.16}$$

The gradient of the misfit functional becomes

$$\frac{\partial \phi_{mea,n}}{\partial \hat{\mathbf{s}}} = \delta\hat{\mathbf{s}}_n = 2\mathbf{G}_p^\dagger \mathbf{r}_{n-1}, \tag{8.17}$$

where $\mathbf{G}_p^\dagger$ refers to the adjoint operator. The gradient weighting factor, β_n is

$$\beta_n = \frac{\sum_i < \delta\hat{\mathbf{s}}_n, \delta\hat{\mathbf{s}}_n - \delta\hat{\mathbf{s}}_{n-1} >}{\sum_i < \delta\hat{\mathbf{s}}_{n-1}, \delta\hat{\mathbf{s}}_{n-1} >}. \tag{8.18}$$

Then, the modified gradient, $\delta\hat{\mathbf{s}}'_n$, is computed such that

$$\delta\hat{\mathbf{s}}'_n = \delta\hat{\mathbf{s}}_{n-1} - \beta_n \delta\hat{\mathbf{s}}' \tag{8.19}$$

and the step length direction, α_n, such that

$$\alpha_n = \frac{\sum < \delta\hat{\mathbf{s}}_n, \delta\hat{\mathbf{s}}'_n >}{\sum \left\| \mathbf{G}_p \delta\hat{\mathbf{s}}'_n \right\|}. \tag{8.20}$$

Finally, the phantom source is then updated, where

$$\hat{\mathbf{s}}_n = \hat{\mathbf{s}}_{n-1} - \alpha_n \delta\hat{\mathbf{s}}_n. \tag{8.21}$$

Estimating the actual operator requires another inverse problem. A different objective functional is then used for deriving the actual operator, $\mathbf{\Omega}$, containing the reflection and augmented transmission operators. The objective functional for this scheme is

$$\phi_{op} = \sum_i \left\| \bar{\mathbf{q}}_i \right\|, \tag{8.22}$$

where $\bar{\mathbf{q}}_i$ is the phantom source residual such that

$$\bar{\mathbf{q}}_i = \hat{\mathbf{s}}_i - \mathbf{\Omega}\mathbf{p}_i. \tag{8.23}$$

We then derive the gradient of the operator objective functional with respect to the desired operators such that

$$\frac{\partial \phi_{op}}{\partial \mathbf{\Omega}_m} = \delta\mathbf{\Omega}_m(\mathbf{x}, \mathbf{x}') = \sum_i \begin{pmatrix} \hat{s}^+_{i,m} {p^+_{i,m}}^\dagger & \hat{s}^+_{i,m} {p^-_{i,m}}^\dagger \\ \hat{s}^-_{i,m} {p^+_{i,m}}^\dagger & \hat{s}^-_{i,m} {p^-_{i,m}}^\dagger \end{pmatrix}, \tag{8.24}$$

which is then used for updating the weighted gradient $\delta\mathbf{\Omega}'_m$ such that

$$\delta\mathbf{\Omega}'_m = \delta\mathbf{\Omega}'_{m-1} - \epsilon_m \delta\mathbf{\Omega}_m. \tag{8.25}$$

Finally, the actual gradient $\mathbf{\Omega}_m$ is updated such that

$$\mathbf{\Omega}_m = \mathbf{\Omega}_{m-1} - \gamma_m \delta\mathbf{\Omega}'_m. \tag{8.26}$$

The weighting factors ϵ_m and γ_m can be derived in a similar manner to the α and β, derived previously.

8.5. NUMERICAL EXAMPLE AND DISCUSSION

The foundation of an inverse problem, like ours, lies on the gradient of the misfit functional for it is used to update the model iteratively. Hence, generating such a gradient reveals the core of the inverse engine and many aspects of the method. The gradient contains essentially the update to the model except for a scale factor and in some cases, it might require some preconditioning or regularizations.

We compute the gradient, using the first framework, for what might seem a peculiar model in Figure 8.2. This model is chosen on purpose — to reveal some keys aspects of this method. It contains only a perturbation with only vertical and horizontal dips.

The gradients of reflection and augmented transmission operators — computed and stacked for a frequency of 10 Hz — are shown in Figure 8.3. The reflection operator

seems to be similar to the reflection images we get in conventional migration, although it is missing entirely the vertical dips. This is expected if we examine the theory closely to realize that the direction of preference is vertical and hence the reflection operator is only that of the vertical direction — not the horizontal one. That is to say that the reflection operator is almost a vertical derivative of the model and thus contains no lateral variations of the model.

The fact that the lateral heterogeneity is missing from the reflection operator seems to be a weakness in this method unless it is obtained via other means. If we examine the augmented transmission, shown in Figure 8.3b, we can see that it does indeed contain the lateral heterogeneity. It also seems relatively smooth and, hence, heavy smoothing or regularization may not be required.

Hence, this method obtains a term (reflection operator) that has no lateral variations but it obtains another term that contains all the lateral variations. One could realize that this fact agrees with the theory by examining the vertical wavenumber operator, which contains all the lateral heterogeneity.

We see that the bulk of this lateral heterogeneity is present in this gradient of augmented transmission shown in Figure 8.3b. It is not completely resolved as we would expect, but it is a reasonable start. As well-known in FWI literature, great amount of research just goes into shaping and steering this gradient to make it closer to reality. In our situation, we start with a reasonable gradient, which is encouraging.

Another encouraging property of this method is the fact that it is capable of separating a term that contains all the lateral heterogeneity, i.e. augmented transmission operator, from a term that contains none of it, i.e. reflection operator. Since lateral heterogeneity is harder to obtain from seismic data as opposed to vertical heterogeneity, otherwise we would not need such complicated methods, we end up with essentially a term that contains information that is easier to obtain — the reflection operator — and a term that contains information that is harder to obtain — the augmented transmission operator. Then, the easier information could assist in obtaining the more difficult one. So, one could think of this method as operator inversion assisted by reflectivity as this kind of assistance makes it seem gradual and hierarchical in nature.

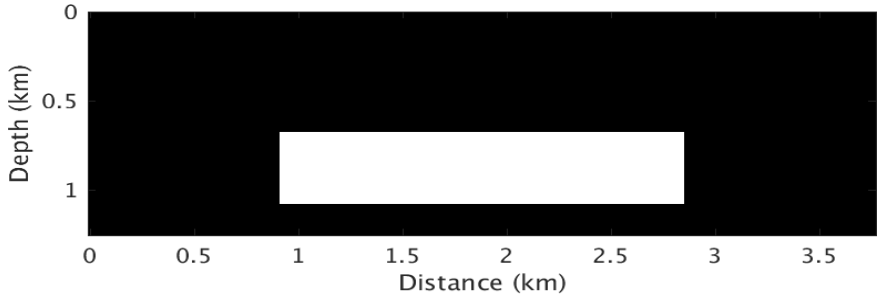

Figure 8.2 *A velocity model containing an anomaly of 2500m/s and a background velocity of 2000 m/s. The model contains two extreme situations; vertical and horizontal dips, which are suitable for illustrating the method.*

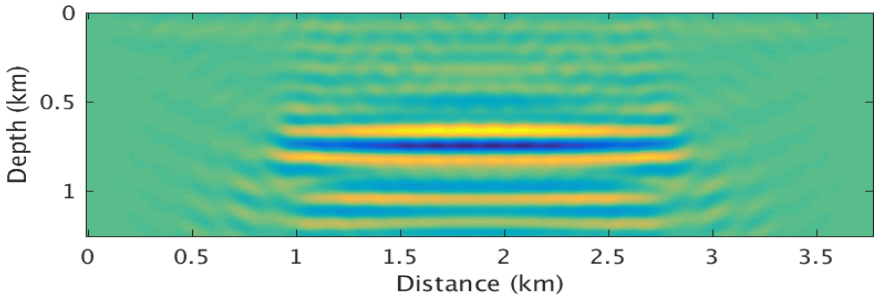

(a)

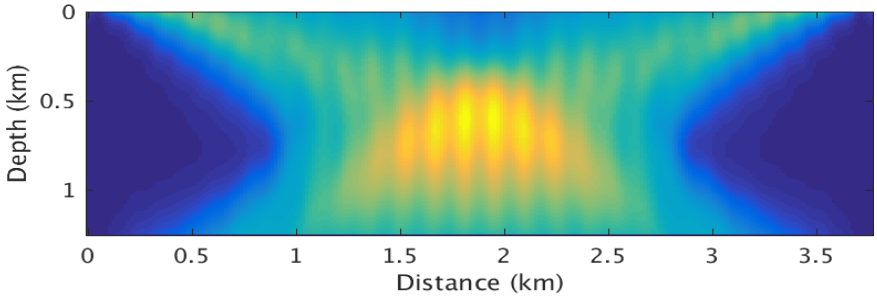

(b)

Figure 8.3 *A stack of of the estimated gradients for the vertical reflection operator from above, R^+, and a stack of the estimated gradient for the augmented transmission operator from below Γ^-. The stacks are for data containing only a single frequency of 10 Hz and are only for the first iteration of inversion. Note that the vertical reflection operator does not contain the vertical dips, but it contains the more easily-obtained horizontal ones. The augmented transmission operator, in contrast, attempts to find the vertical dips and all the difficultly-obtained lateral heterogeneity.*

8.6. CONCLUSION

We have presented a completely operator-based model-independent method for seismic inversion. The method does not require the use of actual physical model parameters, such as velocity and density in the acoustic situation, and only updates operators. The operators are those pertaining to reflection and augmented transmission (the combination of transmission and essentially a slowness perturbation). Two frameworks are proposed; one that directly inverts for the operator and the other inverts for them but via phantom sources, which involve the wavefields and the desired operators. A numerical example demonstrates the implementation of the gradient of misfit functional — an essential step towards analyzing this method. The example shows that while one operator contains all the lateral heterogeneity, the other (reflection operator) contains none — only vertical heterogeneity. So, the method tends to separate information that is easier to obtain, i.e. vertical heterogeneity, from information that is more difficult to obtain, i.e. lateral heterogeneity. We expect that this feature of separating lateral from vertical heterogeneity, among others, to have a positive impact on the inversion process.

REFERENCES

[1] R. P. Feynman, R. B. Leighton, and M. Sands, *The Feynman lectures on physics, Vol. I: The new millennium edition: mainly mechanics, radiation, and heat*, Vol. 1 (Basic books, 2011).

[2] W. Menke, *Geophysical Data Analysis: Discrete Inverse Theory: MATLAB Edition* (Elsevier Science, 2012).

[3] R. Aster, B. Borchers, and C. Thurber, *Parameter Estimation and Inverse Problems*, International Geophysics (Elsevier Science, 2011).

[4] P. Lailly, *The seismic inverse problem as a sequence of before stack migration,* in *Proc. of Conf. on Inverse Scattering, Theory and Applications* (SIAM, Philadelphia, Pennsylvania, 1983) pp. 206–220.

[5] A. Tarantola, *Inversion of seismic reflection data in the acoustic approximation,* GEOPHYSICS **49**, 1259 (1984).

[6] D. Colton and R. Kress, *Inverse Acoustic and Electromagnetic Scattering Theory* (Springer New York, 2012).

[7] P. M. van den Berg and R. E. Kleinman, *A contrast source inversion method,* Inverse Problems **13**, 1607 (1997).

[8] A. J. Berkhout, *Seismic migration, imaging of acoustic energy by wave field extrapolation: A. Theoretical Aspects* (Elsevier Science Publishers B.V., Amsterdam, The Netherlands, 1984).

[9] J. F. Claerbout, *Imaging the Earth's Interior* (Blackwell Scientific Publications, 1985).

[10] Ö. Yilmaz, *Seismic data processing* (Society of exploration geophysicists, 1987).

[11] R. H. Stolt and A. K. Benson, *Seismic Migration: Theory and Practice* (Geophysical Press, 1986).

[12] A. J. Berkhout, *Review paper: An outlook on the future of seismic imaging, part II: Full-wavefield migration,* Geophysical Prospecting **62**, 931 (2014).

[13] T. Nemeth, C. Wu, and G. T. Schuster, *Least-squares migration of incomplete reflection data,* Geophysics **64**, 208 (1999).

[14] J. Schleicher, M. Tygel, and P. Hubral, *Seismic True-amplitude Imaging* (Society of Exploration Geophysicists, 2007).

[15] N. Bleistein, J. Cohen, and J. Stockwell, *Mathematics of Multidimensional Seismic Imaging, Migration, and Inversion*, Interdisciplinary Applied Mathematics (Springer New York, 2013).

[16] M. Davydenko, *Full wavefield migration: Seismic imaging using multiple scattering effects*, Ph.D. thesis, TU Delft (2016).

[17] A. J. Berkhout, *Review paper: An outlook on the future of seismic imaging, part III: Joint migration inversion,* Geophysical Prospecting **62**, 950 (2014).

[18] X. R. Staal, *Combined imaging and velocity estimation by joint migration inversion*, Ph.D. thesis, TU Delft (2015).

[19] B. Biondi and A. Almomin, *Simultaneous inversion of full data bandwidth by tomographic full-waveform inversion,* Geophysics **79**, WA129 (2014).

[20] D. J. Verschuur, A. J. Berkhout, and C. P. A. Wapenaar, *Adaptive surface-related multiple elimination,* GEOPHYSICS **57**, 1166 (1992).

[21] A. B. Weglein, F. A. Gasparotto, P. M. Carvalho, and R. H. Stolt, *An inverse-scattering series method for attenuating multiples in seismic reflection data,* GEOPHYSICS **62**, 1975 (1997).

[22] R. G. van Borselen, J. T. Fokkema, and P. M. van den Berg, *Removal of surface-related wave phenomena—the marine case,* GEOPHYSICS **61**, 202 (1996).

[23] C. P. A. Wapenaar, *One-way representations of seismic data,* Geophysical Journal International **127**, 178 (1996).

[24] G. F. Margrave, *Theory of nonstationary linear filtering in the fourier domain with application to time-variant filtering,* GEOPHYSICS **63**, 244 (1998).

[25] R. H. Stolt, *Migration by fourier transform,* Geophysics **43**, 23 (1978).

9

CONCLUDING REMARKS

" Absence of understanding does not warrant absence of existence."

Avicena

We have started this dissertation with an introduction in which we clarified our objective, which is to investigate operator-based, model-independent methods for modeling, imaging and inversion. We started in chapter 2 by deriving actual representation theorems that can be used for such an objective and we classified them as directional and non-directional, while each is further categorized into operator-based and model-based methods.

We clarified what we mean by model-based methods as those that explicitly define the model — The Earth, in our situation, — as for instance an isotropic, lossless medium; while the operator-based methods allow a more abstract formulation that has less biased tendencies towards such specific models. Although, we have derived several representations, we have investigated two of them for modeling and inversion. Both representations use primary Green's functions, while the full Green's function could also be used and is investigated in Appendix B.

We then investigated those operators and specifically the ones for heterogeneous media. We defined two types of operators: those for heterogeneous but differentiable (i.e. smooth) media and those for heterogeneous but vertically discontinuous media. We implemented the modeling method using current knowledge of boundary conditions using the so-called stretch-coordinate PML and we also looked for curves that show the variation of slowness and reflection coefficients in heterogeneous media; and we found them deviating from the ones for laterally homogeneous media, as one would expect.

We compared the slowness curves for laterally heterogeneous media and the ones that belong to the situation involving two homogeneous half spaces, which is used in the so-called Zoeppritz equations. What we found is that lateral heterogeneity dictates that

those slowness curves deviate from the known circular ones and become dispersive (i.e. change with frequency) unlike the homogeneous situation, where they form a circle that remains frequency-independent. We also compared the propagator, the W operator, and we found that the one commonly used in migration algorithms artificially introduces laterally changing operators but the one we introduce for heterogeneous media changes in both lateral position as well as with local offset.

Although we only described and generated wavefield operators in Chapter 3, we modeled the full wavefields in Chapter 4, using a straight forward implementation using Neumann's iterative method. We first benchmarked the method with an analytical solution, a homogeneous Green's function, with a monopole source, which is what we often assume in exploration seismology, and we find reasonable agreement. We then modeled diving waves and benchmarked the solution with that of the eikonal equation. In this example we showed that one is free to choose the direction of preference and it may be advantageous to not always use the vertical one. We chose to use the horizontal one in this example and we managed to find the solution with a single iteration; thanks to the operators that can handle lateral heterogeneity. We also modeled wavefields for a heterogeneous model where we showed that different Neumann iterations correspond approximately to an order of scattering and, hence, multiples can be modeled and revealed through such a method.

While Neumann's method seems reasonable to start with, it is not guaranteed to converge, as one would suspect. Although it has been theoretically (but not numerically) shown to converge in the time domain, it is known not to always converge in the frequency domain. So, we investigated the convergence in Chapter 5 and we compared it to several methods. We found it surprisingly convergent for both the simple and the complex salt models we used. Although some other methods such as GMRes could converge faster at the expense of saving a few iterations in memory. Nonetheless the difference in saving does not seem to be warranted compared to Neumann's iterations.

Since we are dealing with operators that could be more abstract and hence can accommodate anisotropic or lossy media, we investigated the forward problem for anisotropic media and we implemented the one for transversely isotropic media in Chapter 6. As it turns out, unlike the conventional approach that assumes zero vertical shear-wave velocity, we can directly implement the operator without such an assumption since we are able to evaluate the fractional derivatives. So, it seemed more straightforward to extend this method to anisotropy than the conventional methods based on direct implementation of two-way wave equation.

We then turn our attention to the elastodynamic situation and we derive the equation while pointing our clearly that one would could use directional, polarizational and modal decomposition. The directional decomposition would separate the wavefields into upgoing and downing wavefields, the polarization decomposition decomposed the wavefields into compressional and shear waves, while the modal decomposition incorporated lateral heterogeneity. We could implement the method and computed the wavefield for both compressional and shear waves.

We then look into the inverse problem in Chapter 8; where we make the distinction between two inverse problems; one for imaging where one has reasonable knowledge of the macromodel and would like to obtain reflection and/or transmission operators;

and one where one would like to obtain not only those operators but those of the macro-model represented by the vertical wavenumber or vertical slowness operators. We lay the groundwork in this chapter for both methods and we show that such a methodology is feasible.

In summary, we have investigated the wavefield operators, and developed the full forward problem for acoustic, quasi-elastic anisotropic and elastic media and we looked at those operators and we have also laid the groundwork for the inverse problem using those operators.

While we have investigated many aspects to operator-based modeling and inversion in this dissertation, we do not claim by any means that we have done a perfectly thorough investigation that does not require any further work. On the contrary, many aspects can be investigated further and could be a subject to future research. One of those aspects is a full-fledged implementation of our proposed operator-based inversion method, MI-JMI, with a test of anisotropy or lossy media using the anisotropic modeling framework we propose in this thesis with further application from synthetic to field data. Another aspect could be the full extension of the modeling method to the elastodynamic anisotropic situation with the extension to three dimensions. We have not looked at computational efficiency and many methods could be used to speed up the implementation both for modeling or inversion. The full production-ready solution would require, before hand, thorough investigation of the full extension to three-dimensions and the computational requirements, including CPU and memory requirements. In summary, what is needed next could be similar in breadth to the investigation that was conducted to mature such methods as migration and Full Waveform Inversion.

A

Derivations and Details Related to Chapter 2

A.1. Derivation of operator-based Lippmann-Schwinger Equation

As stated in Equation 2.35, the reciprocity theorem involving the Helmholtz equation [1, p. 172] is

$$\begin{aligned}\chi(\mathbf{x}_d)\, p(\mathbf{x}_d) = &\int_{\mathbb{D}} d^3\mathbf{x}\, G_H(\mathbf{x}_d,\mathbf{x})\, s(\mathbf{x}) \\ &+ \int_{\mathbb{D}} d^3\mathbf{x}\left[\omega^2 G_H(\mathbf{x}_d,\mathbf{x})\delta\kappa(\mathbf{x})\, p(\mathbf{x}) - \partial_k G_H(\mathbf{x}_d,\mathbf{x})\delta l(\mathbf{x})\partial_k p(\mathbf{x})\right] \\ &+ \oint_{\partial\mathbb{D}} d^2\mathbf{x}\left[G_H(\mathbf{x}_d,\mathbf{x})\left\{l(\mathbf{x})\partial_k p(\mathbf{x})\right\} - p(\mathbf{x})\left\{l(\mathbf{x})\partial_k G_H(\mathbf{x}_d,\mathbf{x})\right\}\right] n_k,\end{aligned} \tag{A.1}$$

where the characteristic function $\chi(\mathbf{x}_d)$ is defined in Equation 2.29. Applying the chain rule to the term involving the lightness — inverse density — contrast in Equation A.1, yields the identity

$$\int_{\mathbb{D}} d^3\mathbf{x}\, \partial_k G_H(\mathbf{x}_d,\mathbf{x})\delta l(\mathbf{x})\partial_k p(\mathbf{x}) = \int_{\mathbb{D}} d^3\mathbf{x}\left[\partial_k\{G_H(\mathbf{x}_d,\mathbf{x})\delta l\partial_k p(\mathbf{x})\} - G_H(\mathbf{x}_d,\mathbf{x})\partial_k\{\delta l\partial_k p(\mathbf{x})\}\right]. \tag{A.2}$$

Then, applying Gauss' divergence theorem to the first term in Equation A.2 yields

$$\int_{\mathbb{D}} d^3\mathbf{x}\, \partial_k G_H(\mathbf{x}_d,\mathbf{x})\delta l(\mathbf{x})\partial_k p(\mathbf{x}) = \oint_{\partial\mathbb{D}} d^2\mathbf{x}\, \left[G_H(\mathbf{x}_d,\mathbf{x})\delta l\partial_k p(\mathbf{x})\right] n_k - \int_{\mathbb{D}} d^3\mathbf{x}\left[G_H(\mathbf{x}_d,\mathbf{x})\partial_k\{\delta l\partial_k p(\mathbf{x})\}\right]. \tag{A.3}$$

Substituting Equation A.3 into the main Equation A.1 results in

$$\begin{aligned}\chi(\mathbf{x}_d)\, p(\mathbf{x}_d) = &\int_{\mathbb{D}} d^3\mathbf{x}\, G_H(\mathbf{x}_d,\mathbf{x})\, s(\mathbf{x}) \\ &+ \int_{\mathbb{D}} d^3\mathbf{x}\left[\omega^2 G_H(\mathbf{x}_d,\mathbf{x})\delta\kappa(\mathbf{x})\, p(\mathbf{x}) + G_H(\mathbf{x}_d,\mathbf{x})\partial_k\{\delta l\partial_k p(\mathbf{x})\}\right] \\ &+ \oint_{\partial\mathbb{D}} d^2\mathbf{x}\left[G_H(\mathbf{x}_d,\mathbf{x})\left\{l_0(\mathbf{x})\partial_k p(\mathbf{x})\right\} - p(\mathbf{x})\left\{l(\mathbf{x})\partial_k G_H(\mathbf{x}_d,\mathbf{x})\right\}\right] n_k,\end{aligned} \tag{A.4}$$

which can also be written as

$$\begin{aligned}\chi(\mathbf{x}_d)\, p(\mathbf{x}_d) = &\int_{\mathbb{D}} d^3\mathbf{x}\, G_H(\mathbf{x}_d,\mathbf{x})\, s(\mathbf{x}) \\ &+ \int_{\mathbb{D}} d^3\mathbf{x}\, G_H(\mathbf{x}_d,\mathbf{x}) \underbrace{\left[\omega^2\delta\kappa(\mathbf{x}) + \partial_k\left(\delta l\partial_k\cdot\right)\right]}_{\delta\mathcal{L}} p(\mathbf{x}) \\ &+ \oint_{\partial\mathbb{D}} d^2\mathbf{x}\left[G_H(\mathbf{x}_d,\mathbf{x})\left\{l_0(\mathbf{x})\partial_k p(\mathbf{x})\right\} - p(\mathbf{x})\left\{l(\mathbf{x})\partial_k G_H(\mathbf{x}_d,\mathbf{x})\right\}\right] n_i.\end{aligned} \tag{A.5}$$

Letting the domain be unbounded in a homogeneous embedding [see 2, p. 172] so that the surface integrals vanish when the Sommerfeld radiation condition is applied (see e.g. [see e.g. 1, p.165], we finally arrive at

$$p(\mathbf{x}_d) = \int_{\mathbb{R}^3} d^3\mathbf{x}\, G_H(\mathbf{x}_d,\mathbf{x})\, s(\mathbf{x}) + \int_{\mathbb{R}^3} d^3\mathbf{x}\, G_H(\mathbf{x}_d,\mathbf{x}) \underbrace{\left[\omega^2\delta\kappa(\mathbf{x}) + \partial_k\left(\delta l\partial_k\cdot\right)\right]}_{\delta\mathcal{L}} p(\mathbf{x}), \tag{A.6}$$

which is identical to that derived by Taylor [3, p. 133], albeit it was derived for Schrodinger equation and using a simple operator identity involving forward and inverse operators. The equation is also discussed by Weglein *et al.* [4] and derived by Stolt and Weglein [5, p. 132], although their derivation is different from ours.

A.2. DERIVATION OF OPERATOR-BASED NON-DIRECTIONAL REPRESENTATION

We can also express the wave equation in only vertical particle velocity, v_3, and pressure, p, leading to the coupled equations [e.g. 1]

$$\begin{cases} \partial_3 p + j\omega\rho v_3 = f_3 \\ \partial_3 v_3 - \frac{1}{j\omega\rho} H_2 p = q' - \frac{1}{j\omega}\partial_\alpha(\frac{1}{\rho} f_\alpha), \end{cases} \tag{A.7}$$

where

$$H_2 = \frac{\omega^2}{c^2} + \rho\partial_\alpha(\frac{1}{\rho}\partial_\alpha \cdot). \tag{A.8}$$

Another form is to express Equation A.7 as

$$\partial_3 \mathbf{q} = \mathbf{A}\mathbf{q} + \mathbf{d}, \tag{A.9}$$

where

$$\mathbf{q} = \begin{pmatrix} p \\ v_3 \end{pmatrix}, \tag{A.10}$$

$$\mathbf{A} = \begin{pmatrix} 0 & -j\omega\rho \\ \frac{1}{j\omega\rho} H_2 & 0 \end{pmatrix}, \tag{A.11}$$

and the source term is expressed as

$$\mathbf{d} = \begin{pmatrix} f_3 \\ q' - \frac{1}{j\omega}\partial_\alpha(\frac{1}{\rho} f_\alpha) \end{pmatrix}. \tag{A.12}$$

We derive in this appendix the operator-based non-directional reciprocity theorem. We first start by applying the chain rule to the interaction quantify $\partial_3(p_a v_{3,b} - v_{3,a} p_b)$, after which we substitute the resulting terms using the wave equation and we rearrange the terms as follows:

$$\begin{aligned} \partial_3(p_a v_{3,b} - v_{3,a} p_b) &= v_{3,b}\partial_3 p_a + p_a \partial_3 v_{3,b} - [v_{3,a}\partial_3 p_b + p_b \partial_3 v_{a,3}] \\ &= v_{3,b}[f_{3,a} - j\omega\rho_a v_{3,a}] + p_a[s_b + \frac{1}{j\omega\rho_b} H_{2,b} p_b] \\ &\quad - v_{3,a}[f_{3,b} - j\omega\rho_a v_{3,b}] - p_b[s_a + \frac{1}{j\omega\rho_a} H_{2,a} p_a] \\ &= v_{3,b} f_{3,a} + p_a s_b + v_{3,a} f_{3,b} + p_b s_a \\ &\quad + j\omega v_{3,b} v_{3,a}\delta\rho + \frac{1}{j\omega} p_a p_b \delta\tilde{H}_2. \end{aligned} \tag{A.13}$$

Then we apply Gauss' divergence theorem to obtain

$$\begin{aligned} \int_{\partial\mathbb{D}} d^2\mathbf{x}_h\, [p_a v_{3,b} - v_{3,a} p_b] n_3 &= \int_{\mathbb{D}} d^3\mathbf{x}\, [v_b f_{3,a} + p_a s_b + v_{3,a} f_{3,b} + p_b s_a] \\ &\quad + \int_{\mathbb{D}} d^3\mathbf{x}\, [j\omega v_{3,b}\delta\rho\, v_{3,a} + \frac{1}{j\omega} p_a \delta\tilde{H}_2\, p_b], \end{aligned} \tag{A.14}$$

which can be written as operator form

A

$$\int_{\partial\mathbb{D}} d^2\mathbf{x}_h \, \{\mathbf{q}_a^T \mathbf{N} \mathbf{q}_b\} n_3 = \int_{\mathbb{D}} d^3\mathbf{x} \, \mathbf{q}_a^T \mathbf{N} \delta\mathbf{A} \mathbf{q}_b + \int_{\mathbb{D}} d^3\mathbf{x} \, \left[\mathbf{q}_a^T \mathbf{N} \mathbf{q}_b + \mathbf{d}_a^T \mathbf{N} \mathbf{q}_b\right], \tag{A.15}$$

where

$$\mathbf{N} = \begin{pmatrix} 0 & 1 \\ -1 & 0 \end{pmatrix}, \tag{A.16}$$

$$\mathbf{q}_a = \begin{pmatrix} p_a \\ v_{3,a} \end{pmatrix}, \tag{A.17}$$

and $\mathbf{q}_b$ is similarly defined but with replacing the subscript from a to b. Replacing $\mathbf{q}_a$ with the Green's function, $\mathbf{G}_A$ (and hence $\mathbf{d}_a = \mathbf{I}$), $\mathbf{q}_b$ with $\mathbf{q}$, $\mathbf{d}_b$ with $\mathbf{d}$ and assuming that the medium in unbounded, we then arrive at

$$\mathbf{q}(\mathbf{x}_d) = \int_{\mathbb{R}^3} d^3\mathbf{x} \, \mathbf{G}_A(\mathbf{x}_d, \mathbf{x}) \mathbf{d}(\mathbf{x}) + \int_{\mathbb{R}^3} d^3\mathbf{x} \, \mathbf{G}_A(\mathbf{x}_d, \mathbf{x}) \delta\mathbf{A}(\mathbf{x}) \mathbf{q}(\mathbf{x}). \tag{A.18}$$

A.3. GREEN'S STATES

Green's functions can be normalised, and hence defined, in different ways. In this section, we define explicitly the Green's functions used in different representations. We start with the Green's function for the Helmholtz equation, which can be defined as

$$\{\partial_i (l \, \partial_i \cdot) + \omega^2 \kappa\} G_H(x, x_s) = -\delta(x - x_s). \tag{A.19}$$

We can then define the Green's matrix used in Equation 8, which can be defined as

$$\partial_3 \mathbf{G}_A(\mathbf{x}, \mathbf{x}_s) - \mathbf{A}(\mathbf{x}) \mathbf{G}_A(\mathbf{x}, \mathbf{x}_s) = \mathbf{I}\delta(\mathbf{x} - \mathbf{x}_s), \tag{A.20}$$

where the constituents of $\mathbf{G}_A$ are as follows:

$$\mathbf{G}_A = \begin{pmatrix} G_A^{p,f} & G_A^{v_3,f} \\ G_A^{v_3,q} & G_A^{p,q} \end{pmatrix}, \tag{A.21}$$

where the superscripts indicate the receiver and source types, respectively.

Next, we define the various directional Green's functions used in Section 2.6. The full wavefield Green's matrix, $\mathbf{G}_f$, that encompasses primary and multiple interactions is thoroughly derived and discussed by Wapenaar [6]. It is defined as

$$\partial_3 \mathbf{G}_f(\mathbf{x}, \mathbf{x}_s) - \mathbf{B}(\mathbf{x}) \mathbf{G}_f(\mathbf{x}, \mathbf{x}_s) = \mathbf{I}\delta(\mathbf{x} - \mathbf{x}_s), \tag{A.22}$$

which, for clarity, can also be written as

$$\partial_3 \mathbf{G}_f(\mathbf{x}, \mathbf{x}_s) + \{j\omega\mathbf{\Lambda}(\mathbf{x}) + \mathbf{R} + \mathbf{T}\} \mathbf{G}_f(\mathbf{x}, \mathbf{x}_s) = \mathbf{I}\delta(\mathbf{x} - \mathbf{x}_s), \tag{A.23}$$

where

$$\mathbf{G}_f(x,x_s)=\begin{pmatrix} G_f^{+,+}(x,x_s) & G_f^{+,-}(x,x_s)\\ G_f^{-,+}(x,x_s) & G_f^{-,-}(x,x_s)\end{pmatrix}. \tag{A.24}$$

The superscripts $(\pm,\pm)$ refer to the propagation direction at the detector, at location $\mathbf{x}$, and at the source, at location $\mathbf{x}_s$, respectively.

We then define the Green's matrix $\mathbf{G}_r$ as

$$\partial_3\mathbf{G}_r(\mathbf{x},\mathbf{x}_s)+\{j\omega\mathbf{\Lambda}(\mathbf{x})+\mathbf{R}\}\mathbf{G}_r(\mathbf{x},\mathbf{x}_s)=\mathbf{I}\delta(\mathbf{x}-\mathbf{x}_s), \tag{A.25}$$

where

$$\mathbf{G}_r(x,x_s)=\begin{pmatrix} G_r^{+,+}(x,x_s) & G_r^{+,-}(x,x_s)\\ G_r^{-,+}(x,x_s) & G_r^{-,-}(x,x_s)\end{pmatrix}. \tag{A.26}$$

Note that the Green's matrix $\mathbf{G}_r$ is defined by eliminating the transmission operator, $\mathbf{T}$, while keeping the reflection operator, $\mathbf{R}$, in addition to the slowness operator $\mathbf{\Lambda}(\mathbf{x})$, which so essential that without it no propagation occur.

We can then eliminate the reflection operator while keeping the transmission operator to arrive at the transmission Green's matrix, $\mathbf{G}_t$, defined as

$$\partial_3\mathbf{G}_t(\mathbf{x},\mathbf{x}_s)+\{j\omega\mathbf{\Lambda}(\mathbf{x})+\mathbf{T}\}\mathbf{G}_t(\mathbf{x},\mathbf{x}_s)=\mathbf{I}\delta(\mathbf{x}-\mathbf{x}_s), \tag{A.27}$$

where

$$\mathbf{G}_t(\mathbf{x},\mathbf{x}_s)=\begin{pmatrix} H(x_3-x_{s,3})V^+(\mathbf{x},\mathbf{x}_s) & 0\\ 0 & -H(x_{s,3}-x_3)V^-(\mathbf{x},\mathbf{x}_s)\end{pmatrix}, \tag{A.28}$$

in which H is the Heaviside function and V is the propagator that includes transmission.

We can then define the so-called primary Green's matrix, $\mathbf{G}_p$, as

$$\partial_3\mathbf{G}_p(\mathbf{x},\mathbf{x}_s)+j\omega\mathbf{\Lambda}(\mathbf{x})\mathbf{G}_p(\mathbf{x},\mathbf{x}_s)=\mathbf{I}\delta(\mathbf{x}-\mathbf{x}_s), \tag{A.29}$$

where

$$\mathbf{G}_p(\mathbf{x},\mathbf{x}_s)=\begin{pmatrix} H(x_3-x_{s,3})W^+(\mathbf{x},\mathbf{x}_s) & 0\\ 0 & -H(x_{s,3}-x_3)W^-(\mathbf{x},\mathbf{x}_s)\end{pmatrix}, \tag{A.30}$$

and W is the primary propagator, which — unlike V — does not include transmission. However, those two operators share the feature that they both model primary-only interactions, while the constituents of $\mathbf{G}_f$ and $\mathbf{G}_t$ model both primary and multiple interactions, with the difference being that one includes transmission ($\mathbf{G}_f$) while the other ($\mathbf{G}_t$) does not.

We also note that the Green's matrices, $\mathbf{G}_f^0$, $\mathbf{G}_r^0$,$\mathbf{G}_t^0$ and $\mathbf{G}_p^0$ of the background medium are defined similarly to their counterparts in the actual medium with the exception that the operators used are those of the background medium rather than the actual one.

The Green's functions related to particle velocity and pressure wavefields are defined as

$$\begin{cases} j\omega\rho Q_i^q(\mathbf{x},\mathbf{x}_s)+\partial_i G^q(\mathbf{x},\mathbf{x}_s)=0\\ j\omega\kappa G^q(\mathbf{x},\mathbf{x}_s)+\partial_i Q_i^f(\mathbf{x},\mathbf{x}_s)=\delta(\mathbf{x}-\mathbf{x}_s),\end{cases} \tag{A.31}$$

and

$$\begin{cases} j\omega\rho Q^f_{i,j}(\mathbf{x},\mathbf{x}_s) + \partial_i G^f_j(\mathbf{x},\mathbf{x}_s) = \delta(\mathbf{x}-\mathbf{x}_s)\delta_{i,j} \\ j\omega\kappa G^f_j(\mathbf{x},\mathbf{x}_s) + \partial_i Q^f_{i,j}(\mathbf{x},\mathbf{x}_s) = 0, \end{cases} \tag{A.32}$$

where $\delta_{i,j}$ is the Kronecker delta.

A.4. SIXTEEN-COMPONENT NON-DIRECTIONAL REPRESENTATIONS

Given a volume injection source, such as a marine seismic air-gun or a force source such as a marine seismic vibrator, eight-component data can be acquired with existing technology using four-component receivers, i.e. pressure and and the three components of particle velocity. Eight other components can also be acquired with lateral force sources to make a total of sixteen components.

In order to analyze and invert such data one would need to use the appropriate integral equation with the proper Green functions. We state here the respective representation, all are derived from the general form. The representation of pressure due to vertical or lateral force sources is given as

$$\begin{aligned} p_i(\mathbf{x}_d) = &-\int_{\mathbb{D}} d^3\mathbf{x}\, \delta_{i,j} Q^q_j(\mathbf{x}_d,\mathbf{x}) f_i(\mathbf{x}) \\ &- j\omega \int_{\mathbb{D}} d^3\mathbf{x}\, [G^q(\mathbf{x}_d,\mathbf{x})\delta\kappa(\mathbf{x})\, p(\mathbf{x}) - Q^q_i(\mathbf{x}_d,\mathbf{x})\delta\rho(\mathbf{x})\, v_i(\mathbf{x})]. \end{aligned} \tag{A.33}$$

The representation of pressure due a volume injection source is given as

$$\begin{aligned} p_4(\mathbf{x}_d) = &\int_{\mathbb{D}} d^3\mathbf{x}\, G^q(\mathbf{x}_d,\mathbf{x})\, q(\mathbf{x}) \\ &- j\omega \int_{\mathbb{D}} d^3\mathbf{x}\, [G^q(\mathbf{x}_d,\mathbf{x})\delta\kappa(\mathbf{x})\, p(\mathbf{x}) - Q^q_i(\mathbf{x}_d,\mathbf{x})\delta\rho(\mathbf{x})\, v_i(\mathbf{x})]. \end{aligned} \tag{A.34}$$

The representation of particle velocity due to lateral or vertical forces sources is given as

$$\begin{aligned} v_{j,i}(\mathbf{x}_d) = &\int_{\mathbb{D}} d^3\mathbf{x}\, \delta_{i,k} Q^f_{k,j}(\mathbf{x}_d,\mathbf{x}) f_i(\mathbf{x}) \\ &+ j\omega \int_{\mathbb{D}} d^3\mathbf{x}\, [G^f_j(\mathbf{x}_d,\mathbf{x})\delta\kappa(\mathbf{x})\, p(\mathbf{x}) - Q^f_{i,j}(\mathbf{x}_d,\mathbf{x})\delta\rho(\mathbf{x})\, v_i(\mathbf{x})]. \end{aligned} \tag{A.35}$$

The representation of particle velocity due a volume injection source is given as

$$\begin{aligned} v_{j,4}(\mathbf{x}_d) = &-\int_{\mathbb{D}} d^3\mathbf{x}\, G^f_j(\mathbf{x}_d,\mathbf{x})\, q(\mathbf{x}) \\ &+ j\omega \int_{\mathbb{D}} d^3\mathbf{x}\, [G^f_j(\mathbf{x}_d,\mathbf{x})\delta\kappa(\mathbf{x})\, p(\mathbf{x}) - Q^f_{i,j}(\mathbf{x}_d,\mathbf{x})\delta\rho(\mathbf{x})\, v_i(\mathbf{x})]. \end{aligned} \tag{A.36}$$

A.5. WAVE EQUATION IN PARTICLE-VELOCITY ONLY

For completeness, one can also derive a vector Helmholtz equation containing only particle velocity. The result is

$$\partial_i(K\partial_j v_j) + \omega^2 \rho v_i = \partial_i(Kq) - j\omega f_i, \tag{A.37}$$

where $K = 1/\kappa$, which is the bulk modulus. We can then derive reciprocity theorem and domain-boundary representation and so on. We state here the scalar Helmholtz equation for comparison. The scalar Helmholtz equation states that

$$\partial_i(l\,\partial_i p) + \omega^2 \kappa p = \partial_i(l\,f_i) - j\omega q. \tag{A.38}$$

Note that not only the receiver is assumed different (i.e. particle velocity vs pressure) but also the sources are defined differently and hence the Green functions are also different. The Green's functions can be defined as

$$\{\partial_i(K\partial_j\,\cdot) + \omega^2\rho\}Q_i^v(x - x_s) = \delta(x - x_s). \tag{A.39}$$

Alternatively, one can distinguish between the different Green's functions based on its source and the resulting Green's functions are then $\tilde{Q}^q_{i,j}$ (due to the presence of a spatial derivative) and $\tilde{Q}^f_{i,j}$.

A.6. EXTENDABLE FORM

For completeness, we also state an easily extendable form of the wave equation proposed by de Hoop [7, p. 207]. The form contains all the components of particle velocity and pressure. This formulation can be easily extended to the elastodynamic formulation. It states that

$$(\mathbf{D} + j\omega\mathbf{M})\mathbf{q}' = \mathbf{d}', \tag{A.40}$$

where

$$\mathbf{M} = \begin{bmatrix} \kappa & 0 & 0 & 0 \\ 0 & \rho & 0 & 0 \\ 0 & 0 & \rho & 0 \\ 0 & 0 & 0 & \rho \end{bmatrix}, \tag{A.41}$$

and

$$\mathbf{D} = \begin{bmatrix} 0 & \partial_1 & \partial_2 & \partial_3 \\ \partial_1 & 0 & 0 & 0 \\ \partial_2 & 0 & 0 & 0 \\ \partial_3 & 0 & 0 & 0 \end{bmatrix}. \tag{A.42}$$

In addition,

A

$$\mathbf{d}' = \begin{bmatrix} q \\ f_1 \\ f_2 \\ f_3 \end{bmatrix} \tag{A.43}$$

and

$$\mathbf{q}' = \begin{bmatrix} p \\ v_1 \\ v_2 \\ v_3 \end{bmatrix}. \tag{A.44}$$

The reciprocity theorem then becomes [7, p. 214]

$$\oint_{\partial\mathbb{D}} d^2\mathbf{x}\, \{\mathbf{q}'_a\}^T \mathcal{N}_\delta \mathcal{N} \mathbf{q}'_b = \int_{\mathbb{D}} d^3\mathbf{x}\, [\{\mathbf{q}'_a\}^T \mathcal{N}_\delta \mathbf{d}'_b - \{\mathbf{d}'_a\}^T \mathcal{N}_\delta \mathbf{q}'_b] - \int_{\mathbb{D}} d^3\mathbf{x}\, j\omega\, \{\mathbf{q}'_a\}^T \mathcal{N}_\delta \delta\mathbf{M} \mathbf{q}'_b,$$

where

$$\delta\mathbf{M} = \mathbf{M}_b - \mathbf{M}_a, \tag{A.45}$$

$$\mathcal{N} = \begin{bmatrix} 0 & n_1 & n_2 & n_3 \\ n_1 & 0 & 0 & 0 \\ n_2 & 0 & 0 & 0 \\ n_3 & 0 & 0 & 0 \end{bmatrix}, \tag{A.46}$$

and

$$\mathcal{N}_\delta = \begin{bmatrix} 1 & 0 & 0 & 0 \\ 0 & -1 & 0 & 0 \\ 0 & 0 & -1 & 0 \\ 0 & 0 & 0 & -1 \end{bmatrix}. \tag{A.47}$$

REFERENCES

[1] C. P. A. Wapenaar and A. J. Berkhout, *Elastic Wave Field Extrapolation: Redatuming of Single- and Multi-component Seismic Data* (Elsevier Science Publishers B.V., Amsterdam, The Netherlands, 1989).

[2] A. T. de Hoop, *Handbook of radiation and scattering of waves: Acoustic waves in fluids, elastic waves in solids, electromagnetic waves* (Academic Press Limited, London, U.K., 1995).

[3] J. R. Taylor, *Scattering Theory: The quantum Theory on Nonrelativistic Collisions* (Wiley, New York, 1972).

[4] A. B. Weglein, F. A. Gasparotto, P. M. Carvalho, and R. H. Stolt, *An inverse-scattering series method for attenuating multiples in seismic reflection data,* GEOPHYSICS **62**, 1975 (1997).

[5] R. H. Stolt and A. B. Weglein, *Seismic imaging and inversion: Application of linear inverse theory* (Cambridge University Press, Cambridge, U.K., 2012).

[6] C. P. A. Wapenaar, *One-way representations of seismic data,* Geophysical Journal International **127**, 178 (1996).

[7] M. V. de Hoop, *Directional Decomposition of Transient Acoustic Wave Fields*, Ph.D. thesis, Delft University of Technology, Delft, The Netherlands (1992).

B

ELASTODYNAMIC MODELING

B.1. FORMULATION INCLUDING ONLY DIRECTIONAL AND MODAL DECOMPOSITION

The following formulation contains no polarizational decomposition, only directional and modal decomposition. For applications where directional wavefield decomposition is needed regardless of the polarization, the current formulation is useful. The advantage of this formulation is its simplicity with respect to implementation but the disadvantage is that it contains no decomposition with respect to P- and S-waves. We follow the normalization schemes given in the acoustic situation by de Hoop [1].

For simplicity, let $\gamma_1 = \frac{j\omega}{\mu}$, $\gamma_2 = j\omega\rho$, $\gamma_{11} = \gamma_2 = j\omega\rho$, $\gamma_{12} = -\frac{1}{j\omega}\eta = -\frac{1}{j\omega}$, $\gamma_{13} = -\frac{\lambda}{\lambda+2\mu}$ and $\gamma_{14} = \frac{j\omega}{\lambda+2\mu}$. Also, let the derivative, $\partial_1 = \mathbf{D}_1$. We can then recast matrices $\mathbf{A}_{12}$ and $\mathbf{A}_{21}$ as follows:

$$\mathbf{A}_{12} = \begin{pmatrix} \gamma_1 & -\mathbf{D}_1 \\ -\mathbf{D}_1 & \gamma_2 \end{pmatrix}, \tag{B.1}$$

and

$$\mathbf{A}_{21} = \begin{pmatrix} \gamma_{11} + \gamma_{12}\mathbf{D}_1(\eta\mathbf{D}_1\cdot) & \mathbf{D}_1\gamma_{13} \\ \gamma_{13}\mathbf{D}_1 & \gamma_{14} \end{pmatrix}. \tag{B.2}$$

Next, we consider three formulations. For implementation purposes especially for including a staggered grid implementation, which is absolutely necessary, one would need to implement the operator, $\mathbf{N}_2$, directly rather than through its constituent matrices, i.e. $\mathbf{A}_{21}$ and $\mathbf{A}_{12}$. For this reason, we include the explicit product of the corresponding matrices.

B.2. PRESSURE-NORMALIZED ANALOG

The formulation equivalent of the pressure-normalized formulation in the acoustic situation dictates that

$$\mathbf{N}_{2,pr} = \mathbf{A}_{21}\mathbf{A}_{12} = \begin{pmatrix} \gamma_{11} + \gamma_{12}\mathbf{D}_1(\eta\mathbf{D}_1\cdot) & \mathbf{D}_1\gamma_{13} \\ \gamma_{13}\mathbf{D}_1 & \gamma_{14} \end{pmatrix} \begin{pmatrix} \gamma_1 & -\mathbf{D}_1 \\ -\mathbf{D}_1 & \gamma_2 \end{pmatrix}, \tag{B.3}$$

which results in

$$\mathbf{N}_{2,pr} = \begin{pmatrix} \big(\gamma_{11} + \gamma_{12}\mathbf{D}_1(\eta\mathbf{D}_1\cdot)\big)\gamma_1 - \mathbf{D}_1\gamma_{13}\mathbf{D}_1 & -\big(\gamma_{11} + \gamma_{12}\mathbf{D}_1(\eta\mathbf{D}_1\cdot)\big)\mathbf{D}_1 + \mathbf{D}_1\gamma_{13}\gamma_2 \\ \gamma_{13}\mathbf{D}_1\gamma_1 - \gamma_{14}\mathbf{D}_1 & -\gamma_{13}\mathbf{D}_1^2 + \gamma_{14}\gamma_2 \end{pmatrix}. \tag{B.4}$$

The (de)/composition operator are defined as

$$\mathbf{L} = \begin{pmatrix} \mathbf{A}_{12} & \mathbf{A}_{12} \\ \mathbf{N} & -\mathbf{N} \end{pmatrix}, \tag{B.5}$$

and

$$\mathbf{L}^{-1} = \frac{1}{2}\begin{pmatrix} \mathbf{A}_{12}^{-1} & \mathbf{N}^{-1} \\ \mathbf{A}_{12}^{-1} & -\mathbf{N}^{-1} \end{pmatrix}. \tag{B.6}$$

B.3. PARTICLE-VELOCITY-NORMALIZED ANALOG

The formulation equivalent of the particle-normalized formulation in the acoustic situation dictates that

$$\mathbf{N}_{2,pl} = \mathbf{A}_{12}\mathbf{A}_{21} = \begin{pmatrix} \gamma_1 & -\mathbf{D}_1 \\ -\mathbf{D}_1 & \gamma_2 \end{pmatrix} \begin{pmatrix} \gamma_{11} + \gamma_{12}\mathbf{D}_1(\eta\mathbf{D}_1\cdot) & \mathbf{D}_1\gamma_{13} \\ \gamma_{13}\mathbf{D}_1 & \gamma_{14} \end{pmatrix}, \tag{B.7}$$

which results in

$$\mathbf{N}_{2,pl} = \begin{pmatrix} \gamma_1(\gamma_{11} + \gamma_{12}\mathbf{D}_1(\eta\mathbf{D}_1\cdot)) - \mathbf{D}_1\gamma_{13}\mathbf{D}_1 & \gamma_1\mathbf{D}_1\gamma_{13} - \mathbf{D}_1\gamma_{14} \\ -\mathbf{D}_1(\gamma_{11} + \gamma_{12}\mathbf{D}_1(\eta\mathbf{D}_1\cdot)) + \gamma_2\gamma_{13}\mathbf{D}_1 & -\mathbf{D}_1^2\gamma_{13} + \gamma_2\gamma_{14} \end{pmatrix}. \tag{B.8}$$

The eigenvectors are then

$$\mathbf{L} = \begin{pmatrix} \mathbf{N} & -\mathbf{N} \\ \mathbf{A}_{21} & \mathbf{A}_{21} \end{pmatrix}, \tag{B.9}$$

and its inverse

$$\mathbf{L}^{-1} = \frac{1}{2}\begin{pmatrix} \mathbf{N}^{-1} & \mathbf{A}_{21}^{-1} \\ -\mathbf{N}^{-1} & \mathbf{A}_{21}^{-1} \end{pmatrix}. \tag{B.10}$$

B.4. FLUX-NORMALIZED ANALOG

The formulation equivalent of the flux-normalized formulation in the acoustic situation dictates that

$$\mathbf{N}_{2,fl} = \mathbf{A}_{12}^{1/2}\mathbf{A}_{21}\mathbf{A}_{12}^{1/2} = \begin{pmatrix} \gamma_1 & -\mathbf{D}_1 \\ -\mathbf{D}_1 & \gamma_2 \end{pmatrix}^{1/2} \begin{pmatrix} \gamma_{11} + \gamma_{12}\mathbf{D}_1(\eta\mathbf{D}_1\cdot) & \mathbf{D}_1\gamma_{13} \\ \gamma_{13}\mathbf{D}_1 & \gamma_{14} \end{pmatrix} \begin{pmatrix} \gamma_1 & -\mathbf{D}_1 \\ -\mathbf{D}_1 & \gamma_2 \end{pmatrix}^{1/2}. \tag{B.11}$$

The result is

$$\mathbf{N}_{2,fl} = \begin{pmatrix} E_{11} & E_{12} \\ E_{21} & E_{22} \end{pmatrix}, \tag{B.12}$$

where

$$\begin{aligned} E_{11} &= \gamma_1^{1/2}\left([\gamma_{11}+\gamma_{12}\mathbf{D}_1(\eta\mathbf{D}_1\cdot)]\gamma_1^{1/2}-\mathbf{D}_1\gamma_{13}\mathbf{D}_1^{1/2}\right)-\mathbf{D}_1^{1/2}\left(\gamma_{13}\mathbf{D}_1\gamma_1^{1/2}-\gamma_{14}\mathbf{D}_1^{1/2}\right) \\ &= \gamma_1^{1/2}[\gamma_{11}+\gamma_{12}\mathbf{D}_1(\eta\mathbf{D}_1\cdot)]\gamma_1^{1/2}-\gamma_1^{1/2}\mathbf{D}_1\gamma_{13}\mathbf{D}_1^{1/2}-\mathbf{D}_1^{1/2}\gamma_{13}\mathbf{D}_1\gamma_1^{1/2}+\mathbf{D}_1^{1/2}\gamma_{14}\mathbf{D}_1^{1/2}, \end{aligned}$$

$$\begin{aligned} E_{12} &= \gamma_1^{1/2}\left(-[\gamma_{11}+\gamma_{12}\mathbf{D}_1(\eta\mathbf{D}_1\cdot)]\mathbf{D}_1^{1/2}+\mathbf{D}_1\gamma_{13}\gamma_2^{1/2}\right)-\mathbf{D}_1^{1/2}\left(-\gamma_{13}\mathbf{D}_1\mathbf{D}_1^{1/2}+\gamma_{14}\gamma_2^{1/2}\right) \\ &= -\gamma_1^{1/2}[\gamma_{11}+\gamma_{12}\mathbf{D}_1(\eta\mathbf{D}_1\cdot)]\mathbf{D}_1^{1/2}+\gamma_1^{1/2}\mathbf{D}_1\gamma_{13}\gamma_2^{1/2}+\mathbf{D}_1^{1/2}\gamma_{13}\mathbf{D}_1\mathbf{D}_1^{1/2}-\mathbf{D}_1^{1/2}\gamma_{14}\gamma_2^{1/2}, \end{aligned}$$

$$E_{21} = -\mathbf{D}_1^{1/2}\left([\gamma_{11}+\gamma_{12}\mathbf{D}_1(\eta\mathbf{D}_1\cdot)]\gamma_1^{1/2}-\mathbf{D}_1\gamma_{13}\mathbf{D}_1^{1/2}\right)+\gamma_2^{1/2}\left(\gamma_{13}\mathbf{D}_1\gamma_1^{1/2}-\gamma_{14}\mathbf{D}_1^{1/2}\right), \tag{B.13}$$

and finally

$$E_{22} = -\mathbf{D}_1^{1/2}\left(-[\gamma_{11}+\gamma_{12}\mathbf{D}_1(\eta\mathbf{D}_1\cdot)]\mathbf{D}_1^{1/2}+\mathbf{D}_1\gamma_{13}\gamma_2^{1/2}\right)-\gamma_2^{1/2}\left(-\gamma_{13}\mathbf{D}_1\mathbf{D}_1^{1/2}+\gamma_{14}\gamma_2^{1/2}\right). \tag{B.14}$$

Note that

$$E_{21} = E_{12}^T. \tag{B.15}$$

The eigenvectors are then

$$\mathbf{L} = \frac{1}{\sqrt{2}}\begin{pmatrix} \mathbf{A}_{12}^{1/2}\mathbf{N}^{-1/2} & \mathbf{A}_{12}^{1/2}\mathbf{N}^{-1/2} \\ \mathbf{A}_{12}^{-1/2}\mathbf{N}^{1/2} & -\mathbf{A}_{12}^{-1/2}\mathbf{N}^{1/2} \end{pmatrix}, \tag{B.16}$$

and its inverse

$$\mathbf{L}^{-1} = \frac{1}{\sqrt{2}}\begin{pmatrix} \mathbf{N}^{1/2}\mathbf{A}_{12}^{-1/2} & \mathbf{N}^{-1/2}\mathbf{A}_{12}^{1/2} \\ \mathbf{N}^{1/2}\mathbf{A}_{12}^{-1/2} & -\mathbf{N}^{-1/2}\mathbf{A}_{12}^{1/2} \end{pmatrix}. \tag{B.17}$$

For completeness, we also include the operator $\tilde{\mathbf{N}}$ — the directional-only Square wavenumber operator in the wavenumber domain — which is

$$\tilde{\mathbf{N}} = j\alpha\begin{pmatrix} \tilde{\mathcal{H}}_{1,p}-\tilde{\mathcal{H}}_{1,s}+\alpha^{-1}\tilde{\mathcal{H}}_{1,s} & \tilde{\mathcal{H}}_{1,s}-\tilde{\mathcal{H}}_{1,p}+\alpha^{-1}(\tilde{\mathcal{H}}_{1,p}-\tilde{\mathcal{H}}_{1,s}) \\ \tilde{\mathcal{H}}_{1,p}-\tilde{\mathcal{H}}_{1,s} & \tilde{\mathcal{H}}_{1,s}-\tilde{\mathcal{H}}_{1,p}+\alpha^{-1}\tilde{\mathcal{H}}_{1,p} \end{pmatrix}, \tag{B.18}$$

whereas its inverse is

$$\tilde{\mathbf{N}}^{-1} = j\alpha\begin{pmatrix} \tilde{\mathcal{H}}_{1,p}^{-1}+(1+\alpha^{-1})\tilde{\mathcal{H}}_{1,s}^{-1} & (\alpha^{-1}-1)\tilde{\mathcal{H}}_{1,p}^{-1}+(1-\alpha^{-1})\tilde{\mathcal{H}}_{1,s}^{-1} \\ \tilde{\mathcal{H}}_{1,p}^{-1}-\tilde{\mathcal{H}}_{1,s}^{-1} & (\alpha^{-1}-1)\tilde{\mathcal{H}}_{1,p}^{-1}+\tilde{\mathcal{H}}_{1,s}^{-1} \end{pmatrix}. \tag{B.19}$$

B

REFERENCES

[1] M. V. de Hoop, *Generalization of the bremmer coupling series,* Journal of Mathematical Physics **37**, 3246 (1996).

C

MI-JMI USING FULL GREEN'S FUNCTIONS

In this appendix we derive the formulas for inversion — similar to what we did in Chapter 8 — but using a representation that includes the full directional Green's functions. The representation used here (Equation 2.44) is as follows

$$\mathbf{p}(\mathbf{x}_d) = \int_{\mathbb{D}_s} d^3\mathbf{x}\, \mathbf{G}_f^0(\mathbf{x}_d,\mathbf{x})\mathbf{s}(\mathbf{x}) + \int_{\mathbb{D}_p} d^3\mathbf{x}\, \mathbf{G}_f^0(\mathbf{x}_d,\mathbf{x})\delta\mathbf{B}(\mathbf{x})\mathbf{p}(\mathbf{x}), \tag{C.1}$$

and the objective functional can be written explicitly in terms of the directional wavefields as

$$\phi_d = \sum_i \int d\mathbf{x}_d \;\left\| p^+_{i,mea}(\mathbf{x}_d) - p^+_i(\mathbf{x}_d) \right\| + \sum_i \int d\mathbf{x}_d \;\left\| p^-_{i,mea}(\mathbf{x}_d) - p^-_i(\mathbf{x}_d) \right\|, \tag{C.2}$$

where the summation is over shot index i similar to what is done in Chapter 8.

We minimize such an objective functional by utilizing the previous representation theorem, C.1, in order to obtain Fréchet derivatives, although the adjoint-state method [e.g. 1] can also be used.

Linearizing Equation C.1 gives what we could describe as the directional Born integral equation — akin to that of the non-directional reciprocity theorem — where

$$\mathbf{p}(\mathbf{x}_d) \approx \int_{\mathbb{D}_s} \mathbf{G}_f^0(\mathbf{x}_d,\mathbf{x})\mathbf{s}(\mathbf{x})\; d^3\mathbf{x} + \int_{\mathbb{D}_p} \mathbf{G}_f^0(\mathbf{x}_d,\mathbf{x})\delta\mathbf{B}(\mathbf{x})\bar{\mathbf{p}}(\mathbf{x})\; d^3\mathbf{x}, \tag{C.3}$$

where $\bar{\mathbf{p}}(\mathbf{x})$ is the wavefield of the reference/background state. Then, the wavefield residual can be written as

$$\mathbf{r}(\mathbf{x}_d) = \delta\mathbf{p}(\mathbf{x}_d) = \mathbf{p}_{mea}(\mathbf{x}_d) - \int_{\mathbb{D}_s} \mathbf{G}(\mathbf{x}_d,\mathbf{x})\mathbf{s}(\mathbf{x})\; d^3\mathbf{x} - \int_{\mathbb{D}_p} \mathbf{G}_f^0(\mathbf{x}_d,\mathbf{x})\delta\mathbf{B}(\mathbf{x})\bar{\mathbf{p}}(\mathbf{x})\; d^3\mathbf{x}. \tag{C.4}$$

Next, taking the Fréchet derivatives of the wavefield using the directional Born integral equation gives

$$\mathcal{K}^{+}(\mathbf{x},\mathbf{x}') = \frac{\partial p^{+}(\mathbf{x}')}{\partial \mathbf{B}(\mathbf{x})} = \begin{pmatrix} \frac{\partial p^{+}(\mathbf{x}_d)}{\partial \Gamma^{+}(\mathbf{x})} & \frac{\partial p^{+}(\mathbf{x}_d)}{\partial R^{-}(\mathbf{x})} \\ \frac{\partial p^{+}(\mathbf{x}_d)}{\partial R^{+}(\mathbf{x})} & \frac{\partial p^{+}(\mathbf{x}_d)}{\partial \Gamma^{-}(\mathbf{x})} \end{pmatrix} = \begin{pmatrix} G_f^{+,+}(\mathbf{x}_d,\mathbf{x})\bar{p}^{+}(\mathbf{x}) & G_f^{+,+}(\mathbf{x}_d,\mathbf{x})\bar{p}^{-}(\mathbf{x}) \\ G_f^{+,-}(\mathbf{x}_d,\mathbf{x})\bar{p}^{+}(\mathbf{x}) & G_f^{+,-}(\mathbf{x}_d,\mathbf{x})\bar{p}^{-}(\mathbf{x}) \end{pmatrix} \tag{C.5}$$

and

$$\mathcal{K}^{+}(\mathbf{x},\mathbf{x}_d) = \frac{\partial p^{+}(\mathbf{x}_d)}{\partial \mathbf{B}(\mathbf{x})} = \begin{pmatrix} \frac{\partial p^{-}(\mathbf{x}_d)}{\partial \Gamma^{+}(\mathbf{x})} & \frac{\partial p^{-}(\mathbf{x}_d)}{\partial R^{-}(\mathbf{x})} \\ \frac{\partial p^{-}(\mathbf{x}_d)}{\partial R^{+}(\mathbf{x})} & \frac{\partial p^{-}(\mathbf{x}_d)}{\partial \Gamma^{-}(\mathbf{x})} \end{pmatrix} = \begin{pmatrix} G_f^{-,+}(\mathbf{x}_d,\mathbf{x})\bar{p}^{+}(\mathbf{x}) & G_f^{-,+}(\mathbf{x}_d,\mathbf{x})\bar{p}^{-}(\mathbf{x}) \\ G_f^{-,-}(\mathbf{x}_d,\mathbf{x})\bar{p}^{+}(\mathbf{x}) & G_f^{-,-}(\mathbf{x}_d,\mathbf{x})\bar{p}^{-}(\mathbf{x}) \end{pmatrix}, \tag{C.6}$$

where the superscript 0 is dropped so that the Green functions would change as the reference state changes in the full iterative scheme. Then, the gradient of the objective functional can be obtained such that

$$\mathcal{K}'(\mathbf{x}) = \sum_i \int d\mathbf{x}_d \ \{\mathcal{K}^{+}(\mathbf{x},\mathbf{x}_d)\}^{*} \delta p_i^{+}(\mathbf{x}_d) + \sum_i \int d\mathbf{x}_d \ \{\mathcal{K}^{-}(\mathbf{x},\mathbf{x}_d)\}^{*} \delta p_i^{-}(\mathbf{x}_d). \tag{C.7}$$

Finally, one can iterate using a gradient-based optimization method such that

$$\mathbf{B}_{n+1}(\mathbf{x}) = \mathbf{B}_n(\mathbf{x}) - \alpha_n \mathcal{K}'_n(\mathbf{x}), \tag{C.8}$$

where α_n is a step length. The operator $\mathbf{B}$, once again, includes scattering and slowness operators, see Ch. 2 for details and in particular Equation 2.17.

REFERENCES

[1] P. Lailly, *The seismic inverse problem as a sequence of before stack migration,* in *Proc. of Conf. on Inverse Scattering, Theory and Applications* (SIAM, Philadelphia, Pennsylvania, 1983) pp. 206–220.

ACKNOWLEDGMENTS

"If I have seen further it is by standing on the shoulders of Giants."

Isaac Newton [1, p. 9]

One could safely assume that doing a PhD is rarely like a sprint, but more like a marathon. Since marathons require endurance, every single bit of help is very much needed throughout their journey. This help could range from what is taken for granted — actual existence, being sound, healthy and motivated — to the moral, psychological, logistical and general technical support; to the support with the nitty gritty details.

So, first and foremost, I would like to thank, the Necessary Being — as the Grand Master would say — for his blessings of existence, grace, health, bounty and for enabling me to do this project.

I would like to thank my promotor and teacher dr. Eric Verschuur for his help throughout this project; for his help with the nitty gritty details; and for his understanding, open mindedness and for leading by example and clearly demonstrating his work ethic. I came in a transition period when Professor Berkhout, who set the research path I took, retired. So, many thanks to him for the legacy he left — to Eric and Gerrit, whom I also thank for his help and feedback especially in the so-called go-no-go meeting.

I would like to thank prof. Kees Wapenaar for his help and for answering some of my seemingly technically interrogating questions in his wonderful classes. Many thanks to prof. Peter van den Berg for letting me interrupt and ask him as he enjoyed writing his book — although that did not go quite well sometimes when he had some non-prime time with the intricacies of latex and coding bugs! I was very lucky to have been assigned a mentor: dr. Kees Hagen from Optics. Many thanks go to him for his wisdom, kindness and wonderful advice.

I have received some useful feedback at different stages of this project and had wonderful discussions with many people including dr. Koen van Dongen, prof. N. de Jong and dr. Martin Verweij, from our department.

While I thank my teachers at Delft, I would not forget my previous teachers that have brought me to where I am: prof. Chris Liner, whom I was lucky to meet in SEG meetings as either current of past SEG president, prof. Gary Margrave, who taught me imaging and prof. Christian Constanda who taught me wonderful mathematics.

Many thanks are due to our wonderful retired secretary: Margraet van Fessem, whom we always thought of as a wonderful mother to all of us — even though she might have picked the Treme', a French-sounding Hotel in New Orleans that does not have any resemblance to anything in France — to say the least! Nonetheless, she left us with many memories that we will always cherish. Margaret was succeeded by Angela and Annelies

who were very wonderful and helpful and arranged really nice trips for us especially the one in Rotterdam. In addition, I would like to thank Edo Bergsma, Henry den Bok and Ronald Ligteringen for their technical support.

I would like to thank my friends and colleagues for their help, companionship and the nice environment they help create. Many thanks are due to: Abdulrahman Al-Shuhail, Aayush Garg, Mikhail Davydenko, Ali Al-Farj, Hassan Al-Faraj, J. S. Maciel, J. C. Costa, Aparajita Nath, Shan Qu, Shogo Masaya, Bouchaib el Marfoul, Bander Al-Quaimi, Abdulmehsin Al-Mansoor, Dong Zhang, Tiexing Wang, Leo Hoogerbrugge, Matteo Caporal, GA Lopez-Angarita, S. Sharma, Apostolos Kontakis, Verya Daeichin, Moein Mozaffarzadeh, Elango Selvam, Alberico Sabbadini, Jack Massaad, Ulas Taskin and Jos van Rooij. Jos graciously translated the summary and propositions in Dutch, as my Dutch is currently limited to a little bit beyond "alles goed?".

Many thanks are due to my friends and colleagues from Aramco Delft Global Research Center whom I missed once they moved out of the same floor we were in to a new building. The list include: Hannes Kutscha — who taught me to never ask a Dutch "how are you?" rather than "alles goed?" unless you are prepared to listen to how they really are — Mikhail Belonosov, Yimin Sun, Roald van Borselen and Jewoo Yoo, with whom discussions were a lot of fun! From AOC, I would like to thank Fahad Abdulkareem for fostering a nice home-like environment in which we gathered with our Saudi friends. I would like also to thank my advisor Aggie Cooper from AOC for her help and follow-up.

From Saudi Aramco I would like thank my mentor and teacher Pano Kelamis — who originally comes from the land of the First Teacher and perhaps has some resemblance to him! I would like to thank many wonderful people of Saudi Aramco for their help and support including but not limited to: Mohammaed Al-Otaibi, Ayman Bakhorji, Saleh Al-Saleh, Mohammed Albannagi, Mohammad Al-Husain and Ramzy Al-Zayer.

Nothing can be done without family! I would like to thank my family: my mother, brothers, sisters, nephews and nieces for their support, especially my eldest brother, Mohammad, who sadly passed away while writing this thesis. I will miss him dearly. My wonderful wife, Naqa, and kids, Ali and Khawlah, endured with me this wonderful journey. Many thanks to them for their endless love and support. I would like to thank our families for their visits, especially my father and mother in-law for their wonderful frequent stays that lessened the feeling of home sickness we sometimes felt away from home.

Nonetheless, friends really made us feel home away from home. Many thanks to Bashar and Katrina; Ben and Linda; Leo and Bidia; Astrid and Mateen and their wonderful families.

I tried my best to mention all the people I could remember, but I might have unintentionally left some. So, for those I left out, my heartfelt sincere apologies to you. But remember, you know who you are.

It goes without saying that while I thank those people, they bear no responsibility for any errors in this document. All errors are to be attributed to the author alone.

REFERENCES

[1] R. Merton, *On the Shoulders of Giants: The Post-Italianate Edition* (University of Chicago Press, 1993).

LIST OF PUBLICATIONS

International Publications:

1. **Hammad, H. I.** and Verschuur, D. J., *Joint migration inversion for laterally varying media*, 78th EAGE Conference and Exhibition, (2016).

2. **Hammad, H. I.** and Verschuur, D. J., *Towards forward modeling beyond Zoeppritz's: Full-wavefield modeling for inhomogeneous media*, SEG Technical Program Expanded Abstracts, (2016).

3. **Hammad, H. I.** and Verschuur, D. J., *Augmented Full Wavefield Modeling-An Iterative Directional Modeling Scheme for Inhomogeneous Media*, 79th EAGE Conference and Exhibition, (2017).

4. **Hammad, H. I.** and Verschuur, D. J., *Model-Independent Joint Migration Inversion-An Operator Approach to the Seismic Inverse Problem*, 79th EAGE Conference and Exhibition, (2017).

5. **Hammad, H. I.** and Verschuur, D. J., *Scattering Order Decomposition-Separating Multiples by Order of Scattering*, 79th EAGE Conference and Exhibition, (2017).

6. **Hammad, H. I.** and Verschuur, D. J., *Practical aspects of full-wavefield modeling*, SEG Technical Program Expanded Abstracts, (2017).

7. **Hammad, H. I.** and Verschuur, D. J., *Nonlinear model-independent joint migration inversion*, SEG Technical Program Expanded Abstracts, (2017).

8. **Hammad, H. I.** and Verschuur, D. J., *Non-Linear Model-Independent Joint Migration Inversion: An Operator Approach to the Seismic Full Waveform Inverse Problem*, SEG FWI Workshop - Bahrain, (2017).

9. **Hammad, H. I.** and Verschuur, D. J., *Generalized Full Wavefield Modeling: Beyond Neumann*, 80th EAGE Conference and Exhibition, (2018).

10. **Hammad, H. I.** and Verschuur, D. J., *Quasielastic generalized full-wavefield modeling with extension to transversely isotropic media*, SEG Technical Program Expanded Abstracts, (2018).

11. **Hammad, H. I.** and Verschuur, D. J., *Iterative solutions to generalized full-wavefield modeling*, SEG Technical Program Expanded Abstracts, (2018).

12. **Hammad, H. I.** and Verschuur, D. J., *Causality-constrained model-independent joint migration inversion*, SEG Technical Program Expanded Abstracts, (2018).

13. **Hammad, H. I.** and Verschuur, D. J., *Elastodynamic Full Wavefield Modeling*, 81st EAGE Conference and Exhibition, (2019).

14. **Hammad, H. I.** and Verschuur, D. J., *Slowness and reflection coefficient curves for laterally heterogeneous media*, 81st EAGE Conference and Exhibition, (2019).

15. **Hammad, H. I.** and Verschuur, D. J., *Modeling Slowness and Transfer Coefficient Curves in Laterally Heterogeneous Media*, Geophysics (in submission), (2021).

16. **Hammad, H. I.** and Verschuur, D. J., *Modeling Diving Waves Iteratively Using Directional Wavefield Extrapolation*, Geophysical Prospecting (in submission), (2021).

Book Chapters:

1. **Hammad, H. I.** and Verschuur, D. J., *Full wavefield modeling and inversion for laterally varying media*, Delphi: The Multiple Estimation and Structural Imaging Project, Volume XXVII (2016).

2. **Hammad, H. I.** and Verschuur, D. J., *Augmented Full Wavefield Modeling*, Delphi: The Multiple Estimation and Structural Imaging Project, Volume XXVIII (2017).

3. **Hammad, H. I.** and Verschuur, D. J., *Scattering order decomposition: a method for separating multiples by order of scattering*, Delphi: The Multiple Estimation and Structural Imaging Project, Volume XXVIII (2017).

4. **Hammad, H. I.** and Verschuur, D. J., *Augmented Full Wavefield Modeling*, Delphi: The Multiple Estimation and Structural Imaging Project, Volume XXVIII (2017).

5. **Hammad, H. I.** and Verschuur, D. J., *Generalized Full Wavefield Modeling: Beyond Neumann*, Delphi: The Multiple Estimation and Structural Imaging Project, Volume XXIX (2018).

6. **Hammad, H. I.** and Verschuur, D. J., *Generalized Full Wavefield Modeling For Quasi-elastic Anisotropic Media* , Delphi: The Multiple Estimation and Structural Imaging Project, Volume XXIX (2018).

7. **Hammad, H. I.** and Verschuur, D. J., *Model-Independent Joint Migration Inversion Directly Characterized by Reflection and Augmented Transmission Operators*, Delphi: The Multiple Estimation and Structural Imaging Project, Volume XXIX (2018).

8. **Hammad, H. I.** and Verschuur, D. J., *Elastodynamic Generalized Full Wavefield Modeling Embedding Amplitudes Beyond Those of Knott-Zoeppritz*, Delphi: The Multiple Estimation and Structural Imaging Project, Volume XXIX (2018).

9. **Hammad, H. I.** and Verschuur, D. J., *Integral Representation Theorems for Model-Based, Operator-Based, Directional and Non-Directional Modeling, Imaging and Inversion of Single and Multi-Component Wavefields*, Delphi: The Multiple Estimation and Structural Imaging Project, Volume XXIX (2018).

10. **Hammad, H. I.** and Verschuur, D. J., *Generalised Full Wavefield Modelling For Inhomogeneous Isotropic and Transversely Isotropic Media with Vertical Axis of Symmetry*, Delphi: The Multiple Estimation and Structural Imaging Project, Volume XXX (2019).

11. **Hammad, H. I.** and Verschuur, D. J., *Model- and Operator-Based Representations for Directional and Non-Directional Wavefields*, Delphi: The Multiple Estimation and Structural Imaging Project, Volume XXX (2019).

12. **Hammad, H. I.** and Verschuur, D. J., *Model-Independent Joint migration Inversion via Homogenous Green's Functions Reconstruction*, Delphi: The Multiple Estimation and Structural Imaging Project, Volume XXX (2019).

13. **Hammad, H. I.** and Verschuur, D. J., *Elastodynamic Full Wavefield Modeling using a Power-Flux Normalisation Scheme*, Delphi: The Multiple Estimation and Structural Imaging Project, Volume XXX (2019).

About the Author

Hussain holds Bachelor of Science degrees with double major in both geosciences and mathematics with a minor specialization in computer science from University of Tulsa, U.S. He also holds a Master of Science degree in geophysics from University of Calgary, Canada, with a thesis titled "Full Waveform Inversion for Areas with Complex Near Surface". He is a recipient of Saudi Aramco scholarship for CDPNEs (College Degree Program for Non-Employees). He is also a recipient of Saudi Aramco employee professional development programs for completing a master and a PhD degrees. He has worked for Saudi Aramco with work assignments in seismic processing, acquisition and briefly in reservoir characterization division, as well as in CGG office in Crawley, U.K. His professional experience is primarily related to seismic imaging and model building in rift basins — working closely with Red Sea geophysicists and geologists of various disciplines. His work included deep water areas of the Red Sea, transition zone and land seismic including the basin of Midyan. His work on operation included seismic reimaging while drilling for one of Saudi Arabia's first deep water wells. He is currently part of the Saudi Aramco Exploration Technology Development Group which is in charge of developing, transferring and maintaining production seismic technology, in addition to contributing to the Company's intellectual property portfolio.